Universitat Autònoma de Barcelona

Departament de Biologia cel·lular, de Fisiologia i

d'Immunologia

Effects of oxidative stress on plasma membrane fluidity: biological consequences

Carlos de la Haba Fonteboa

Laboratori d'Immunologia Aplicada
Departament de Biologia cel·lular, de Fisiologia i d'Immunologia
Institut de Biotecnologia i de Biomedicina (IBB)

Unitat de Biofísica, Facultat de Medicina
Departament de Bioquímica i de Biologia Molecular
Centre d'Estudis en Biofísica (CEB)

Effects of oxidative stress on plasma membrane fluidity: biological consequences

Tesis para optar al grado de Doctor en Inmunologia

Carlos de la Haba Fonteboa

Directores:

Dra. Paz Martínez   Dr. Antoni Morros   Dr. José Ramón Palacio

Bellaterra, Marzo 2015

Este trabajo ha sido financiado gracias a los siguientes proyectos y ayudas:

Agradecimientos

Gracias a los doctores Paz Martinez, Antoni Morros y José Ramón Palacio por darme la oportunidad de formarme en este proyecto. Gracias por la paciencia y la ayuda a la hora de dirigir esta tesis doctoral.

Agradezco a la Unitat de Biofísica la concesión de la beca para personal investigador en formación (PIF) subvencionada por la UAB.

Me gustaria resaltar la ayuda recibida por el grupo de la Dra. Szekeres-Bartho en la obtención de la línea celular MEC-1 y del PIBF con marcador fluorescente.

También agradezco todo la ayuda del Servei de Microscòpia (UAB) y en especial a Mónica Roldán por el soporte recibido durante todo el trabajo.

Gracias a Pau Coma por toda la ayuda recibida para mejorar los programas informáticos que se han utilizado para el análisis de los resultados; a James Bolt y Armand Mensen por la corrección lingüística de la memoria escrita.

También quería dar las gracias a todos mis compañeros de laboratorio del IBB por el apoyo recibido durante estos años: Arais Sierra, Antoni Iborra, Roger Badia, Susanna Estany, Laia Viñals, así como a los profesores y compañeros de la Unitat de Biofísica.

Esto ya se acaba, gracias a todos por el apoyo durante todo el tiempo que ha durado este trabajo. Agradezco especialmente a Neus y Aritz por todo el cariño, por levantaros tan felices todos los días y aguantarme aunque yo no sea un "mourning person", os quiero. Y por supuesto muchas gracias a mis padres, a mi familia y mis amigos por estar siempre a mi lado y por todo el apoyo recibido.

Abbreviation List

ASM	Acid sphingomyelinase
ATP	Adenosine triphosphate
B-cell	B-lymphocytes
CD	Cluster of differentiation
Cer	Ceramide
DMSO	Dimethyl sulfoxide
DNA	Deoxyribonucleic acid
DPH	Diphenylhexatriene
DPPC	Dipalmitoylphosphatidylcholine
DRMs	Detergent resistant membranes
EGF	Epidermal growth factor
FAD	Flavin adenine dinucleotide
FBS	Fetal bovine serum
GDP	Guanosine diphosphate
GP	Generalized polarization
GPI	Glycosylphosphatidylinositol
GTP	Guanosine-5'-triphosphate
GUV	Giant unilamellar vesicles
HLA	Human leucocyte antigen
IκB	Inhibitor of kappa B
IKK	Inhibitor of kappa B kinase
IL	Interleukin
KO	Knockout
l_α	Fluid phase
l_β	Gel phase
l_d	Liquid-disordered phase
l_o	Liquid-ordered phase
LLIR	Lectin-like inhibitory receptor
LPS	Lipopolysaccharide
LRRs	Leucine-rich repeat
MHC	Major histocompatibility complex
MTT	3-[4,5-dimethylthiazol-2-yl]-2,5-diphenyltetrazolium bromide
MyD88	Myeloid differentiation primary response gene 88
NADP+	Oxidized nicotinamide adenine dinucleotide phosphate
NADPH	Reduced nicotinamide adenine dinucleotide phosphate
NF-κB	Nuclear factor kappa B
NK	Natural killer
NKT	Natural killer T-cell
NLRs	NOD-like receptors
NOD	Nucleotide-binding oligomerization domain
NOS	Nitric oxide synthases
PAMPs	Pathogen-associated molecular patterns
PGE$_2$	Prostaglandin E
PIBF	Progesterone induced blocking factor
PIBF-R	Progesterone induced blocking factor-receptor
PMA	Phorbol 12-myristate 13-acetate
PRRs	Pathogen recognition receptors
RIG	Retinoic acid-inducible gene

RLRs	RIG-I-like receptors
RNA	Ribonucleic acid
RNS	Reactive nitrogen species
ROS	Reactive oxygen species
SNARE	Soluble N-ethylmaleimide-sensitive factor attachment protein receptor
SOD	Superoxide dismutase
STAT	Signal Transducer and Activator of Transcription
T-cell	T-lymphocyte
Th	T-CD4+ helper
TGF-β	Transforming growth factor β
TIR	Toll-interleukin receptor
TLRs	Toll-like receptors
TNFα	Tumor necrosis factor α
T-reg	T-regulatory
TRIF	TIR-domain containing adaptor inducing interferon-β
uDC	Uterine dendritic cell
uNK	Uterine natural killer cell

Summary

Oxidative stress is present in many diseases and it is produced in cells when an imbalance between oxidants and antioxidants occurs, favoring an oxidant status which produce reactive oxygen and nitrogen species. Lipids in plasma membrane are one of the preferential targets giving rise to lipid peroxidation. This process modifies membrane properties such as membrane fluidity, a very important physical feature known to modulate membrane protein localization and receptor-ligand binding.

Aims: 1) To evaluate the effect of oxidative stress on plasma membrane fluidity regionalization of single living THP-1 macrophages and MEC-1 lymphocytes. 2) To analyze, in these cells, the relationship between lipid peroxidation and membrane fluidity. 3) To study the effect of oxidative stress on receptor-ligand binding and membrane fluidity: lipopolysaccharide/toll-like receptors (TLR2/4) in macrophages and progesterone-induced blocking factor (PIBF)/PIBF-receptor in lymphocytes.

Material and Methods: Two-photon microscopy was standardized for the first time in Universidad Autónoma de Barcelona by our laboratory, to analyze membrane fluidity in single living cells. It was also developed a new software application to analyze membrane lipid domain **size** and **number**. Cellular oxidative stress was induced by H_2O_2; the fluorescent probe Laurdan was applied to evaluate plasma membrane fluidity changes. LPS in macrophages or soluble PIBF in lymphocytes were used to analyze receptor-ligand interactions under oxidative stress.

Results:

Macrophages showed a significant H_2O_2 concentration dependent increase in the frequency of rigid lipid regions, mainly attributable to lipid rafts, at the expense of the intermediate fluidity regions. Under oxidative stress conditions, an increase in **number**, but not in **size**, of lipid raft domains was detected. Macrophage activation by LPS increase the frequency of fluid regions, which was inhibited by oxidative stress. Concerning macrophage function, secretion of TNFα under oxidative conditions was decreased.

Lymphocytes showed a significant increase in the frequency of rigid lipid regions, at the expense of fluid regions, under oxidative stress conditions. Upon PIBF binding to its receptor, lymphocyte plasma membrane became more rigid due to clustering of lipid rafts. However, when PIBF bound lymphocytes were placed in oxidizing conditions, lipid raft clustering was inhibited and PIBF binding to its receptor was also decreased.

Conclusions: 1) In single living cells plasma membrane lipid dynamics was evaluated. 2) An important general consequence of oxidative stress is that both in macrophages and lymphocytes plasma membrane becomes more rigid. 3) Receptor-ligand interactions have an effect on membrane fluidity, which vary greatly between the two cell types studied: macrophages and lymphocytes. Upon receptor-ligand binding, macrophage plasma membrane became more fluid while lymphocytes plasma membrane became more rigid. Our results suggest that lipid raft clustering is linked to cell function: upon PIBF binding to its receptor lipid raft clustering occurs in lymphocytes; however, upon LPS/TLR2/4 lipid raft clustering does not occur in macrophages. 4) Nevertheless, the effect induced by receptor-ligand binding on membrane fluidity was inhibited during oxidative stress in both cases.

Index

1- Introduction

1.1- Plasma membrane lipid organization

The plasma membrane is the intricate barrier between the extracellular matrix and the intracellular cytoplasm that allows the interactions of cells with their external components and with other cells. It is mainly composed by a complex phospholipid bilayer in an organized manner with embedded proteins, such as receptors, which link the outside of the cell with the cytoplasm and the nucleus.

The molecular structure of phospholipids is divided into three regions of great diversity: a hydrophilic head group, an interface or core body and, normally, two hydrophobic aliphatic tails or fatty acid moieties. The diversity can reside in different polar heads, in the core body which can structurally derive from glycerol or from sphingosine, or in the fatty acid tails which can have varying lengths and/or different number of unsaturations placed along distinct carbon-carbon chain positions (Fig. 1). The different combinations in lipid structure provide an endless possibility for lipid
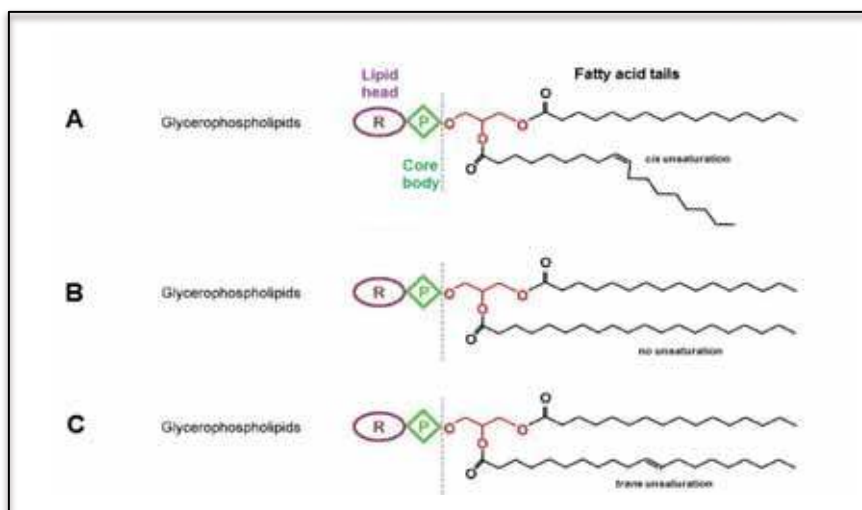
*Figure 1.- **Phospholipid structure**. Three moieties can be distinguished in the molecular structure of a phospholipid: a polar head section (purple), a core body (green) and the fatty acid tails (black). A) Glycerophospholipid with one cis-unsaturation. B) Saturated glycerophospholipid. C) Glycerophospholipid with one trans-unsaturation.*

structures and functions: strikingly, over 1000 different lipid structures exist in the membranes of any eukaryotic cell [9-11]; the role of this lipid diversity still remains elusive.

In 1972, Singer and Nicolson proposed their *Fluid-Mosaic Model* for biological membrane structures [12] was based on a large amount of previously existing experimental observations and ideas collected over the previous thirty years on membrane protein, lipid structure and dynamics. The *Fluid-Mosaic Model* states that lipids, due to their amphipathic character, are able to organize themselves in a bilayer, and that the peripheral membrane proteins are associated to the lipid bilayers polar headgroups while integral proteins are associated to the hydrophobic matrix. Both lipids and proteins are in constant motion with lateral diffusion along the plane of the membrane, or rotation around an axis perpendicular to the membrane plane. Even though the essential framework of that model remains valid today, it has been complemented and expanded with new concepts described below:

1) Different lipid phases or types of physical organization have been described in biomembranes where rigid phases as well as fluid phases coexist. However it is presently thought that, in certain circumstances, a small region of a cell membrane may transiently adopt a non-bilayer architecture: hexagonal or cubic phases [13, 14].

2) Several researchers have shown that cell membranes are formed by heterogeneous patches or laterally differentiated regions, known as lipid domains. These domains have diameters ranging between 0.1 and 1.0μm, and are enriched in certain lipids and proteins, providing them with characteristic physical, structural and functional properties. Specialized rigid membrane domains, known as *lipid rafts*, are critical for many important cellular functions [15-17].

3) More recent findings by several authors [18-20] state that lateral diffusion of lipids and proteins in the plasma membrane is not a completely free process. Diffusion barriers are presently known in the biomembranes, like membrane-associated cytoskeletal fences and extracellular matrix structures, which can selectively restrain lateral translational mobility of lipids and proteins, thus helping to define and maintain lipid domains like *lipid rafts.*

4) From Singer and Nicolson´s initial model and the more recent findings, stated above, the *Fluid-Mosaic Model* has evolved into the *hydrophobic matching principle,* widely accepted as the *mattress model*. This new model establishes that the thickness of the hydrophobic portion of an integral protein must match with the hydrophobic core thickness of the lipid domain where it resides [21-23]. This helps to explain why a certain plasma membrane receptor is able to specifically reside in a certain lipid domain.

1.2- Fluidity of the plasma membrane

Membrane fluidity is a critical physical feature of biomembranes, as it is involved in cell functions such as: regulation of enzyme activity, permeability, transport, lateral motion of membrane constituents and osmotic stability of cells [24]. Membrane fluidity is referred to as the lipid mobility within a membrane; lipids are able to move in different ways, mainly rotational and lateral diffusion.

Based on the model of Singer and Nicholson membrane fluidity was thought to be a property of the overall membrane lipid compartment. This statement by Singer and Nicholson was reflected in experimental terms as a single mean membrane fluidity value for every cell. Certain techniques such as fluorescence anisotropy are able only to obtain this average measure, so that individual lipid domains cannot be detected. Nevertheless, it is presently accepted that plasma membrane fluidity is not homogenous

around the entire plasma membrane, such that different areas within membranes can possess different fluidities [25].

Since the 1980s, two major phases have been described in studies with model membranes: the fluid phase or liquid-disordered phase ($l\alpha$ or l_d) and the gel phase (l_β) which are schematically depicted in figure 2. Recently it has been described, both in model membranes and in living cells, the presence of a new phase with intermediate properties: the liquid-ordered phase (l_o) [26, 27], mainly composed of cholesterol and sphingolipids, two kinds of lipids showing physical properties which facilitate their mutual interaction. Sphingolipids usually have saturated acyl chains which are longer
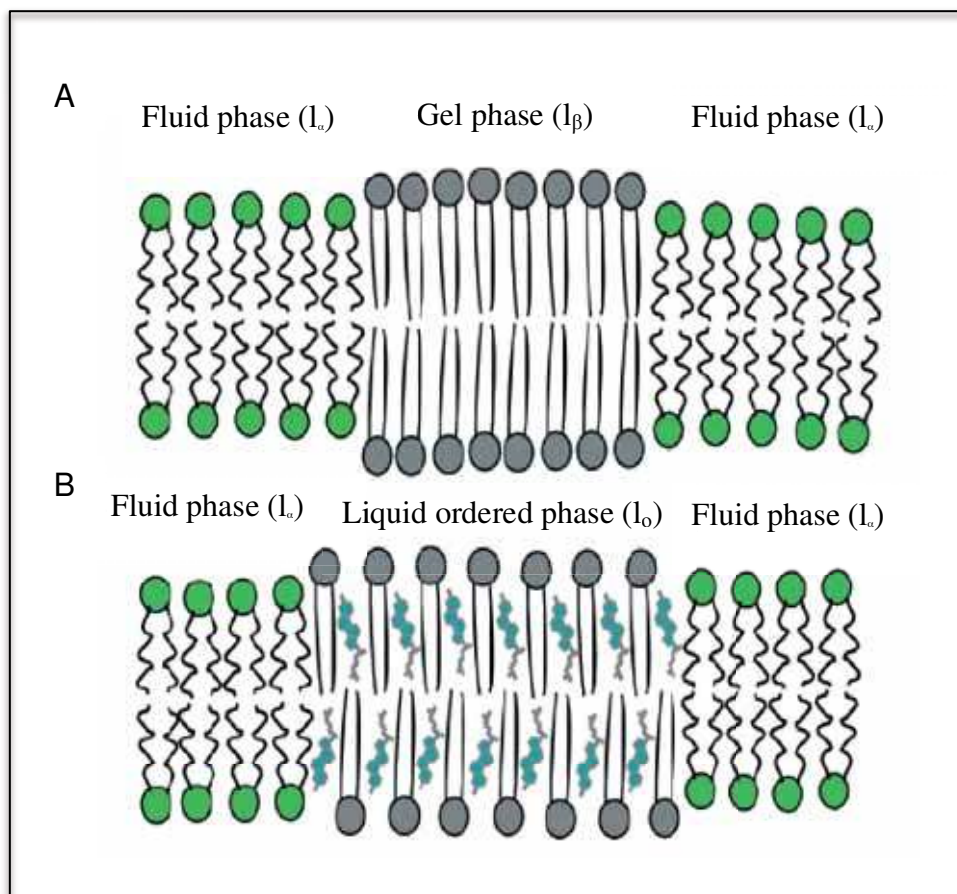
*Figure 2.- **Schematic depiction of different lipid phases.** Three main types of lipid organization or lipid phases are believed to coexist both in model and biological membranes: the fluid phase or liquid-disordered phase ($l\alpha$ or l_d), the gel phase (l_β) and the liquid ordered phase (l_o). Green heads have unsaturated tails; grey heads have saturated tails; blue molecules correspond to cholesterol. Image adapted from L.J. Johnston et al. (2007) [8].*

than the lipid tails of the surrounding membrane matrix. This is why this phase, termed the liquid-ordered phase (l_o) (Fig. 2B), appears to be more tightly packed than the neighbouring loosely packed domains and, as a consequence, the l_o bilayer is more compact than the fluid phase ($l\alpha$ or l_d) bilayer. Therefore, the l_o phase is a rigid phase, although it is not as ordered as the gel phase (l_β) [28]; it has physical properties midway between those of the liquid-disordered and the gel phase [29]. The liquid ordered phase has been observed as lipid structures that "float" in a liquid-disordered matrix [29]. It is presently accepted that these "floating structures" are also present in biological conditions, commonly named *lipid rafts* after their properties, later described in section 1.4.

Membrane fluidity is mainly determined by the ratio of cholesterol to phospholipids and by the structure of the fatty acid tails of phospholipids, number of carbons or chain length, number of unsaturations (C=C double bonds) and the position of these double bonds. In the absence of *cis*-unsaturations (Fig. 1B), fatty acyl chains become longer and the number of chain-chain van der Waals interactions increases; this yields a compact and rigid lipid domain, whose molecules show high order and low mobility, such as the gel or solid phase (l_β) [29-31] (Fig. 2A).

The presence of a *cis*-unsaturation in a phospholipid fatty acid chain causes a "kink" in the tail increasing spatial area (Fig. 1A), separating neighbor molecules and drastically impairing the lipid-lipid van der Waals weak interactions. This causes the phospholipids to have more mobility and would increase the fluidity of the lipid domain as occurs in the fluid or liquid-disordered phase ($l\alpha$) of lipids (Fig. 2) [32]. The presence of a second unsaturation in a fatty acid chain also increases membrane fluidity, although its contribution is moderate. In contrast, *trans*-unsaturations (Fig. 1C) do not induce an increase in fluidity, as they do not cause any "kink" in the acyl chain [33].

1.3- Plasma membrane receptors

Plasma membrane fluidity is a physicochemical property of the lipid components of plasma membrane, which is reflected as lipid motion. Nevertheless, membrane proteins, such as membrane receptors, also have different types of molecular movement, like lateral diffusion, rotation, and conformational fluctuations, all of them necessary for their specific function. However, this receptor mobility is not an intrinsic property of proteins; it is instead a feature determined by the fluidity of its specific lipid environment [34]. Consequently, one of the ideas on biological membranes, which has been consolidated in recent years, is that receptor structure and function are modulated by the composition, structure and dynamics of its lipid environment [34, 35]. As a result, the lipid bilayer is now accepted to be more than just a structural support for plasma membrane receptors to perform their actions [21, 36-39].

Another key feature, presently accepted, of plasma membranes is the compartmentalization of certain receptors within the plasma membrane in order to facilitate the encountering for receptor interaction and function. Van Meer, Voelker, and Feigenson reviewed [9] that certain receptors show higher affinity towards one type of lipid phase in the plasma membrane. This means that adequate lipid mobility must be an important property for an efficient function of plasma membrane receptors. Membrane receptors have numerous ways in which they can partition into the different lipid phases. Receptors containing α-helices that span across the plasma membrane, tend to have higher affinity towards fluid lipid phases, while other receptors such as glycosylphosphatidylinositol (GPI) anchored proteins tend to have a higher affinity towards ordered lipid phases like l_o phase [9].

1.4- Lipid raft hypothesis

Since 1999, most of the research in membrane biology has been focused in the area of lipid raft domains. Lipid rafts are described as liquid-ordered (l_o), fluctuant, highly dynamic, nanoscale domains which have a large amount of resident proteins [28]. Raft domains, which are enriched in sphingolipids and cholesterol, have sizes
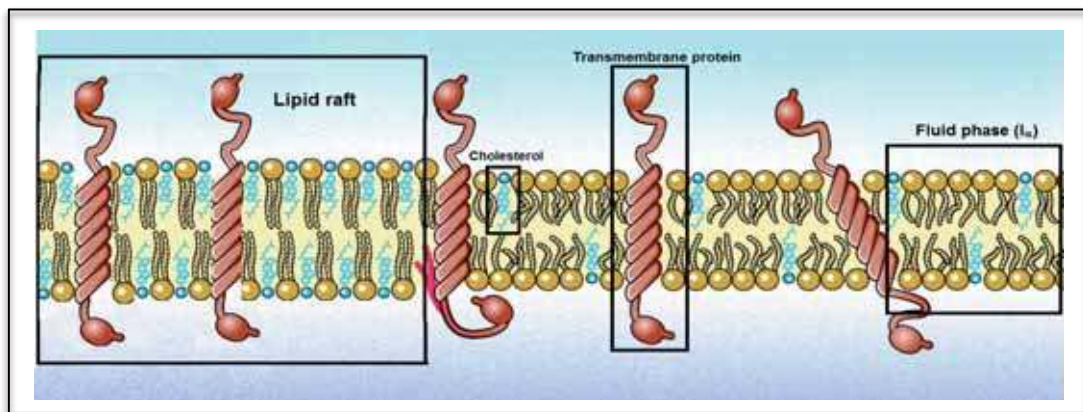
*Figure 3.- **Structure of a lipid raft.** Plasma membrane specialized domains called lipid rafts. Lipid raft tend to be thicker than fluid phases and contain a high proportion of sphingolipids and cholesterol. Image adapted from D.A. Brown et al. (2006) [5].*

ranging from 10–200nm. Smaller rafts tend to be unstable platforms while larger rafts are much more stable and aid cell signaling. Rafts are able to cluster, through fusion of small domains, giving rise to larger domains upon receptor-ligand interactions.

Lipid rafts have been extensively associated to certain membrane proteins that play essential roles, such as in the immunological synapse [16, 19, 40-43]. Certain nonresident receptors in lipid rafts are able to migrate upon receptor-ligand interactions into lipid rafts causing clustering, although the molecular mechanisms regarding this migration remain unclear. This clustering effect stabilizes the receptor-ligand interaction and aids the intracellular signaling cascade. In summary, lipid rafts act as a "meeting point", sorting proteins from the plasma membrane into the lipid raft to aid cell signaling after receptor-ligand interaction [44] (Fig. 3).

To date, there are two main experimental approaches in which lipid rafts can be studied: the use of invasive techniques such as membrane lipid extracts or the use of noninvasive image techniques. One of the invasive techniques involves the use of detergents to lyse cells, which allows isolating membrane fractions called detergent resistant membranes (DRMs). Several authors [45-48] refer to these DRMs as being lipid rafts, although several concerns have been reported that DRMs might not truly correspond to the lipid raft organization present on the biological membrane [49-51].

Nevertheless, to overcome the disadvantage of being invasive, several techniques have recently emerged which allow to obtain high-resolution fluorescence images [28]. These techniques are not only noninvasive for cells, but they are able to analyze living cells and produce high-resolution images overcoming the 200nm × 200nm spatial resolution limit. Consequently, obtaining images that distinguish domains smaller than 200nm allow us to visualize individual lipid rafts.

Two-photon microscopy is a preferred technique of this high-resolution fluorescence microscopy family, as its noninvasiveness makes it suitable for the study of membrane fluidity regionalization in individual living cells. Two-photon microscopy in combination with the fluorescent probe Laurdan allow us to visualize membrane fluidity. This probe is an analogue of a fatty acid which intercalates among phospholipids homogenously across the lipid bilayer. The technique is able to produce high-resolution images of membrane fluidity distribution in living cells, so that individual membrane domains may be visualized across the plasma membrane. This two-photon microscopy approach can also be used to perform colocalization experiments with certain receptors, combining both, membrane fluidity analysis with the probe Laurdan and membrane receptor staining, to locate the distribution of one receptor in its lipid environment. This colocalization approach, of which no studies have

yet been performed, can result in a very powerful tool for determining receptors distribution in different lipid domains. This approach would allow us to visualize the affinity of the receptor for different lipid phases or domains in living cells.

1.5- Oxidative stress

Oxidative stress is produced when an imbalance between oxidants and antioxidants occurs, favoring oxidants which can finally cause lipid peroxidation. Unsaturated lipids, which are key elements in maintaining membrane fluidity, are the preferential target of oxidative stress. Cells under normal conditions produce oxidants as a product of aerobic metabolism but under certain pathological conditions, the production of oxidants is increased [52]. Cells have several molecules that help to eliminate oxidants such as glutathione, vitamin C and vitamin E, as well as enzymes such as catalase, superoxide dismutase (SOD) and peroxidases [52].
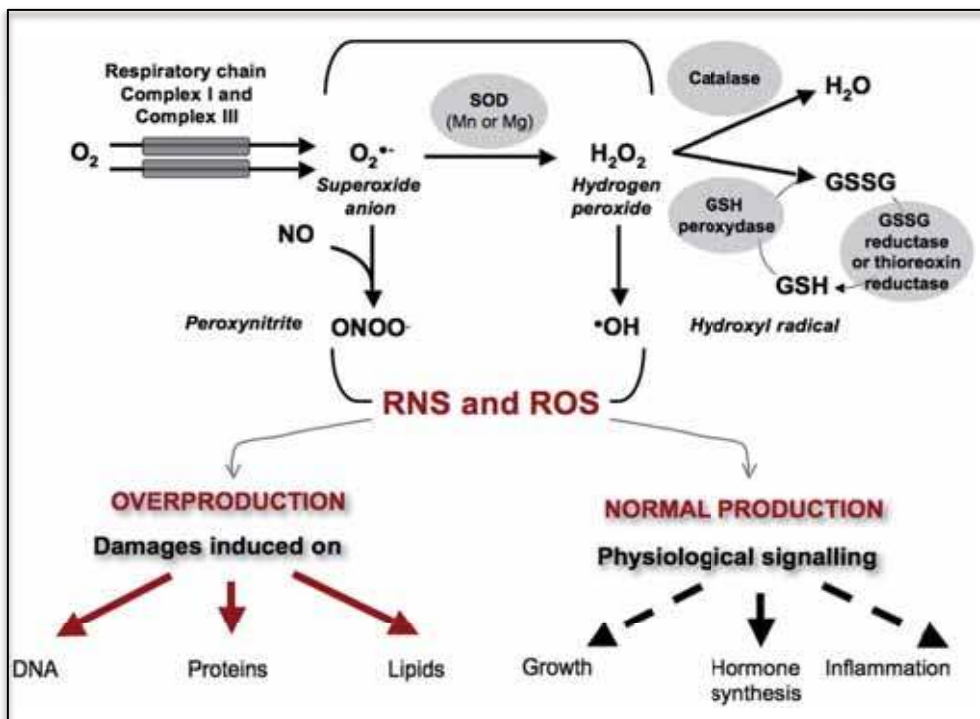
*Figure 4. **ROS and RNS production.** Free radical posses beneficial effects, however an excessive production of these can cause negative effects. Image from N. Bellance (2009) [4].*

Glutathione and vitamin C are particularly important for cells. Glutathione is synthesized by cells and contains a thiol group which acts as a reducing agent, while Vitamin C and E are not synthesized by human cells and therefore must be taken in the diet. Vitamin C neutralizes oxidants by donating an electron to the oxidant inducing the inactivation of these; while Vitamin E, present in the lipid bilayer, reacts with lipid radicals which stop the propagation step during peroxidation [53, 54]. The SOD is one of the enzymes with antioxidant capabilities which is particularly important for cells, catalyzing the dismutation of O_2^- to H_2O_2 [55]. The H_2O_2 produced is not a radical but is a precursor of the hydroxyl radical which is generated by the Fenton reaction [56]. This radical can then be eliminated by glutathione [57].

Although free radicals are potentially harmful for the cell, they can also be beneficial. In phagocytic cells, such as macrophages, free radicals are generated in the phagosome to degradate and eliminate bacterial biomolecules during phagocytosis [58]. Free radicals are generated mainly by two separate systems: *reactive oxygen species* (ROS) and *reactive nitrogen species* (RNS) which is produced by the enzyme nitric oxide synthase (NOS). The NOS enzyme can be present in three isoforms: NOS I, NOS II and NOS III [59] and these isoforms are expressed in a different manner depending on the tissue. NOS I, or neuronal isoform, is constitutively expressed in brain and skeletal muscle tissue. NOS III, or endothial isoform, is constitutively expressed in vascular endothelial cells (NOS III) [59], while NOS II, or inducible isoform, is expressed predominantly in phagocytic cells [60]. The production of ROS, by phagocytic cells, is carried out by the enzyme NADPH oxidase, which converts NADPH into NADP+, producing two electrons and a proton as byproducts. These two electrons are accepted by two oxygen molecules to generate the superoxide anion ($O_2^{\bullet -}$) [61, 62] (Fig. 4).

Under oxidative stress conditions, free radicals target the C=C double bonds present in polyunsaturated lipids and modify their chemical structure; a process termed lipid peroxidation. In the initial stages of lipid peroxidation, a free radical removes a hydrogen atom from the carbon adjacent to a double bond, forming a lipid radical. The polyunsaturated lipid radical generated, reorders its double bonds to form a conjugated diene. In the second stage of lipid peroxidation, the diene reacts with oxygen to give rise to a lipid radical peroxyl. Lipid peroxidation can propagate through the reaction of the radical peroxyl with another polyunsaturated acid, or instead terminate through the reaction of the radical peroxyl with another peroxyl radical (Fig. 5).

Finally, the collective modifications in lipids caused by lipid peroxidation would alter the physical organization of the lipid bilayer leading to damage in living cells.
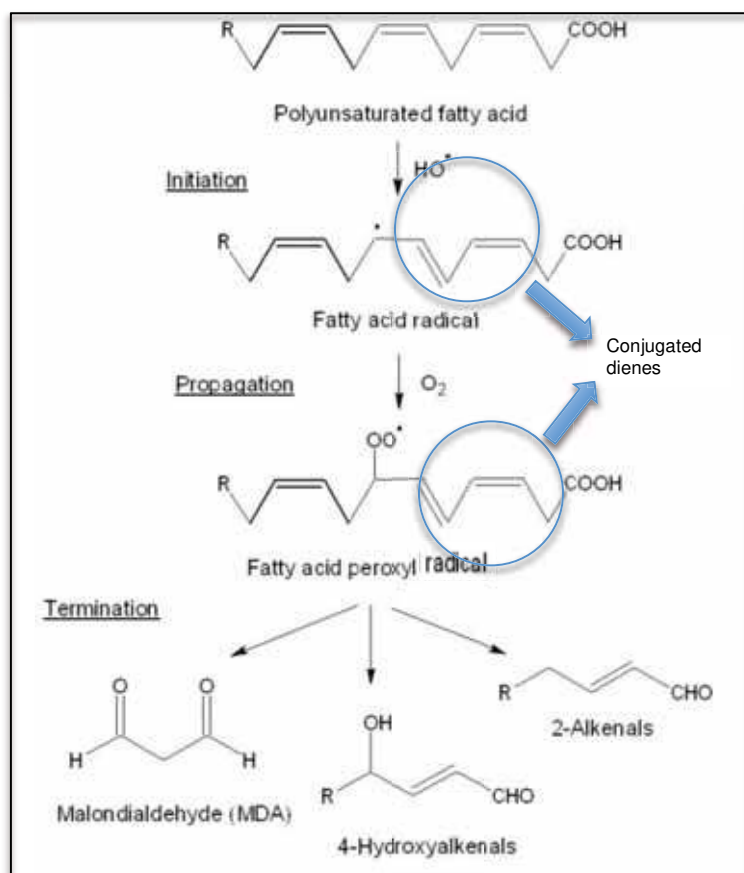
*Figure 5. **Lipid peroxidation**. Three stages of lipid peroxidation: initiation, propagation and termination. Image from N. Mimica-Dukic et al. (2012) [3].*

Several reports [63-65] have shown that cells are constantly under attack by free radicals although little is known about the effects of oxidative modifications of lipids on membrane fluidity and dynamics of living cell membranes.

Lipids are the preferential target of free radicals but proteins can also modified by oxidative stress conditions. Modifications due to oxidative stress have already been studied in several receptors: cholinergic and glutaminergic receptors [66], SNARE receptors important in neurotransmission [67] and epidermal growth factor receptor [68].

The oxidative conditions induce receptor and ligand modifications and may cause an impaired receptor activation. Nevertheless, as lipids are the preferential target of oxidative stress, it also may contribute to the impaired receptor activation through lipid dynamcis modifications in plasma membrane.

1.6- Receptor-ligand interactions in the innate immune system: the macrophage

An efficient interaction between the receptor and its ligand is crucial for biological functions, which incude the immune response. The innate and adaptative immune responses protect the body from invading pathogens. During an infection, the innate immune response is the first line of defense that is able to recognize specific pathogen-associated molecular patterns (PAMPs) present in bacteria, viruses and fungi. These molecular patterns are recognized through specific receptors called pattern recognition receptors (PRRs) which bind to different PAMPs. This PRR-PAMP interaction allows the innate immune system to recognize, engulf and trigger phagocytosis of a wide variety of pathogens. Several PRRs have been described so far: Toll-Like Receptors (TLR), RIG-I-like receptors (RLRs), NOD-like receptors (NLRs) [69].

One of the most relevant members of the PRRs family are the TLRs, which are transmembrane proteins that exist in both plasma membrane and in endosomal membranes. To date, in humans eleven TLRs have been identified which recognize: lipopolysaccharides (LPS), lipoproteins, double-stranded RNA, bacterial flagellin, among others (Fig. 6). During infection of Gram-negative bacteria, LPS present on the bacterial wall is recognized by the TLR2/4. In macrophages, binding of TLR4 to a lipopolysaccharide (LPS) ligand induces the production of proinflammatory cytokines through two different pathways: MyD88 dependent and MyD88 independent pathway. The MyD88 dependent signaling pathway induces cytokines production of several cytokines such as tumor necrosis factor α (TNFα); while, MyD88 independent pathway induces production of type I interferons among others (Fig. 6) [70].
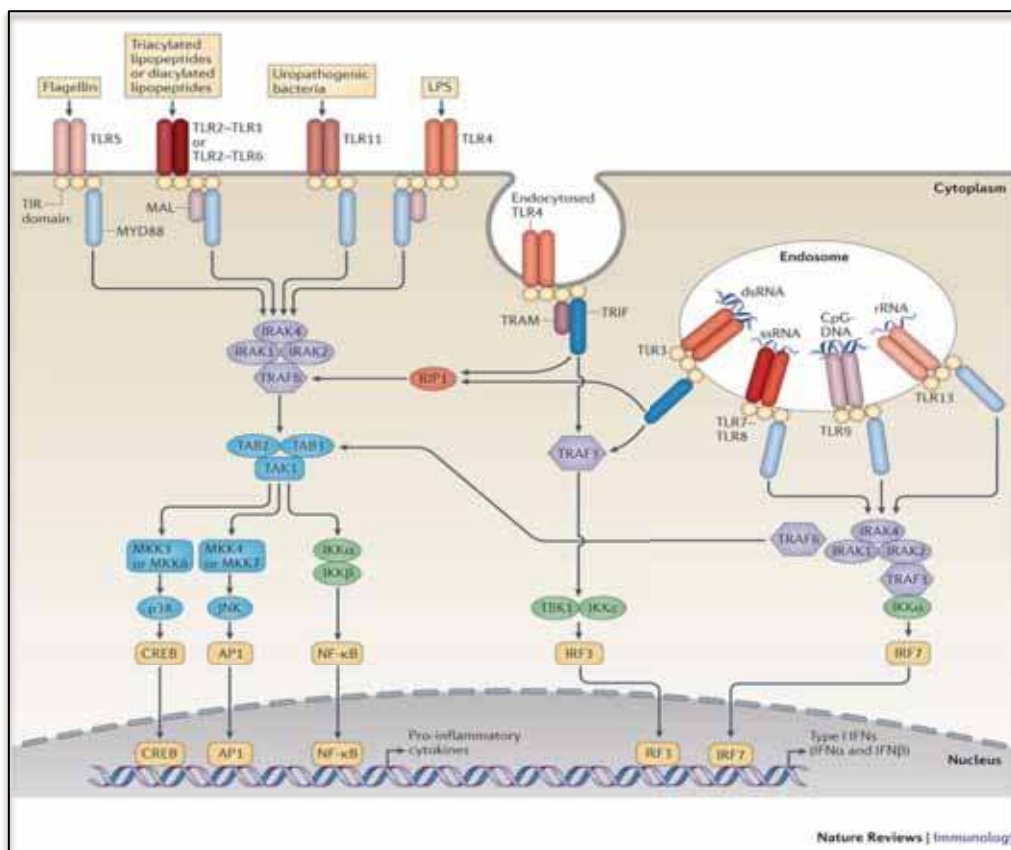
*Figure 6.- **TLRs signalling cascade upon stimulation.** TLRs present in plasma membrane with their specific ligands, present in bacteria or viruses, activate proinflamatory cytokines. Image from L.A. O´Neill et al. (2013) [2].*

As described in section 1.2, membrane fluidity plays an important role in allowing an efficient receptor-ligand binding and in aiding cell signaling. Any modification of the lipid microenvironment of the receptor could lead to an impaired binding, leading to an inefficient signaling. Therefore, as described in section 1.5, oxidative stress can cause lipid modifications that could account for an impaired interaction between TLR2/4 and LPS. If this crucial interaction was not able to occur efficiently, it would cause impaired macrophage phagocytosis and it would inefficiently mount the proinflammatory response and/or inefficiently activate the adaptive response. In turn, this modified membrane fluidity could lead to an altered function of the immune system causing an inefficient elimination of Gram-negative bacteria, as the immune system is not able to detect correctly bacteria through the TLR2/4.

1.7- Receptor-ligand interactions in the adaptive immune system: the lymphocyte

Throughout evolution, animals have developed mechanisms that protect themselves against pathogens by detecting and destroying foreign antigens by mechanisms of the immune system. It is also able to regulate the immune response in mucosa [71] or during pregnancy [72].

The intimate association between mother and embryo in placental mammals creates the potential problem of two genetically distinct individuals having to coexist during pregnancy. This means that during pregnancy, the mother immune system has to be tolerant to the presence of paternal alloantigens from the placenta and/or the fetus [72]. This ability of the immune system to tolerate the fetus relies in a potent immunoregulation that involves the action of many cells including uterine Natural Killer cells (uNKs), decidual Macrophages, uterine Dendritic Cells (uDCs) and T-reg cells. During early pregnancy, the endometrium and the trophoblast induce a large

production of soluble factors: PGE$_2$ and important regulatory cytokines such as TGF-β, IL-4 and IL-10 which favor the immune tolerance towards pregnancy [73].

Among the most abundant cells of the immune system present in the endometrium are the uNK cells, a subpopulation of the systemic natural killer cells (NKs). Before and during early pregnancy, circulating uNK migrate to the uterus by the action of progesterone where they proliferate and contribute to the Th2 cytokine microenvironment [74]. One of the characteristic the uNK cells is that the cytolytic function present in systemic NK cells is absent and they reinforce their cytokine producing ability [75]. Interestingly, invading trophoblast express principally non-classical MHC class I molecules such as HLA-G, HLA-E and HLA-F. The expression of these non-classical MHC molecules would inhibit any uNK cell mediated cytolysis activity and favor the activation of a microenvironment of regulatory cytokines during pregnancy [76].

Decidual macrophages are present in approximately constant numbers during early pregnancy and are mainly located adjacent to the invading trophoblast [77]. These macrophages have the characteristic of secreting anti-inflammatory cytokines such as the IL-10, and they interact with the invading trophoblast to allow preganancy to proceed to term [77]. In normal pregnancy, uterine macrophages develop their phagocytic ability and tissue remodeling, but no pro-inflammatory microenvironment is induced [77]. The presence of trophoblast HLA-G reinforces the inhibition of the pro-inflammatory response of macrophages [78]. However, in dysfunctional pregnancy this situation is reverted.

Other important cells are the uterine DCs (uDC) that during early pregnancy are mostly present in an immature state. These cells become activated by the presence of syncytiotrophoblast microparticles, during trophoblast invasion, and they induce a

limited production of IL-12, IL-18 and TNFα, which in turn activate NK and NKT cells to induce Th2 microenvironment in normal pregnancy. However, in pathological conditions with the presence of oxidative stress in preeclampsia, the syncytiotrophoblast microparticles increase and the microenvironment produced by uDCs is altered favoring a high concentration of IL-18, which induces NK and NKT cells to shift towards a Th1 microenvironment [79].
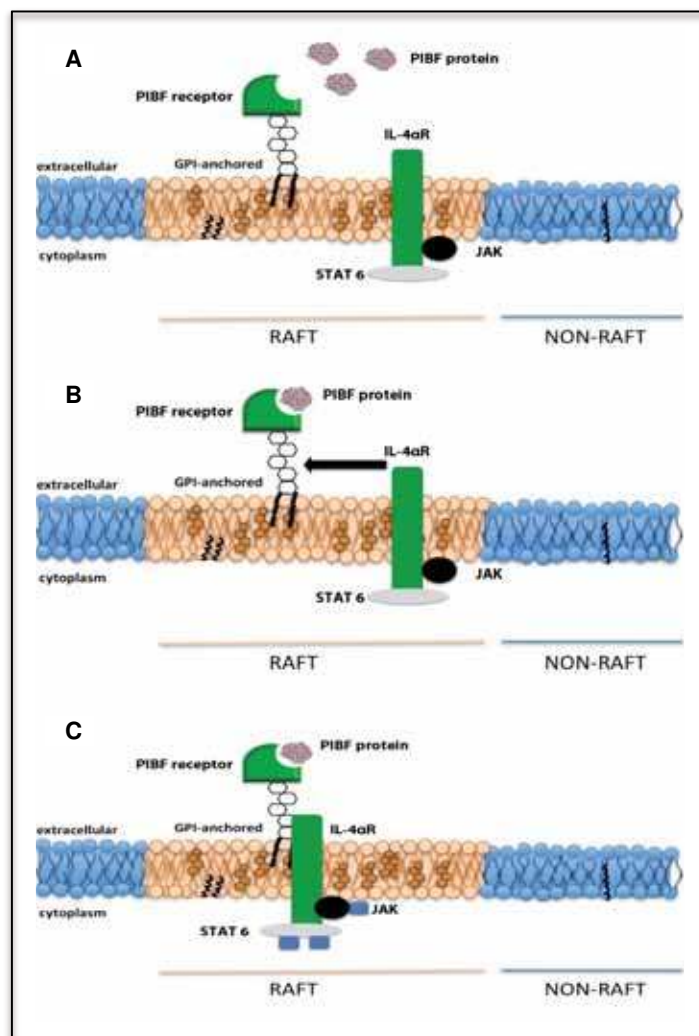
*Figure 7.- **PIBF receptor signaling.** The molecular mechanisms of the PIBF receptor are still under investigation. Studies have shown that PIBF receptor associates with the IL-4α chain [1]. Non-activated PIBF receptor (A) binding to PIBF induces IL-4α chain migration that forms a complex with PIBF-R (B). After PIBF-R/IL-4α association, JAK and STAT6 become phosphorylated (C) which then induces gene activation.*

Most of the T-lymphocytes present during early pregnancy are γδT and Treg cells, both have been shown to play an important regulatory role. Depletion of CD4+ CD25+ (Treg) cells from peripheral blood and decidua are related to pregnancy failure [80]. These Tregs expand in the decidua giving rise to an enriched CD4+ CD25+ FOXP3+ Treg which contributes to a suppressive microenvironment by secreting IL-10 and transforming growth factor-β1 (TGF-β1) [80, 81]. Furthermore, Tregs can also interact with trophoblasts inducing the upregulation of HLA-G [82].

Progesterone is the central hormone for pregnancy, regulating the immune system at several levels: inducing Th2 cytokines, inducing progesterone-induced blocking factor (PIBF), homing of uNK cells to the endometrium and secretion of many factors which allow pregnancy to proceed to term [83]. One of the many immunologic effects of progesterone is mediated by the protein PIBF which induces a Th2 cytokine production by lymphocytes both *in vitro* and *in vivo* [1, 84]. PIBF-R is a member of the glycosylphosphatidylinositol (GPI) anchored receptor family, upon ligand binding, PIBF-R combines with the alpha chain of the IL-4R for signaling [1]. The importance of IL-4αR was experimentally observed by blocking IL-4αR with monoclonal antibodies, which was shown to inhibit the PIBF signaling pathway [1] (Fig. 7).

This interaction PIBF/PIBF-R contributes to the maintenance of pregnancy; it has been reported that women with recurrent miscarriages have significantly lower levels of PIBF in urine and serum [85-88]. Altered membrane fluidity in the PIBF-R microenvironment could modify PIBF binding. This alteration would in turn cause the immune system to not be so efficiently immunoregulated to favour pregnancy.

1.8- Lipid rafts in cells of the immune system

Since lipid rafts have emerged, data are appearing on the role of lipid rafts in cells of the immune system [89-91]. The distribution of several receptors such as the T-

17

cell receptor, B-cell receptor and others within the plasma membrane, and their association with lipid rafts has already been reviewed [89]. Certain receptors in macrophage plasma membrane such as CD14, a GPI-linked protein, reside within lipid rafts [92]. In lymphocytes the coreceptors CD4 and CD8 are also present in lipid rafts [93, 94]. Although there are reports emerging on the distribution and localization of receptors of the immune system, limited data are available on the significance of receptor localization in the plasma membrane domains.

At present, there are few studies on how lipid modifications, caused by oxidative stress, may disturb membrane dynamics or how these alterations could affect normal cellular functions. Although research on receptor modifications due to oxidative stress has been performed, limited studies have shown the importance of membrane dynamics changes on cellular functions, or how oxidative stress can alter lipid structure and then modify the physicochemical state of membrane lipids. Consequently these altered lipids may not be able to act in their prescribed manner which would impair functions. Lipid rafts are thought to allow mechanisms by which the plasma membrane aids cell signaling; upon receptor-ligand interaction lipid rafts are able to cluster into larger domains which favor intracellular signaling.

Plasma membrane lipid peroxidation, membrane fluidity changes and receptor-ligand interactions are important subject of interest to elucidate the role of oxidative stress on cell function. Our aim is to study under oxidative stress conditions how modified plasma membrane lipids of macrophages and lymphocytes could lead to an inefficient receptor-ligand binding leading to an impaired phagocytosis or an immunoregulation failure.

2- Hypothesis

Lipid peroxidation induced by oxidative stress conditions alters membrane fluidity, including lipid raft dynamics. This causes inefficient receptor-ligand binding and may inhibit cell function. This binding is essential for cells of the immune system, although during oxidative stress, recognition of ligand molecules is impaired; moreover, immune response and regulation may be altered. If this hypothesis is true, it can be applied to all kind of cells in our organism and would become a universal event.

3- Aims

Our general aim is to study the effect of oxidative modifications on membrane fluidity in immune cells and on receptor-ligand interactions.

Methodological aim:

To establish a technique able to detect regionalized membrane fluidity changes in single living cells: two-photon microscopy

Specific aims:

1. To evaluate regionalized membrane fluidity changes in macrophages and lymphocytes…

    1.1. under oxidative stress conditions.

    1.2. upon receptor-ligand binding.

    1.3. during receptor-ligand interactions under oxidative stress conditions.

    1.4. related to cell function.

2. To analyze, in living macrophages and lymphocytes, the relationship between lipid peroxidation induced by oxidative stress and membrane fluidity.

3. To assess progesterone-induced blocking factor receptor (PIBF-R) localization in different kinds of membrane lipid domains.

4- Material and methods

4.1- Materials

THP-1 monocytes were obtained from the American Type Culture Collection (ATCC No. TIB- 202, Manassas, VA, USA) and MEC-1 lymphocytes were supplied by Dr. Szekeres-Bartho from the Department of Medical Microbiology and Immunology at Pécs University in Hungary. PIBF conjugated to AlexFluor647 was also supplied by Dr. Szekeres-Bartho.

At Life Technologies (Paisley, UK): RPMI medium 1640 ref. 11835-063, Fetal Bovine Serum (FBS) ref. 10270-106, phosphate buffered saline (PBS) ref. 14190-094, GluMax ref. 35050-038, Laurdan (6-dodecanoyl-2-dimethylamino-naphthalene) ref. D-250, dimethyl sulfoxide (DMSO) ref. D-2650 and C11-BODIPY$^{581/591}$ (4,4-difluoro-5-(4-phenyl-1,3-butadienyl)-4-bora-3a,4a-diaza-s-indacene-3-undecanoic acid) ref. D-3861 was purchased.

At Sigma-Aldrich: Hydrogen peroxide (H_2O_2) ref. H-1009, phorbol 12-myristate 13-acetate (PMA) (P8139-5MG), 2,2´-azobis (2-amidinopropane) dihydrochloride (AAPH) ref. 440914-25G and Escherichia coli lipopolysaccharide (LPS) ref. L-4391 was purchased.

The phospholipid dipalmitoylphosphatidylcholine was purchased at Avanti Polar Lipids (Alabaster, AL) ref. 850355-C. 35mm MatTek glass bottom dishes for the two-photon microscope were purchased from MatTek Corporation in Ashland, MA ref. P350-1.5-14-C. Sterile 96 well plates were purchased from NUNC (Nunc A/S, Kamstrupvej, Denmark) ref. 167008. TNFα kit (BD™ Cytometric Bead Array (CBA), BD) was purchased from Becton Dickinsons (San Diego, CA, USA) ref. 558264 and the

cell viability MTT (3-[4,5-dimethylthiazol-2-yl]-2,5-diphenyltetrazolium bromide) was purschased from Biomedica Gruppe (EZ4U Cell Proliferation Assay, Biomedica Gruppe, Wein, Austria) ref. BI-5000 kit.

Membrane fluidity was analyzed with a two-photon confocal microscope Leica TCS-SP5 (Leica Microsystems, Heidelberg GmbH) at the Servei de Microscòpia (UAB). MTT assay was evaluated with a spectrofluoremeter (Victor3, Perkin-Elmer) at the Servei de Cultius Cel·lulars, Producció d'Anticossos i Citometria (SCAC), UAB. Cells were maintained and treated in sterile conditions with the cell line sterile cabin BHA 48 (Faster). All cellular centrifugations were performed with a Heraeus Multifuge 3SR+ (Thermo Scientific). The TNFα cytometric assay was analyzed in a BD FACS Canto cytometer (BD Biosciences, San José, California).

4.2- Preparative methods

4.2.1- Cellular samples

4.2.1.1- THP-1 monocyte cell line

THP-1 monocyte cells were induced to macrophages for our study. The human monocytic cell line THP-1 was cultured in RPMI medium 1640 containing 10% FBS, GlutaMax and in the absence of phenol red. THP-1 monocytes were maintained at 37°C in 5% CO_2. All experiments were performed within cell passages 20-50. THP-1 monocytes were induced to macrophages with PMA.

4.2.1.1.1- Induction of THP-1 monocyte to macrophages

THP-1 induction was performed to achieve an optimal cellular density (less 50% confluent) to minimize cell-to-cell contact, because this contact increases membrane rigidity as described by Gaus [43]. 1 ml of THP-1 monocytes were induced to macrophages in 35mm MatTek glass bottom dishes at 4×10^5 cells/plate for 72h at 37°C

and 5% CO_2, in the presence of 0.16μM phorbol 12-myristate 13-acetate (PMA). In our study the optimal cellular concentration was $4x10^5$ cells/plate.

4.2.1.2- MEC-1 lymphocyte cell line

MEC-1 lymphocyte cell line were established and characterized from peripheral blood of a patient with B-chronic lymphocytic leukemia [95]. These cells were cultured in RPMI medium 1640 containing 10% FBS, GlutaMax and in the absence phenol red. Cells were maintained at 37^oC in 5% CO_2. All experiments were performed within the cell passages 20-50.

4.2.2- Study of cell viability and evaluation of the suitable oxidative stress conditions for membrane fluidity studies

To evaluate changes in membrane fluidity due to oxidative stress, the optimal H_2O_2 concentration that induced oxidative stress without decreasing cell viability below 75% was initially determined. The MTT assay was then used to analyze cell viability.

The MTT assay is a colorimetric assay that measures the reduction of MTT to formazan (1-(4,5-dimethyl-thiazol-2-yl)-3,5-diphenylformazan) by mitochondrial activity to evaluate cellular viability. The yellow MTT compound is converted to the red compound formazan in living cells, by mitochondrial dehydrogenase catalysis of the reaction, in functional mitochondria. Dead cells do not have functional mitochondria; therefore the catalysis of MTT to formazan cannot occur. This in turn is reflected by a difference in the colour between living cells and dead cells.

The change in colour which reflects cell viability was assessed using a multi-well spectrofluorometer: MTT absorbance was measured at 450nm, while the absorbance at 620nm was used as a reference value to correct the background values, mainly caused by cellular debris.

After determining the H_2O_2 concentration range that induces oxidative stress without affecting cell viability below 75%, for both macrophages and lymphocytes, cells were incubated with H_2O_2 up to 2.0mM and membrane fluidity was evaluated as described in section 4.3.

4.2.2.1- Oxidative stress conditions for THP-1 macrophages

Macrophages were induced at 5×10^5 cells/ml in 96 micro well plates for viability analysis, each well containing 1.25×10^5 cells. After the macrophage induction described in section 4.2.1.1.1, cells were washed three times with PBS. 0.1 to 10mM H_2O_2 in fresh medium without FBS was added to the cells. After 24h at 37^oC and 5% CO_2 cells were washed and viability was assessed by MTT assay. The MTT assay showed that the H_2O_2 concentrations range suitable for our study ranged from 0.5mM to 2mM, which maintained cell viability above 75%.

4.2.2.2- Oxidative stress conditions in MEC-1 lymphocytes

MEC-1 lymphocytes at 5×10^5 cells/ml were placed in each well of 96 micro well plates for viability analysis, each well containing 1.25×10^5 cells. Lymphocytes were then centrifuged at 300×g for 5min and washed three times with PBS. 0.1mM to 10mM H_2O_2 in fresh medium without FBS was added to cells. After 2h at 37^oC and 5% CO_2 cells were centrifuged, washed and viability was assessed by MTT assay. The MTT assay showed that the H_2O_2 concentrations suitable for our study ranged from 0.5mM to 2mM, which maintained cell viability above 75%.

4.2.3- Evaluation of lipid peroxidation

Lipid peroxidation was evaluated in membranes of macrophages and lymphocytes by using C11-BODIPY[581/591], a fluorescent fatty acid analogue which

incorporates into membranes. Upon oxidation, both the excitation and emission fluorescence spectra of the dye shift to shorter wavelengths [96, 97].
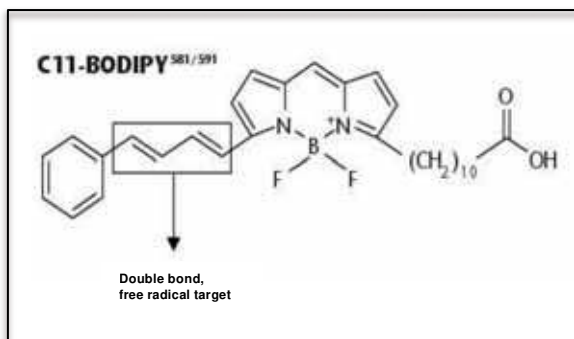
*Figure 8. **C11-BODIPY$^{581/591}$**. Chemical structure of the fluorescent probe C11-BODIPY$^{581/591}$.*

4.2.3.1- Lipid peroxidation in THP-1 macrophages and lymphocytes

A 2mM stock solution of C11-BODIPY$^{581/591}$ was prepared by dissolving the probe in DMSO which was then stored at −20ºC in the dark. For both cell types, 200µl of THP-1 monocytes or MEC-1 lymphocytes at $1×10^6$cells/ml were seeded in each well of 96-microwell plates for probe incorporation. THP-1 monocytes were initially induced to macrophages as described previously in section 4.2.1.1.1 before analysis of lipid peroxidation. To stain cells, macrophages and lymphocytes were centrifuged in the 96-microwell plates, washed three times with PBS and stained in medium without FBS at a final concentration of 10µM C11-BODIPY$^{581/591}$ for 45min at 37ºC and 5% CO_2. After BODIPY incubation, both cell types were centrifuged and washed three times with PBS. H_2O_2 was then added to a final concentration ranging from 0.25mM to 5mM, and cells were incubated for 24h for macrophages and 2h for lymphocytes, at 37ºC. Control macrophages and lymphocytes were incubated in the same conditions without H_2O_2. A multi-well spectrofluorometer was used to measure the emissions corresponding to the oxidized (green fluorescence: $\lambda_{excitation}$, 488nm; $\lambda_{emission}$, 520nm) and non-oxidized (red

fluorescence: $\lambda_{excitation}$, 545nm; $\lambda_{emission}$, 590nm) states of the probe. Oxidation of C11-BODIPY[581/591] was estimated by calculating the ratio between green fluorescence (oxidized) and total fluorescence (oxidized plus non oxidized), to normalize for probe uptake and distribution into cellular membranes [98].

Lipid peroxidation induced by H_2O_2 was compared to the effect of the free radical initiator AAPH. To assess the azo compound oxidizing effect, 5mM AAPH solution in medium without FBS was added to both macrophages and lymphocytes loaded with C11-BODIPY[581/591], as described above, in 96-well plates. The plates were incubated for 2h at 37ºC.

4.2.4- Determination of receptor-ligand interactions under oxidative stress conditions

In this section two receptor-ligand interactions were studied: binding of LPS to the TLR2/4 receptor in macrophages and binding of PIBF to its receptor in lymphocytes.

4.2.4.1- Binding of LPS to TLR4 in macrophages

To evaluate the possible effect of oxidative stress on macrophage function, we quantified TNFα cytokine production in LPS activated macrophages.

After monocyte-macrophage induction, fresh medium with serum was added to the cells and incubated for 24h. THP-1 macrophages were then simultaneously activated with LPS (1µg/ml) and H_2O_2 at 0.5, 1 and 2mM, for 24h. After incubation, the supernatant was removed to evaluate TNFα production by the Human Inflammation Cytometric Bead Array (CBA) kit. TNFα in supernatant was quantified by flow cytometry as described in the manufacturer instructions.

The remaining THP-1 macrophages were then washed three times with PBS to eliminate excess LPS and H_2O_2, and macrophages were stained with Laurdan, as

described in section 4.3.2.2 to evaluate membrane fluidity in the two-photon confocal microscope (Leica Microsystems, Heidelberg GmbH), at the Servei de Microscòpia (UAB).

4.2.4.2- Binding of PIBF to PIBF-R in MEC-1 lymphocyte cell line

To evaluate the possible effect of oxidative stress on PIBF-R function, we analyzed the distribution of PIBF/PIBF-R in MEC-1 lymphocytes. Soluble PIBF conjugated to the AlexaFluor647 fluorochrome was used to obtain confocal images of PIBF bound to its receptor. PIBF/PIBF-R distribution was obtained through the superposition of membrane fluidity GP images, obtained at the two-photon microscope, and PIBF receptor images, obtained at the conventional confocal microscope.

MEC-1 lymphocytes were incubated 2h with 0.5, 1 and 2mM H_2O_2. Cells were then washed and incubated with soluble PIBF-AlexaFluor647. 1.25µg of fluorescent ligand, in 50µl of PBS, was added to the 2×10^6 cell pellet and it was incubated for 1h at 37^oC. Membrane fluidity GP images from lymphocyte membranes, obtained by the two-photon microscopy, and PIBF receptor fluorescence images, obtained by conventional confocal microscopy, were consecutively acquired for comparison. PIBF receptor distribution in the lymphocyte membranes was then analyzed by co-localizing PIBF bound to its receptor in the different lipid phases of plasma membrane.

4.3- Analytical methods

4.3.1- Evaluation of membrane fluidity by two-photon confocal microscopy

Several imaging methods are presently used for investigating cell membrane lipid dynamics as recently reviewed [42, 99, 100]. Many of these techniques use fluorescent dyes sensitive to the packing of its lipid microenvironment, thus allowing to analyze membrane fluidity [101]. One of the more suitable fluorescent probes to study

the regionalization of membrane fluidity is Laurdan, which exhibits an emission spectral maximum shift from 440nm to 490nm in the transition from a gel phase to a liquid phase [102, 103]. By using a multiphoton confocal microscope it is possible to excite the fluorophore with two photons at double the wavelength causing it to fluoresce. This technique, known as two-photon confocal microscopy, allows obtaining high resolution images of Laurdan-stained single living cells, which enables visualizing the distribution of membrane fluidity in different domains within the plasma membrane [102-108].
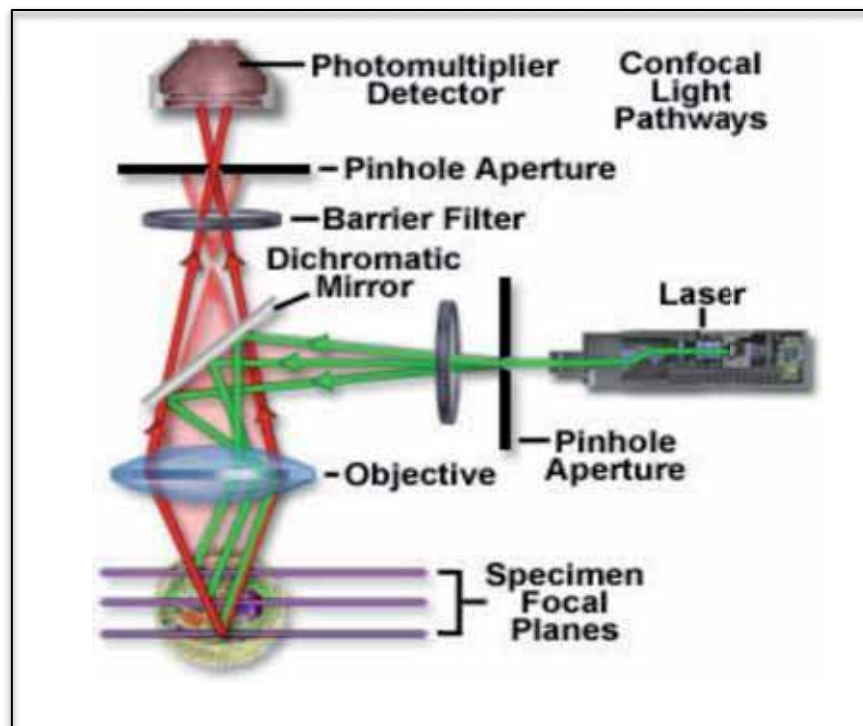
*Figure 9. **Confocal microscope configuration**. (www.olympusfluoview.com)*

Confocal microscopy (Fig. 9) is an optical technique which produces high resolution images. The sample is entirely excited with a light source and the fluorescence is detected by the photo-detector and camera. Confocal microscopy uses point illumination and a pinhole in an optically conjugated plane in front of the detector, this eliminates out of focus fluorescence producing images of better resolution and depth compared to wide-field microscopes [109].

28

4.3.2- Two-photon fundamentals:

Two-photon is a technique developed for confocal microscopes which excites the fluorophore with two simultaneous photons whereas conventional one photon techniques excite the fluorophore with only one photon. These two photons are usually in the ultraviolet or blue/red spectral range. This excitation of the probe involves the sum of the energies of both photons. The fluorophore excited by one photon at a wavelength, l, receives 100% of the energy to emit light, while two-photon at twice the wavelength, 2l, also produce 100% of the energy needed. This is because one photon at double the wavelength only carries about 50% of the energy needed for the excitation [110].
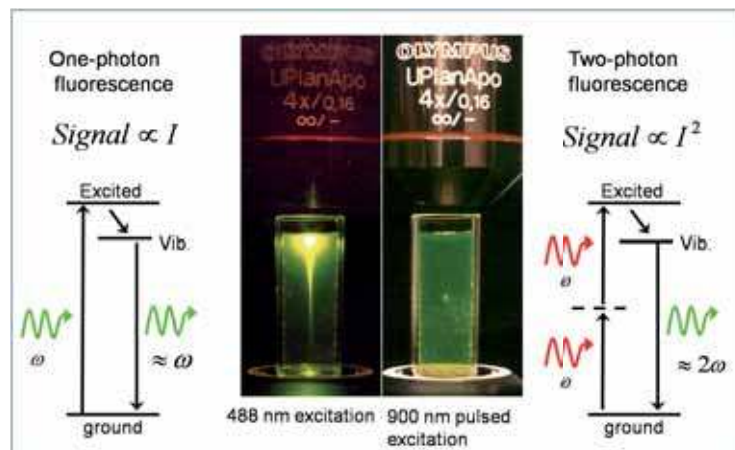
*Figure 10. **Two-photon microscopy**. One-photon confocal microscope excitation compared to a two-photon excitation. (http://cleoqels2010.blogspot.com.es/2010/05/expo-idea-generation-and-multiphoton.html)*

Membrane fluidity was evaluated with a multiphoton scanning confocal microscope after THP-1 macrophages and MEC-1 lymphocytes were stained with Laurdan. For macrophages or lym8phocytes a ×63 objective lenses oil inmersion and a 1.4 numerical aperture was used. Images were obtained at a resolution of 512 × 512 pixels and at a scan speed of 400Hz with LEICA LAS AF software. After fluorescence excitation with the multiphoton laser at 800nm, the two-photon microscope captures

two simultaneous emission images, with wavelengths ranging from 400-460nm and 470-530nm.

Emission intensities from every image pixel were introduced into the generalized polarization (GP) equation 1 providing a final GP value, which is a measure of membrane fluidity:

$$GP = \frac{I_{(400-460)} - G \times I_{(470-530)}}{I_{(400-460)} + G \times I_{(470-530)}} \qquad \textit{Equation 1}$$

where G is a correction factor for the microscope being used, which was calculated by using equation 2:

$$G = \frac{GP_{theo} + GP_{theo} \times GP_{exp} - 1 - GP_{exp}}{GP_{theo} \times GP_{exp} - GP_{theo} + GP_{exp} - 1} \qquad \textit{Equation 2}$$

where GP_{theo} is the GP theoretical value of a standard solution of 5μM Laurdan in DMSO, which has a known value ($GP_{theo} = 0.207$), whereas GP_{exp} is the GP value of the same solution measured in our confocal microscope [111]. GP values range from −1, corresponding to the highest fluidity, to +1 for the lowest fluidity [26].

4.3.2.1- Standardization of two-photon microscopy with DPPC liposomes

Before performing the analysis of membrane fluidity distribution in cell plasma membranes, the technique two-photon microscopy was standardized in our laboratory by using suitable model membranes, i.e. liposomes, stained with Laurdan. Changing the temperature of these liposomes it allows obtaining microscope images of the drastic

fluidity changes produced in the bilayers throughout the transition from the gel phase to the liquid-crystalline phase.

For the standardization of two-photon microscopy, liposomes were placed on MatTek plates with a cover slip to prevent liposome movement. Liposomes were placed in the two-photon confocal microscope which was then calibrated. For the calibration: first the two-photon microscope sample chamber was heated to 30ºC and the photodetector in channel 1 (at 440nm) was set to maximum detection. Then the chamber containing the liposomes was heated to 50ºC and channel 2 (490nm) was set to maximum detection.

After calibration, images of DPPC liposomes were obtained to validate our calibration with previous references. DPPC liposomes were heated to temperatures ranging from 30ºC to 50ºC and images were obtained. These images were then converted to Generalised Polarisation (GP) images and GP histograms for comparison. After validating our technique with liposomes, two-photon microscopy was adapted for living cells.

4.3.2.2- Laurdan-staining of macrophage and lymphocyte membranes

To evaluate membrane fluidity, THP-1 macrophages and MEC-1 lymphocytes were stained with the fluorescent probe Laurdan and analyzed by two-photon microscopy. Laurdan was dissolved to a concentration of 2mM in DMSO and stored at -20°C at the dark. For membrane labeling, cells were incubated in medium without FBS at a final concentration of 5µM Laurdan for 30-60min at 37°C and 5% CO_2 with agitation. In the Laurdan-stained cells the final concentration of DMSO was less than 0.25% (v/v).

4.3.2.3- Image analysis

A WiT 8.3 imaging software (Dalsa Digital Imaging, Canada) was used and adapted for the image processing to obtain a GP value for each pixel. Images obtained from the confocal microscope were all analyzed in floating point format and converted to 8-bit unsigned format [26]. Then, images were processed with a custom made sub-program generated by WiT 8.3 imaging software. Background values were set to zero: equation 1 denominator was converted to a binary image with background values set to zero and nonbackground values set to one, then the binary image was multiplied by the GP image [107]. To obtain the colored GP images, the black and white GP images were then pseudo colored by means of Adobe Photoshop 7.0 by an arbitrary color palette (Fig. 11). The blue spectrum of the colour palette represents fluid phases while the red spectrum represents rigid phases. GP distributions were obtained from the histograms of the GP images.

*Figure 11. **GP arbitrary colour pallete**. GP value are assigned a colour which corresponds to their value, which range from −1 to +1.*

4.4- Statistics

Statistical analyses were performed by using SigmaPlot for Windows 11.0 (Systat Software, Inc.). The sample size, n, was 70 to 94 in macrophages and lymphocytes. Comparisons between control and oxidation treatments were performed by one-way analysis of variance based on ranks (Kruskal-Wallis) followed by post-hoc Dunn's test. Statistical significance was set at $p < 0.05$.

5- Results

5.1- Methodological results

5.1.1- Optimization of two-photon microscopy with model membranes

To perform our studies on membrane fluidity by means of two-photon microscopy and the fluorescent probe Laurdan, we initially standardized the technique. The standardization was performed by using one type of liposome, giant unilamellar vesicles (GUVs) made of the phospholipid dipalmitoylphosphatidylcholine (DPPC), as model membranes (for GUV preparation, see Annex I). GUVs were used as a well established model membrane for microscopy studies, taking advantage of its very slow brownian movement. DPPC is one of the most well known phospholipids available: its membrane fluidity and phase behavior has been described by means of a great deal of techniques [112-114], including two-photon microscopy [115].

One of the characteristics of the fluorescent probe Laurdan, which allows membrane fluidity analysis, is its simultaneous fluorescence emission in two bands centered near 440nm and near 490nm. When Laurdan molecules incorporate into the lipid bilayer they emit fluorescence in both 440nm and 490nm wavelengths. The intensity ratio depends on the motion of the lipid microenvironment in which the probe is present. In DPPC liposomes, when the probe movement is constrained in a tightly packed bilayer (gel phase at low temperature) the 440nm channel is favored and higher relative fluorescence intensity is obtained for this band. However, when the probe is freely moving (fluid phase at high temperature), the 490nm channel is favored. The relative values of both emission intensities images are measured and introduced into a mathematical formula, called generalized polarization (GP). This provides a final GP value, which is a measure of membrane fluidity.

For a better understanding of the probe emission, we initially determined the fluorescent emission spectrum of Laurdan both in fluid and rigid liposomes. Figure 12 shows the fluorescence emission spectra, obtained with a two-photon microscope, of Laurdan stained giant liposomes at different temperatures. At 30ºC, which corresponds to the DPPC gel phase, Laurdan has higher fluorescence intensity, at the 440nm peak, when compared to liposomes in the fluid phase, at 50ºC. The peak at 490nm has higher fluorescence intensity in DPPC liposomes at 50ºC if compared to 30ºC liposomes. These differences in emission intensities, between 440nm and 490nm, will allow us to discriminate rigid and fluid regions in more complex biological membranes.
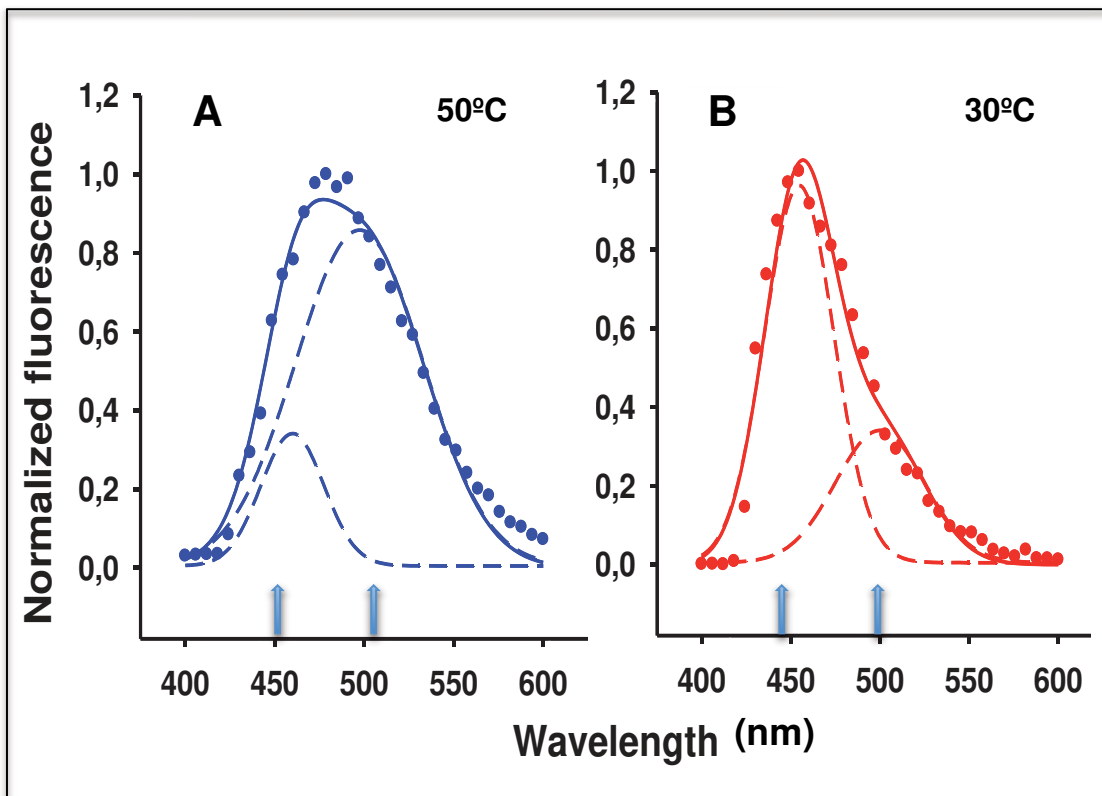
*Figure 12. **Laurdan emission spectra in fluid phase (50ºC) and in gel phase (30ºC) of DPPC.** Fluorescence intensities of Laurdan stained DPPC liposomes were normalized to show the maximum intensity as the value 1. Normalized fluorescence emission intensity of DPPC GUVs stained with 5μM Laurdan in PBS, at 50ºC in A and 30ºC in B, as a function of wavelength. Laurdan stained DPPC liposome fluorescent images were converted to histograms and normalized. Dots represent the normalized fluorescence intensities of DPPC liposomes at 50ºC and 30ºC. Excitation was done at 800nm. Dashed lines represent the best fitting of two gaussian functions, corresponding to the two emission bands. The experimental points and continuous lines represent the sum of the two theoretical gaussian curves.*

Membrane fluidity of DPPC liposomes was analyzed at the fluid phase, at the transition temperature and at the gel phase, to validate the technique in our laboratory. Laurdan stained DPPC liposomes were placed in the two-photon microscope and heated to 30ºC; at this temperature the channel which records the fluorescent image at 440nm was set to the maximum detection. Then the liposomes were heated again up to 50°C; in this case the channel at 490nm was set the maximum detection. After setting the photodetectors to maximum, DPPC liposomes were analyzed at different temperatures, corresponding to the different phases.

Two-photon microscopy was used in order to follow the drastic fluidity changes produced in the bilayers throughout the gel to liquid-crystalline phase transition. Figure 13A–C shows the Laurdan generalized polarization (GP) images of DPPC GUVs at temperatures corresponding to the fluid phase at 50°C (A), to the phase transition temperature at 42°C (B) and to the gel phase at 30°C (C). GP images (A–C) were pseudocolored with an arbitrary color palette (D), the pseudocolored GP images show very fluid lipid domains (GP value −1) in purple color and very rigid domains (GP value +1) in red color. Coherently, liquid crystalline phase liposome (A) appears with predominant blue color, the liposome near the phase transition temperature is shown in yellow-green color (B), and the gel phase liposome (C) shows orange-red color. GP images were transformed to GP distribution graphs (E) to evaluate liposome membrane fluidity distribution at each temperature.

The coincidence of our results, shown in figure 13, with those obtained in the literature [112-114] validates the standardization of the technique two-photon microscopy in our laboratory. Nevertheless, as this was the first time this technique was to be used in the *Servei de Microscòpia* of our University we performed an in-depth and comprehensive standardization by evaluating the full transition phase curve of DPPC by

the technique. By using the maximum GP values obtained from the GP distribution curves shown in figure 13E, we compared these maximum GP frequencies and plotted them at different temperatures, ranging from 30°C to 50°C, to generate a phase transition graph of DPPC liposomes. As it can be observed in figure 14, the *S*-shaped GP *versus* temperature plot describes the DPPC gel to liquid-crystalline phase transition
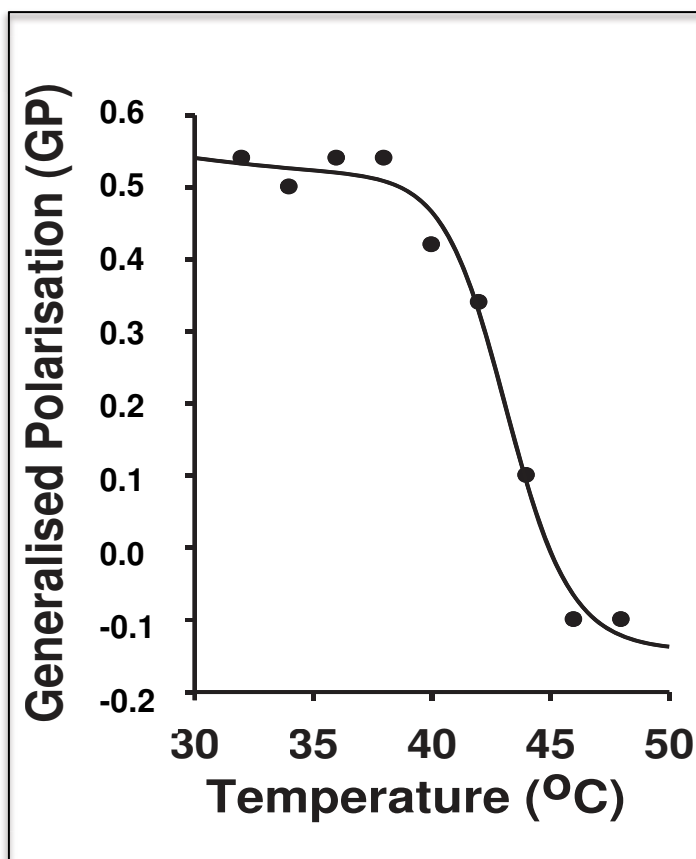
Figure 14. ***Phase transition of DPPC liposomes.*** *Temperature dependence of GP maxima for DPPC GUVs: dots represent the experimental GP peak values of GP histograms at different temperatures (from 30°C to 50°C). The continuous line respresents the best fitting to the experimental data.*

curve. This kind of curves are characterized by a phase transition temperature (T_m), which is the temperature at which half of the phospholipid molecules have yet "transited" to the fluid phase whereas the other half still remains in the rigid, gel phase. We found for our transition curve a T_m value near 43°C, which fits well in the narrow range of 41-43°C expected for DPPC liposomes [112-114].

Once two-photon microscopy has been validated in our laboratory for DPPC liposomes, several modifications were still needed for studies in living cells: macrophages and lymphocytes, as described in the following paragraphs.
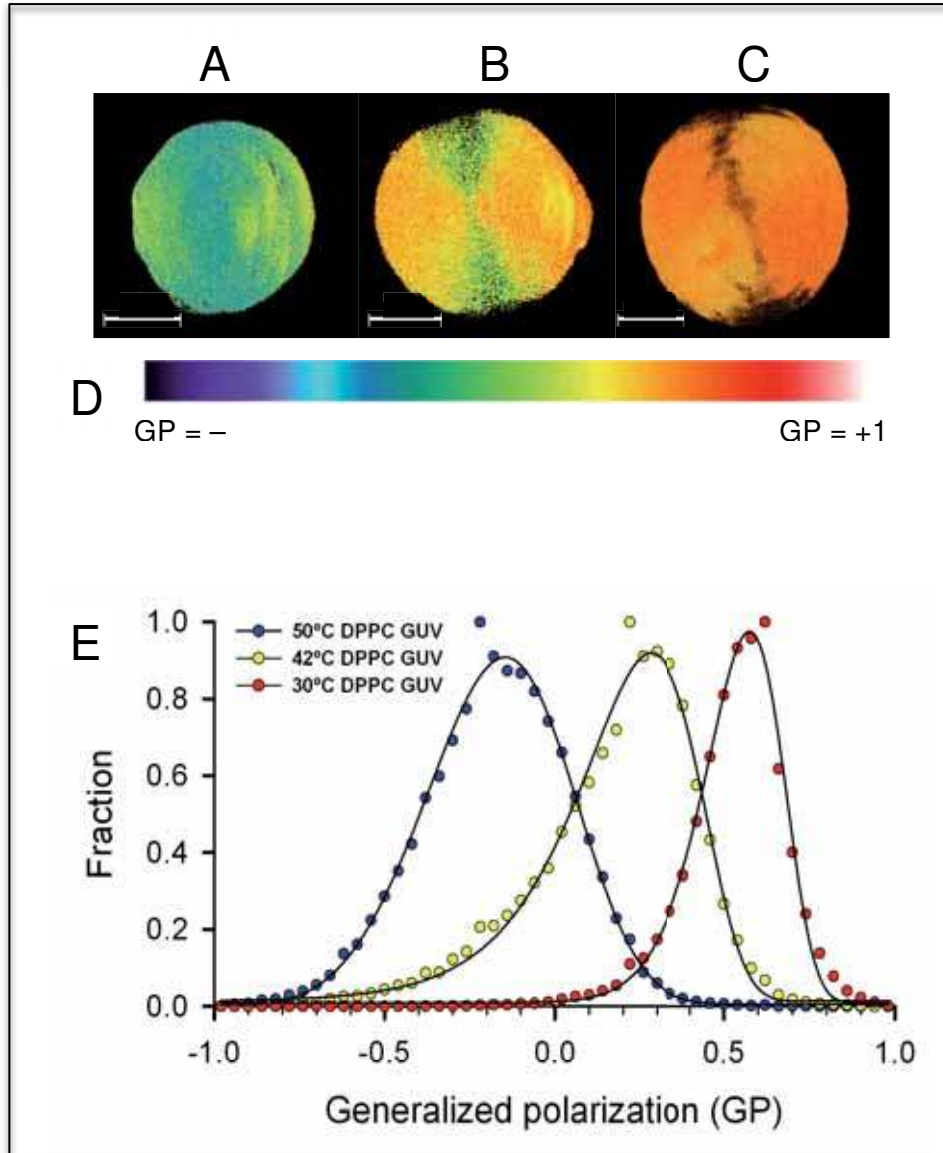
*Figure 13. **Frequency distribution of DPPC.** Validation of the technique two-photon microscopy with Laurdan-labeled DPPC GUVs: GP images of DPPC giant unilamellar vesicles (GUVs) stained with 5μM Laurdan, in PBS at 50°C, fluid phase (A), 42°C, near the gel to liquid phase transition (B) and 30°C, gel phase (C). Scale bar, 10μm. GP images were pseudocolored with an arbitrary color palette (D). Experimental (dots) and fitted (continuous lines) normalized GP frequency distribution curves (E) corresponding to the three images presented in (A–C). GP values range from −1 to +1, −1 being very fluid lipid domains and +1 very rigid lipid domains. For the fitting procedure we have used Gaussian or Weibul functions for asymmetric curves.*

5.1.2- Optimization of two photon microscopy with living cell samples

After standardization of the technique with liposomes, we applied the same conditions to the study of cellular plasma membrane. When these conditions were applied to macrophages, it was observed a significant decreased fluorescence emission of Laurdan in the two-photon microscope. We hypothesized that the serum present in the staining medium of cells was causing this decrease. This hypothesis arose because the serum was the main difference in the staining protocol when compared to DPPC liposomes. To ascertain our hypothesis and solve this problem, THP-1 macrophages
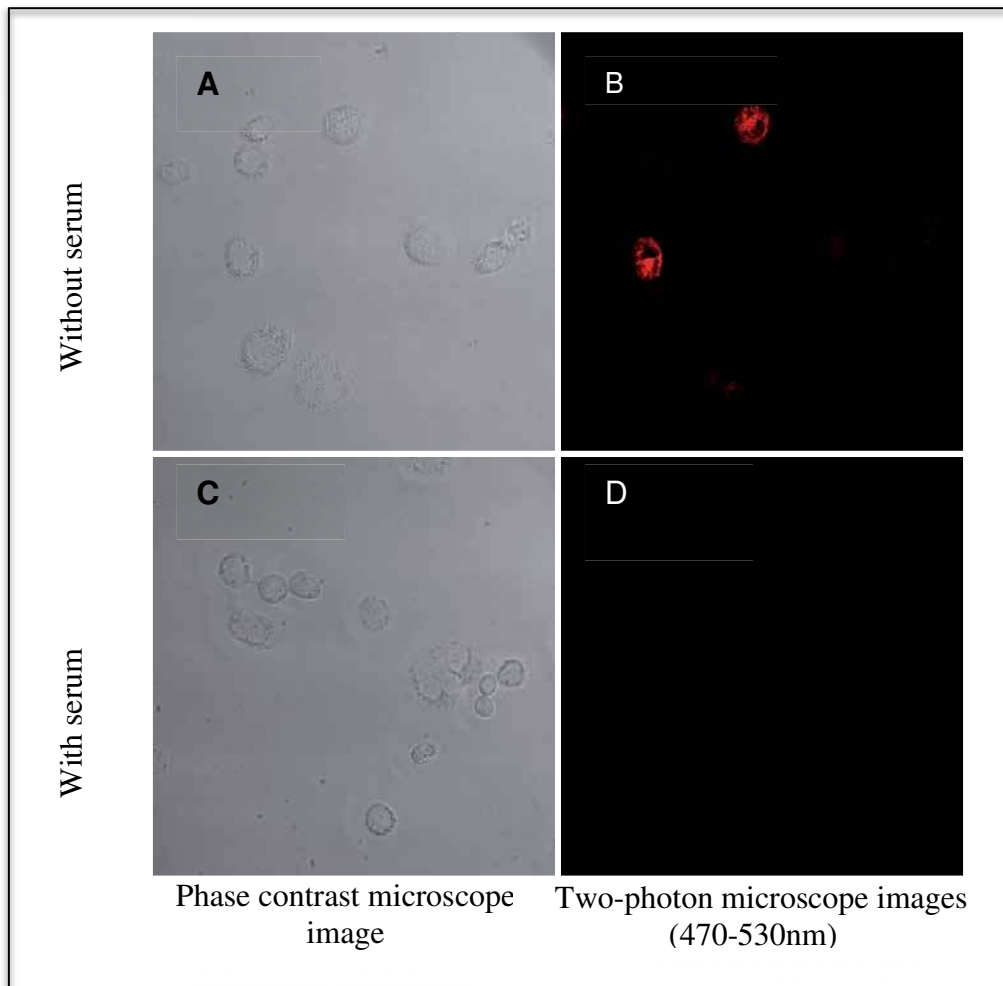
*Figure 15. **Effect of Laurdan staining medium.** Differences in Laurdan fluorescence emission intensity of macrophages were observed depending on the suspension medium used in the staining process. A and C show the corresponding light transmission images of each sample. Two-photon microscope fluorescent images were obtained through channel 2 (490nm) from Laurdan stained macrophages in with RPMI 1640 medium without bovine serum (B) and in medium with 10% serum (D).*

were stained with Laurdan in medium without serum instead of the standard medium, containing 10% bovine serum. In figure 15 phase contrast microscope images (A & C) and the two-photon microscope image of macrophages (B & D) are shown: in medium without serum (A & B), the appropriate fluorescence emission intensity at 490nm is observed, whereas macrophages in medium with 10% serum (C & D) did not produce any fluorescence. The red color observed in the image does not reflect any membrane fluidity values; instead it is an arbitrary color showing raw probe fluorescence intensity.
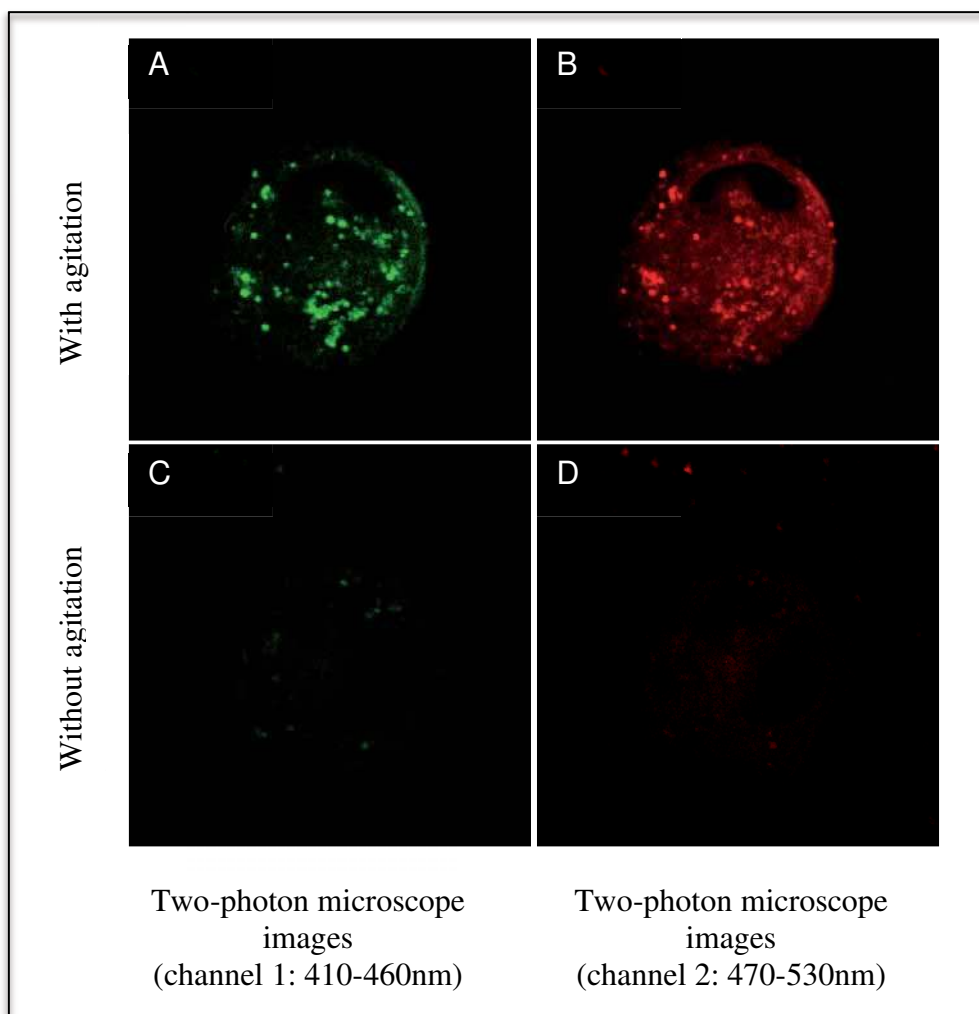
*Figure 16. **Effect of agitation.** Macrophages were stained with Laurdan in medium without serum and under gentle agitation. Two-photon microscope fluorescent images were then obtained at both, channel 1 at 440nm (A and C) and channel 2 at 490nm (B and D). Images obtained of macrophages stained with agitation are shown in A and B, while macrophages stained without agitation are shown in C and D.*

The images obtained from channels 1 and 2 are the used in order to obtain membrane fluidity value as described in section 4.3.2.

During our staining procedure, it was also observed that a gentle agitation of the Laurdan made a dramatic increase of the fluorescence intensity efficiency. As described section 4.3.2.2, cells were stained for 1h with Laurdan; this incubation was carried out under gentle agitation. Figure 16 shows the difference in fluorescence obtained by the introduction of a gentle agitation in the staining procedure. As it can be seen, fluorescent Laurdan stained macrophages increased as a gentle agitation was applied during the staining. We obtained the raw fluorescence intensity images from channels 1 and 2 in Laurdan stained macrophages under gentle agitation or without.

Thus, the introduction of these two optimization changes, the staining without serum and applying gentle agitating, in the Laurdan staining procedure of living cell samples, increased dramatically the fluorescence of cells. A few minor adjustments were also performed for an ideal acquisition of images by two-photon microscopy.

5.1.2.1- Optimization of the confocal microscopy parameters

THP-1 macrophages adhered to the bottom of the plate, which has been previously described [116] to rigidify the plasma membrane in contact with the base of the plate. Therefore, we used macrophages as samples in order to optimize the different experimental parameters implicated in two-photon image acquisition.

To analyze in depth this artifact in macrophage membrane fluidity due to cellular adherence, we recreated a 3D image of Laurdan stained macrophages to view the membrane fluidity across the whole cell and select the optimal cut section, from the top of the cell to the bottom of the cell, which is in contact with the base of the plate. This 3D image was recreated by obtaining 30 cut sections of the cell, from the top of the cell to the bottom in contact with the plate. When the 3D image was reconstructed (Fig.

40

17), we observed a change in membrane fluidity in the section of the cell which was adhered to the plate. In figure 17 it can be seen, that the part of the plasma membrane which is in contact with the plate has an increased amount of rigid pixels compared to the macrophage top section membrane fluidity. When the 3D image was obtained, not only we observed an increased rigidity at the bottom of the cell in contact with the plate but we also observed a large amount of cellular debris present at the base of the plate which affected the final membrane fluidity values of the cut section.
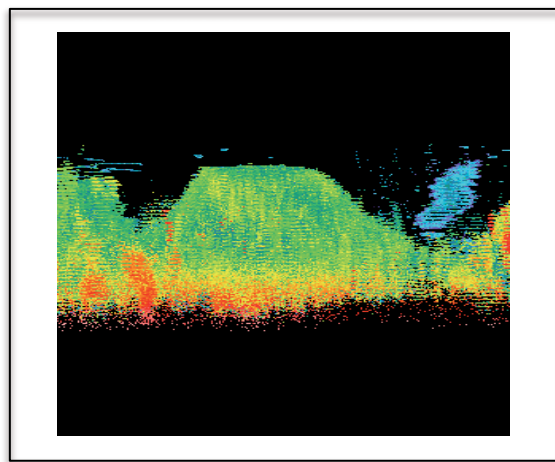
Figure 17. **Frontal plane of a 3D macrophage.** *GP images of Laurdan-stained THP-1 macrophages were obtained from over 30 thin sections from top to bottom of the cell. Macrophaes were induced in MatTek plates with phenol free media and stained with 5µM Laurdan in serum free media. Images were collected at 37°C in a two-photon microscope. GP images were calculated and then pseudocolored with an arbitrary colour palette. Images were then stacked in ImageJ software and 3D images reconstructed.*

Lymphocytes were studied in suspension, in a similar manner to liposomes, and sedimented before membrane fluidity analysis. Sedimented lymphocytes did not adhere to the plate; therefore, the contact of these cells with the bottom did not alter membrane fluidity values, so that no further studies were needed for this cell type.

To show the quantitative differences in plasma membrane fluidity of the bottom section compared to the top section, the GP images were transformed into GP frequency distribution plots. One vertical line has been drawn in figures 18A and B crossing the GP point with common GP frequencies (GP ~ +0.20), to help defining two zones with

41

different behavior in the GP scale. For a better observation of these frequency changes, GP frequency distribution values of top cut section macrophages were subtracted from the corresponding values of each GP distribution of bottom cut section, in contact with the plate, macrophages. The resulting frequency difference curves are shown in figure 18B where the three above defined GP zones can also been observed. Both A and B graphs were fitted with a sum of two Gaussian function for a better visualization and understanding of our results, as it can be seen the fitting positively adjusted to our experimental data (back and white dots). It can be observed in figure 18, the frequency distribution GP curve corresponding to the images from the bottom of the cell, which is
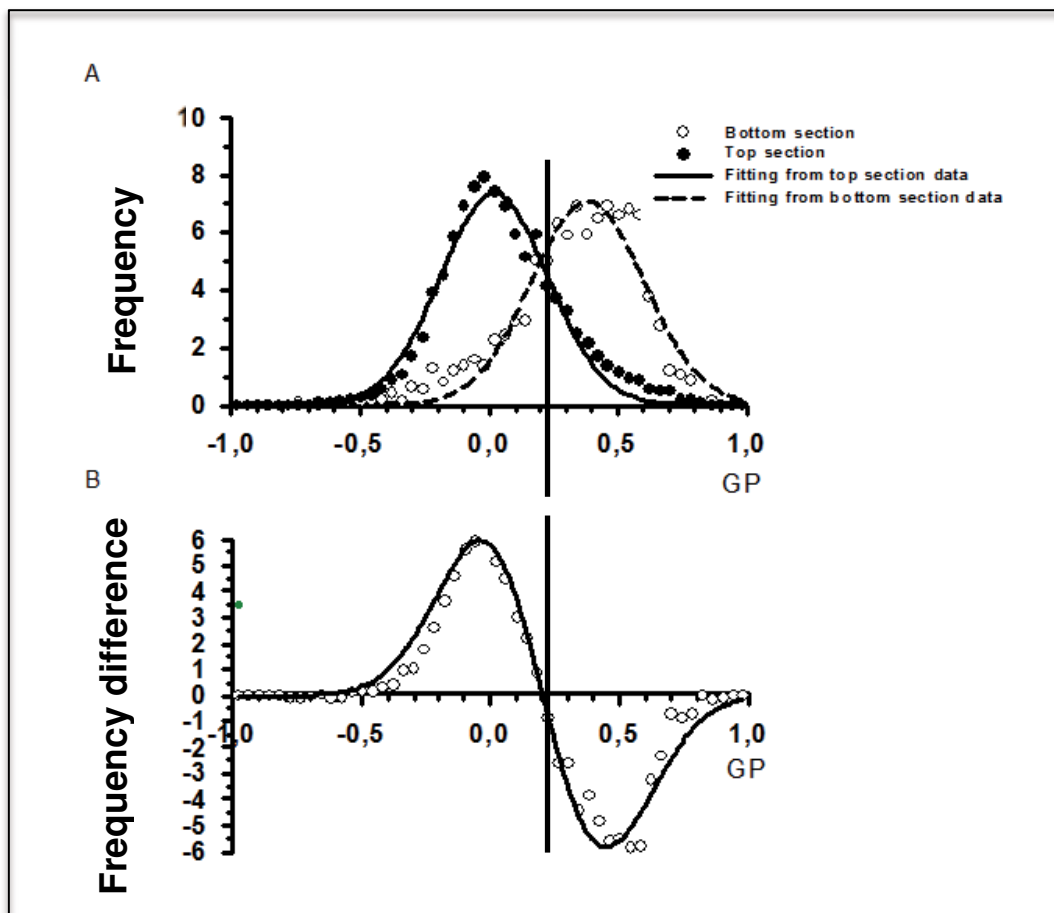
Figure 18. **Macrophage membrane fluidity distribution of the top and bottom cut sections of the cell.** *GP images were transformed to GP frequency distribution curves and normalizad at the sum of 100 (A). Dots show experimental data and lines show best fitting curves to the experimental data using Gaussian functions or Weibul functions for asymmetric curves. GP frequency distribution values of the top section macrophage were subtracted from the corresponding values of the bottom section macrophage and the resulting frequency difference distribution curves are shown in B.*

in contact with the plate, was shifted to the higher GP values, with increased frequencies in GP values from +0.20 to +1.00, which indicate membrane rigidity, compared to those obtained at the top of the cell.

The results showed in figures 17 and 18, indicated that the most suitable section to obtain the GP image for our study is the top section of the plasma membrane of macrophages. This condition, top section image, was then also applied to the study with lymphocytes to maintain the same experimental condition and to produce comparable results between both cell types.

5.1.2.3- Optimization of the number of images to be obtained

Laurdan is a fluorescent probe highly sensitive to photobleaching; this is why two-photon microscopy is a preferable technique to be used as it minimizes this effect compared to conventional confocal microscopy. We then analyzed the number of cut sections we could obtain from every section. It is preferable to use a low zoom with the microscope and then digitally increase the zoom; in this manner we prevent photobleaching. To evaluate this effect on Laurdan and consequently the maximum number of images that could be obtained from a single area, we analyzed consecutive Laurdan images acquired at two different zoom conditions at the two-photon microscope: a low $1X$ zoom and at a high $8X$ zoom. At both zooms, we obtained raw fluorescence intensity images of Laurdan stained THP-1 macrophages from channel 1 and quantified the average fluorescence intensity of the whole image in consecutive images. Figure 19 shows that, at high zoom levels Laurdan becomes photobleached, showing a decreased fluorescence emission compared to a $1X$ zoom. Both at $1X$ zoom and at $8X$ zoom the initial image had the same intensity but after obtaining a secondary image of the same section at $8X$ zoom, the fluorescence intensity decreases up to 30%. Therefore, low zoom intensities were used during our image acquisitions.
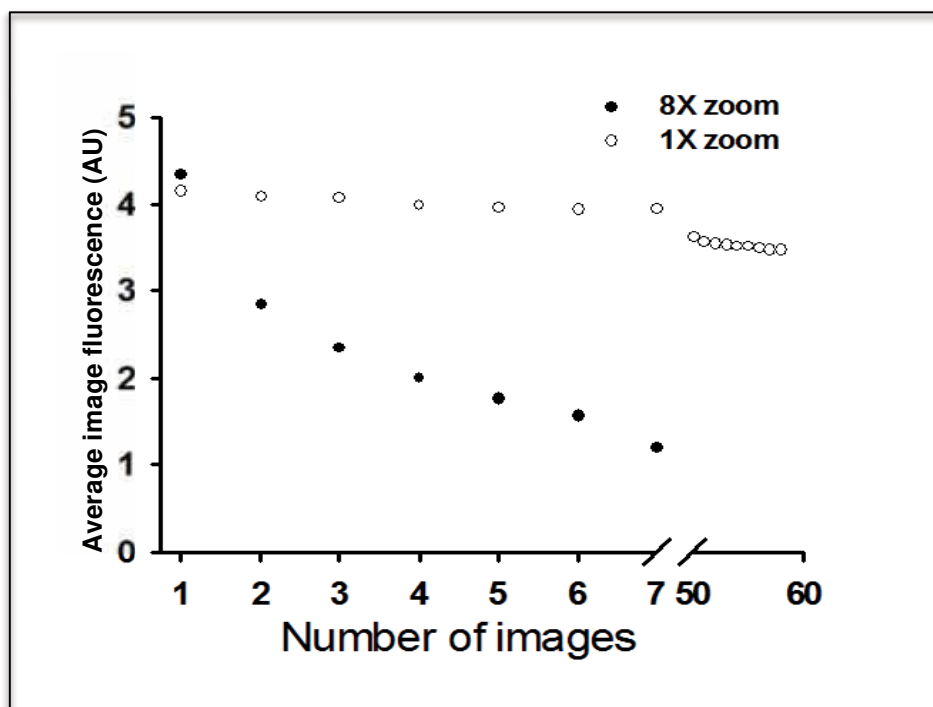
*Figure 19. **Effect of consecutive image acquisition on Laurdan photobleaching.** THP-1 monocytes were induced to macrophages in MatTek plates with 0.16μM PMA and incubated for 72h. THP-1 macrophages were washed with phenol free media and stained with 5μM Laurdan in serum free media. Consecutive images were obtained at 1X and 8X zoom and at 37°C in a two-photon microscope. The photobleaching effects on Laurdan fluorescence intensity were plotted as a function of the number of consecutive images acquired.*

5.1.2.4- Cell viability control under oxidative conditions

After optimizing all the confocal parameters and conditions, we only needed to analyze the oxidative stress in which our experiment would take place. We evaluated the H_2O_2 concentration range at which cells were treated to produce the maximum oxidative effects on macrophages and lymphocytes without affecting cellular viability. We performed a MTT assay in macrophages and lymphocytes at different H_2O_2 concentrations.

As can be seen in figure 20, results for macrophages showed that cell viability was maintained above 75% for H_2O_2 concentrations up to 2mM. At a concentration of 10mM, cell viability drastically decreased below 20%. Consequently, we considered the

H_2O_2 concentration range of 0.5 to 2mM with 24h incubation, as the oxidative stress conditions for studies in macrophages.

After obtaining cell viability results for macrophages, we applied the same conditions, a 24h incubation period with H_2O_2 concentration ranging from 0.1 to 10mM, to lymphocytes. When the same H_2O_2 concentration range and time of incubation was applied to lymphocyte we observed a low viability rate; even at very low concentrations (0.1mM) of H_2O_2 lymphocytes were not able to survive with viability over 60% (data not shown). This means that lymphocytes are more susceptible to H_2O_2 than macrophages. As lymphocyte were not able to withstand the same H_2O_2 conditions, time and concentration, as macrophages we decided to reduce the incubation time of lymphocytes in H_2O_2 to 2 hours for our experiments.
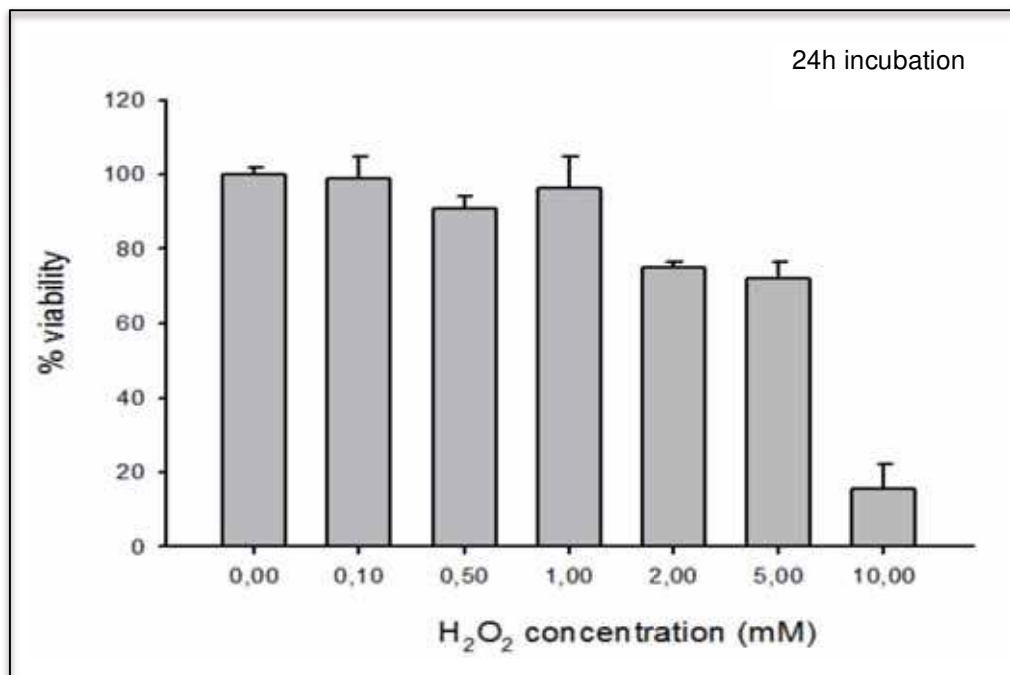
*Figure 20. **Effect of H_2O_2 concentration on macrophage viability**. THP-1 monocytes were induced to THP-1 macrophages in a 96 well plate with 0.16μM PMA and incubated for 72 hours. THP-1 macrophages were washed with phenol free media. H_2O_2 was added at different concentrations and incubated at 37ºC for 24h. After the incubation, cells were washed and viability was assessed by MTT assay. Bars indicate average viability percentage found at every H_2O_2 concentration; error bars are SEM.*

45

As shown in figure 21, a shorter incubation time of 2h with H_2O_2 maintained lymphocyte viability above 75% for H_2O_2 concentrations upto 5mM. At concentrations above 10mM cell viability drastically decreased below 60%. Then we considered the H_2O_2 concentration range of 0.5 - 2mM with an incubation time of 2h suitable for the studies on lymphocytes under oxidative stress conditions.
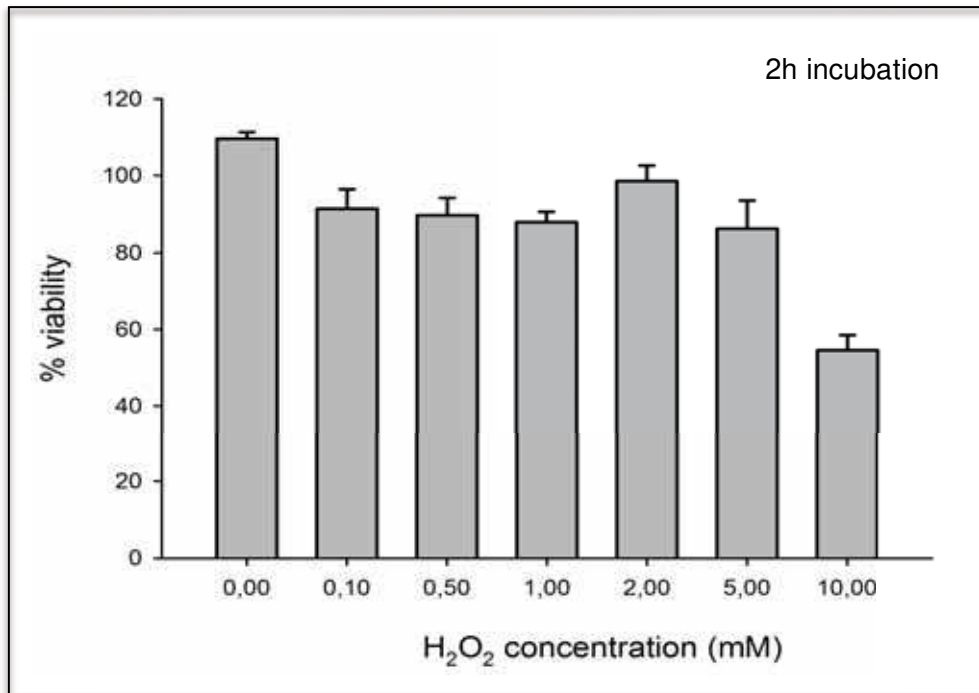
*Figure 21. **Effect of H_2O_2 concentration on lymphocyte viability.** Figure shows cell viability at H_2O_2 concentrations ranging from 0.05 to 10mM. MEC-1 lymphocytes were seeded in a 96 well, washed with phenol free media. H_2O_2 was added at different concentrations and incubated at 37ºC for 2h. After the incubation, cells were washed and viability was assessed by MTT assay. Bars indicate average viability percentage found at every H_2O_2 concentration; error bars are SEM.*

5.2- Effects of oxidative stress induced by H_2O_2 on membrane dynamics in cells of the innate immunity

5.2.1- Membrane fluidity changes due to oxidative stress in macrophages

After all conditions were set for the evaluation of the effect of oxidative stress on macrophage membrane fluidity, THP-1 macrophages were incubated with H_2O_2, stained with Laurdan, and membrane fluidity distribution was then analyzed by two-photon microscopy. For every treatment and for the control over 70 cells were

46

individually analyzed. Figure 22A-D shows examples of GP images obtained from cut sections of macrophages, at 37ºC, in control conditions (A) and in oxidizing conditions, in 0.5mM H_2O_2 (B), 1mM H_2O_2 (C) and 2mM H_2O_2 (D), pseudocolored with an arbitrary color palette (E). The black areas present in the images represent background values which correspond to non-lipid material. It can be detected a substantial enrichment in high GP areas orange-red colored in the macrophage surface, corresponding to rigid domains, as H_2O_2 concentration increases.

GP frequency distributions, at 37ºC, of control and treated macrophages, which presented interesting differences when compared, are shown in figure 22F. Two common vertical lines have been drawn in figure 22F crossing the two GP points with common frequencies (GP ~ −0.28 and GP ~ +0.22), to help defining three zones with different behavior in the GP scale. For a better observation of these frequency changes, GP frequency distribution values of control macrophages were subtracted from the corresponding values of each GP distribution of H_2O_2 treated macrophages (Fig. 22F). The resulting frequency difference curves are shown in figure 22G where the three above defined GP zones can also been observed. As it can be clearly seen, oxidation induces an increase of frequency difference in both ends of the GP scale (from −1.00 to −0.28, and from +0.22 to +1.00), whereas middle GP values (from −0.28 to +0.22) decrease in frequency.

To statistically analyze the frequency changes for every single cell, the area under the frequency distribution curve (Fig. 22F) of these three GP zones was measured and compared. The results of this analysis are shown in figure 23. In the intermediate and positive GP zones, significant differences ($p < 0.05$) were found between the control and each oxidation treatment. In summary, GP values above +0.22 show a significant increase of frequency for macrophages under oxidative stress. These
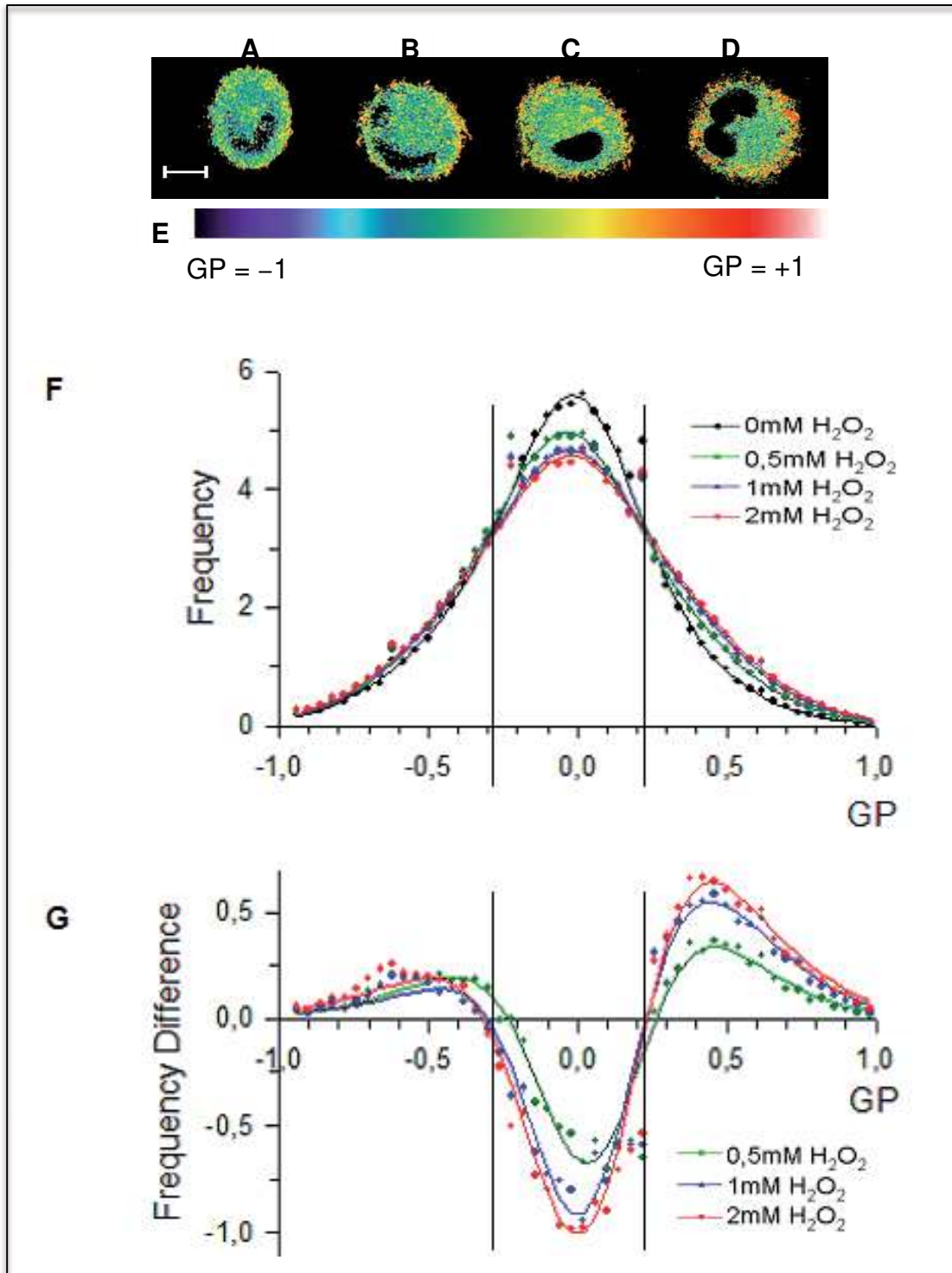
Figure 22. ***GP images and GP frequency distributions of control and oxidized Laurdan stained THP-1 macrophages:*** *THP-1 monocytes were induced in MatTek plates with 0.16μM PMA and incubated for 72h. THP-1 macrophages were washed with phenol free media and 0mM H₂O₂, control cells (A), 0.5mM H₂O₂ (B), 1mM H₂O₂ (C) and 2mM H₂O₂ (D) was added. Scale bar, 10μm. After a 24h incubation period TPH-1 macrophages were stained with 5.0μM Laurdan in serum free media. Images were collected (n=70 to 94) at 37°C in a two-photon microscope, GP images were calculated and then pseudocolored with an arbitrary color palette (E). GP images were transformed to GP frequency distribution curves and normalized to the sum of 100 (F): dots show experimental data and continuous lines show best fitting curves to the experimental data using Gaussian functions or Weibul functions for asymmetric curves. GP frequency distribution values of control macrophages were subtracted from the corresponding values of each GP distribution of H₂O₂ treated macrophages. The resulting frequency difference distribution curves are shown in G. Symbols indicate values of the resulting frequency differences and smoothed lines were obtained using a Savitsky–Golay algorithm.*

frequency differences increase with H_2O_2 concentration and occur at the expense of a significant frequency decrease in the GP interval between -0.28 and $+0.22$. This means that more rigid regions are generated in macrophage plasma membrane as a consequence of oxidative stress.

It is interesting to attribute the above described GP frequency changes to the different kinds of lipid phases, as it is accepted for lipid bilayers of living cell membranes. As two-photon microscopy allows visualizing the distribution of lipid
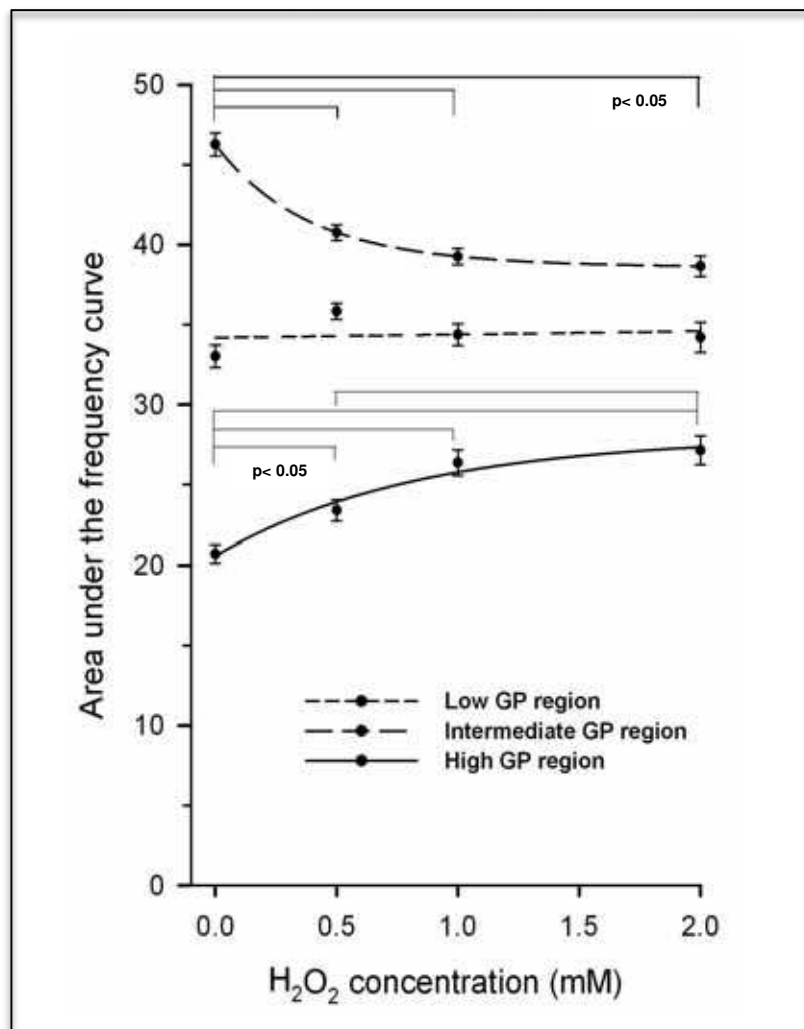
*Figure 23. **Statistical analysis of the area of the three GP regions.** The mean values of the area under the distribution curve for the three GP regions, defined in Figure 22F, were plotted as a function of H_2O_2 concentration. Error bars correspond to SEM. Statistical analysis showed significant differences ($p < 0.05$) between control and treated macrophages in the mean area of both intermediate and rigid regions.*

domains, an accurate quantification of the **size** and the **number** of every type of domains can be obtained from the experimental data. The GP values corresponding to these different lipid phases have been estimated by comparison with membrane models showing compositions similar to those of cell membranes [26, 117, 118]. GP values above +0.55 and below −0.05 represent membranes in gel and fluid phase, respectively [26, 117]. GP values approximately between +0.25 and +0.55 have been attributed to liquid-ordered (l_o) or lipid raft domains whereas GP values between −0.05 and +0.25 would correspond to the surrounding nonraft regions or liquid-disordered (l_d) phase [43,
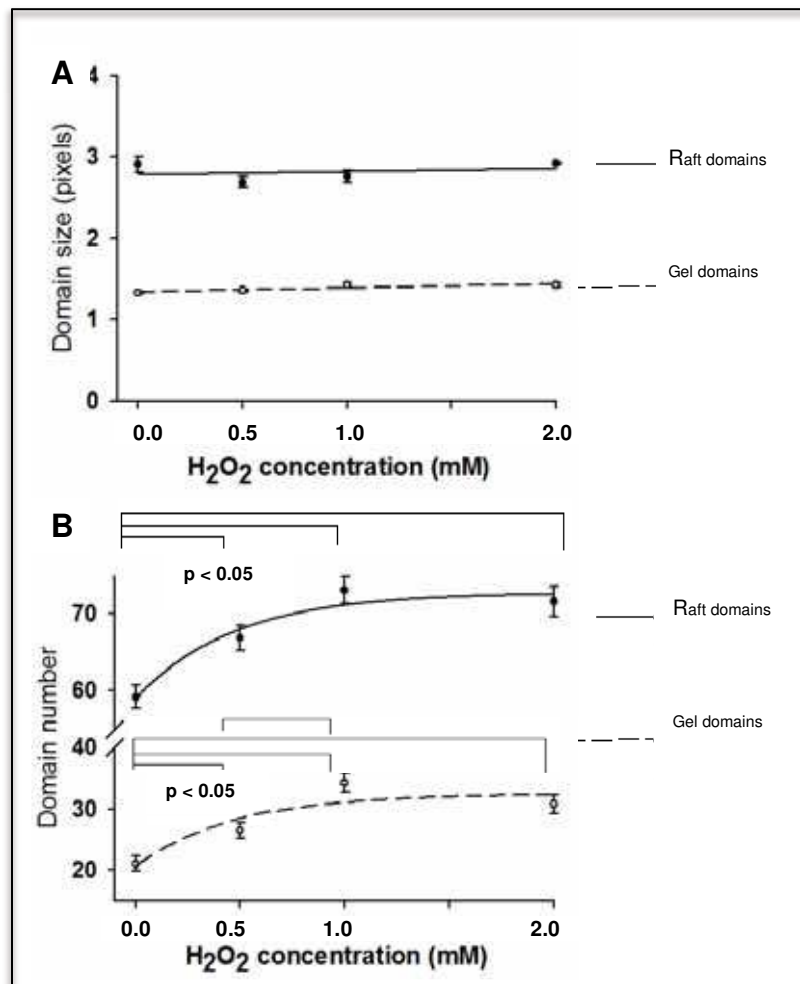
Figure 24. **Statistical analysis of the size and the number of rigid domains in macrophage membranes.** *The mean* **size,** *in pixels, (A) and the mean domain* **number** *(B) of the raft (+0.25 < GP > +0.55) and gel phase domains (GP > +0.55) were plotted as a function of H_2O_2 concentration. Error bars correspond to SEM. Statistical analysis showed significant differences (p < 0.05) between control and treated macrophages in the mean domain* **number** *of both raft and gel phase domains.*

104]. A frequency increase in the high GP range, as observed here for macrophages under oxidative stress (Fig. 22F and G), may reflect an increase in the corresponding mean domain **size** and/or in the **number** of this kind of domains, as suggested by Gaus [26]. To perform this analysis, we specially devised a suitable software capable of analyzing every type of lipid domain from the GP images obtained for every single cell. This new tool allows calculating for first time the **size** and the **number** of every type of lipid domain. This approach can be applied directly to two-photon microscopy experimental data and it allows to analyze results obtained by different laboratories.

We further investigated if raft domains, as platforms for efficient signaling, could increase in **number** or in **size**. Therefore, a novel software was developed in our laboratory to statistically analyze these two parameters from the data obtained for every single cell. The mean and SEM obtained for the **size** of domains with +0.25 < GP > +0.55 (lipid rafts) and for the **size** of domains with GP > +0.55 (gel phase), for control or macrophage under oxidative stress are shown in figure 24A. No significant changes were found in the **size** of raft domains or in the **size** of gel phase domains as a consequence of H_2O_2 treatment on macrophages. However, the **number** of both lipid raft and gel phase domains significantly increased as the H_2O_2 concentration rises (Fig. 24B). This means that oxidative stress rigidifies the plasma membrane by increasing the **number** of raft and gel phase domains.

5.2.2- Assessment of macrophage lipid peroxidation in our oxidative stress conditions

Lipids are the preferential targets of free radicals, and these altered lipids in turn modify plasma membrane fluidity (Fig. 22). Lipid peroxidation is a biological process derived by the action of free radical on polyunsaturated lipids, leading to modification of lipid structure and physicochemical properties. We further investigated if the changes

in membrane fluidity were due to modifications in fatty acids. Therefore we analyzed macrophage lipid peroxidation under oxidative stress conditions.

Lipid peroxidation in cell membranes was assessed by using C11-BODIPY[581/591], a fluorescent fatty acid analogue which incorporates into membranes. Upon oxidation, both the excitation and emission fluorescence spectra of this dye shift to shorter wavelengths. Oxidation of C11-BODIPY[581/591] was estimated from the normalized wavelength shift and plotted as a function of H_2O_2 concentration. Oxidation of C11-BODIPY[581/591] was estimated by calculating the ratio between green fluorescence and total fluorescence. Lipid peroxidation values increase as the probe becomes oxidized in a similar manner to its environment. Therefore, larger values will show more oxidative modifications of the plasma membrane due to oxidative stress.

As shown in figure 25, for macrophages, oxidation of the dye C11-BODIPY[581/591] showed a significant ($p < 0.05$) level of lipid peroxidation under H_2O_2, at concentrations ranging from 0.5mM to 2mM and for 5mM AAPH ($p < 0.05$). However,
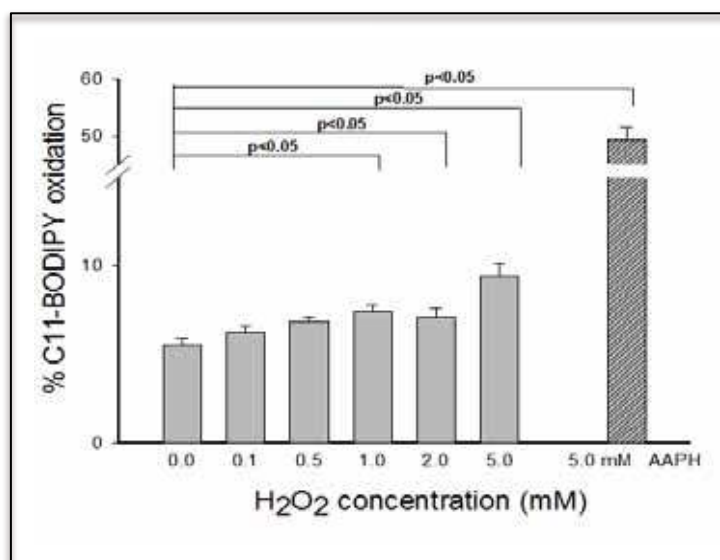
*Figure 25. **Macrophage membrane lipid peroxidation under oxidative stress induced by H_2O_2.** The lipid analog C11-BODIPY[581/591] was incorporated into THP-1 macrophages and treated with H_2O_2 for 24h at 37°C. Bars indicate the mean percentage values of C11-BODIPY oxidation. Error bars correspond to SEM (n=3). Statistical analysis showed significant differences between oxidizing conditions and control macrophages: $p < 0.05$ for concentrations ranging from 0.5mM to 5mM H_2O_2. 5mM azo initiator (AAPH) was used as a positive lipid peroxidation control.*

lipid peroxidation does not appear significantly at H_2O_2 concentrations below 0.1mM, being probably prevented by the inner antioxidative activity of the cell at low H_2O_2 concentrations.

Lipid peroxidation induced by H_2O_2 was compared to the effect of a free radical initiator, the azo compound 2,2´-azobis(2-amidinopropane) dihydrochloride (AAPH). It is known that azo compounds generate free radicals at a constant rate by their spontaneous thermal decomposition and, through a chain mechanism, they induce biochemical modifications in the biological molecules. AAPH has been used successfully to study the action of free radicals upon cell membrane lipid peroxidation [37,39,40] and it was used here as a standard or positive control for lipid peroxidation. To assess the azo compound oxidizing effect, 5mM AAPH solution was added to macrophages loaded with C11-BODIPY[581/591], and oxidation of C11-BODIPY[581/591] was estimated from the normalized wavelength shift in its emission fluorescence spectra. As can be seen in figure 25, after 30min incubation of macrophages with AAPH, there was a significant increase of C11-BODIPY581/591 peroxidation as compared to control cells.

5.2.3- Effect of oxidative stress on macrophage function

After observing changes in macrophages membrane fluidity and lipid peroxidation due to oxidative stress, we evaluated if cellular function was also modified under oxidative stress conditions. Macrophage function can be evaluated by quantifying secretion of cytokines, such as TNFα, in the supernatant upon LPS activation. We therefore quantified TNFα production in macrophages under oxidative stress conditions.

As shown in figure 26, TNFα production, by LPS activated macrophages for 24h, was at its highest peak at about 1500pg/ml; by contrast, control macrophages secreted less than 100pg/ml of TNFα. Oxidative stress itself induced minimal

production of TNFα in non-activated macrophages compared to control cells. When cells were activated with LPS under oxidative stress conditions, the production of TNFα decreased, from 15% at 0.5mM H_2O_2 to 50% at 2mM H_2O_2, as compared to LPS-activated cells without oxidative stress. Therefore, TNFα presence in the supernatant of LPS activated THP-1 macrophages is significantly reduced by oxidative stress.
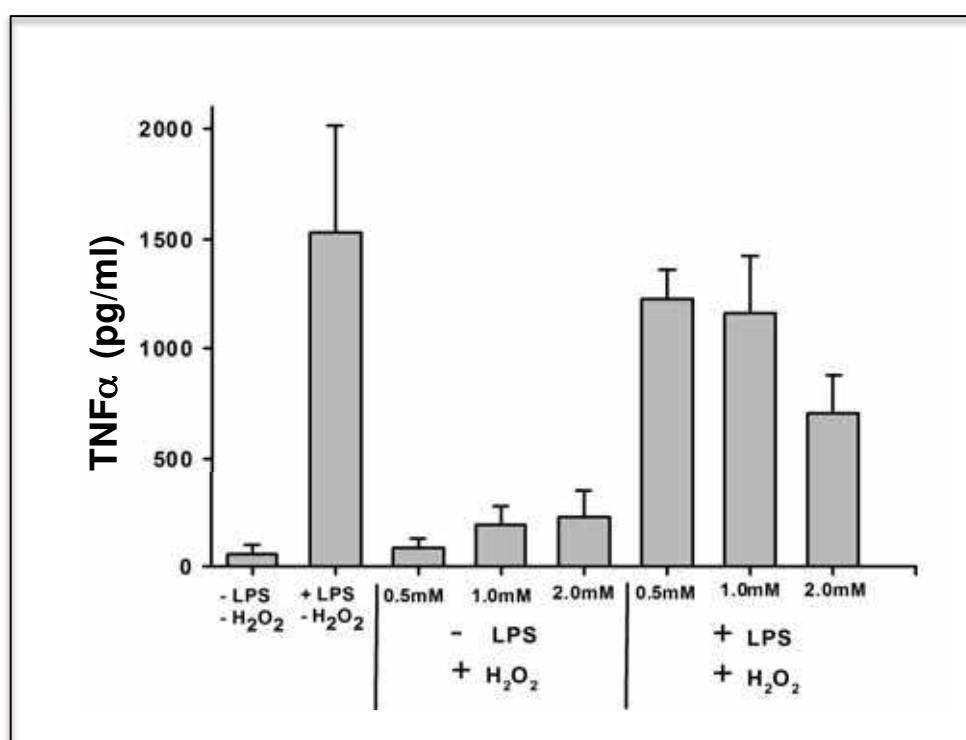
*Figure 26. **TNFα production by LPS activated THP-1 macrophages under oxidative stress conditions**. THP-1 macrophages were placed under oxidative stress conditions and/or stimulated with LPS (1µg/ml) for 24h. Supernatant was then removed and TNFα (pg/ml) present in the supernatant was evaluated by flow cytometry. Data was acquired from 3 independent experiments.*

5.2.4- Membrane dynamics in LPS activated macrophages

To understand the molecular changes in lipid dynamics and structure associated to an impaired cellular function, membrane fluidity was analyzed upon LPS activation under oxidative stress conditions. Our previous results, in figures 22 and 26, confirmed that oxidative stress modifies plasma membrane dynamics, lipid structure and macrophage function. We then analyzed if the reduced macrophage function, induced by oxidative stress, could be due to the modifications detected in membrane
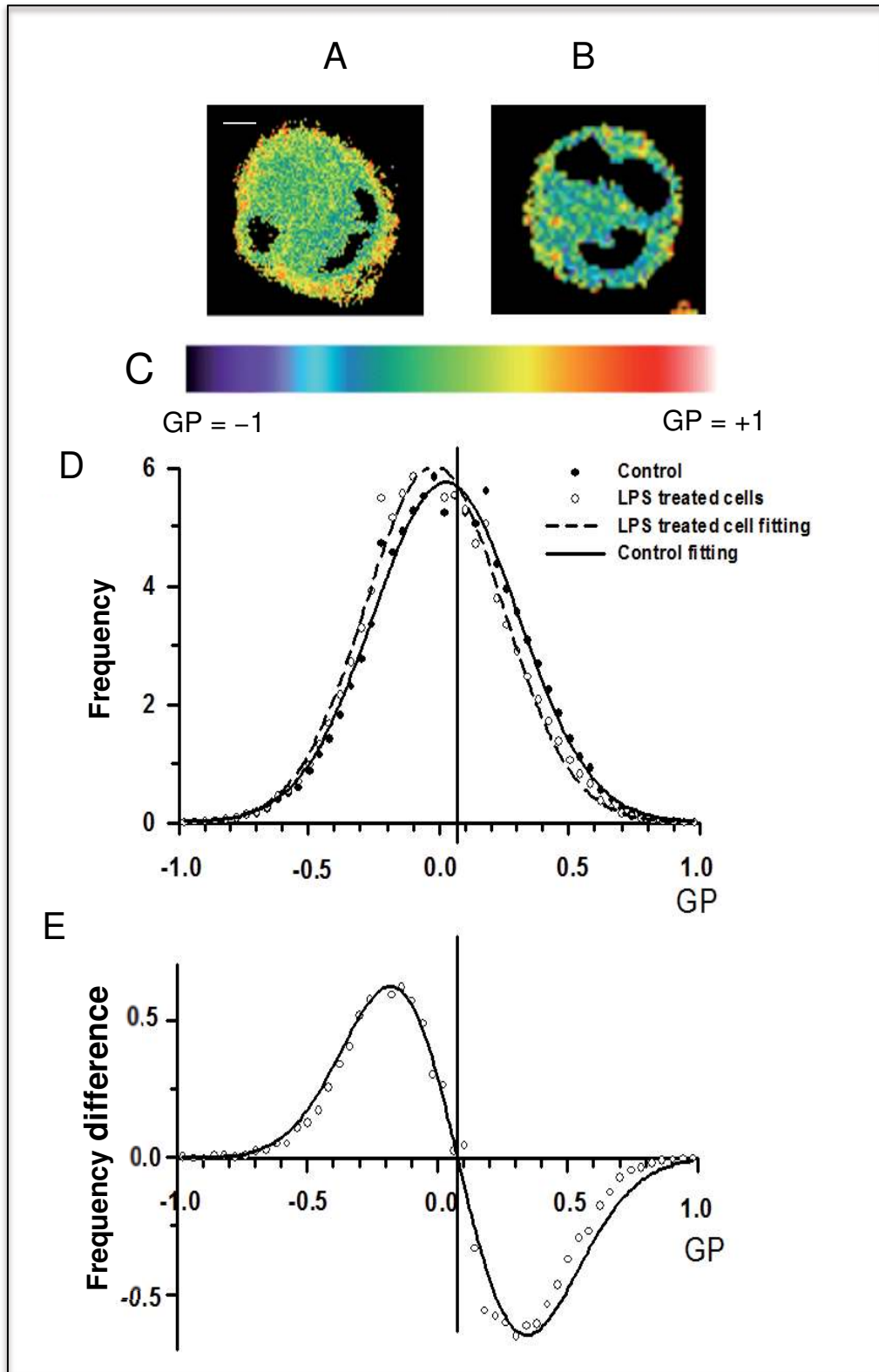
Figure 27. ***Effect of LPS binding on macrophage plasma membrane fluidity.*** *THP-1 macrophages were incubated without LPS as control cells (A) and with 1μg/ml LPS (B) for 24h at 37°C. Scale bar, 5μm. After incubation macrophages were stained with 5μM Laurdan. Images were collected (n = 50) at 37°C in a two-photon microscope. GP images were calculated and then pseudocolored with an arbitrary color palette (C). GP images were transformed to GP frequency distribution curves and normalized to the sum of 100 (D). The frequency difference distribution curves are shown in (E). A vertical line has been drawn in D and E diagrams, crossing the GP point with common frequencies (GP ~ +0.1), to help defining two zones with different behavior in the GP scale.*

55

fluidity. We evaluated changes in membrane fluidity due to LPS activation in physiological conditions, and then we analyzed membrane fluidity of LPS activated macrophages under oxidative stress conditions.

LPS activated macrophages stained with Laurdan were evaluated by two-photon microscopy and membrane fluidity distribution analyzed. The GP images (Fig. 27A-B) show a loss of high GP areas orange-red colored, corresponding to rigid regions, and an
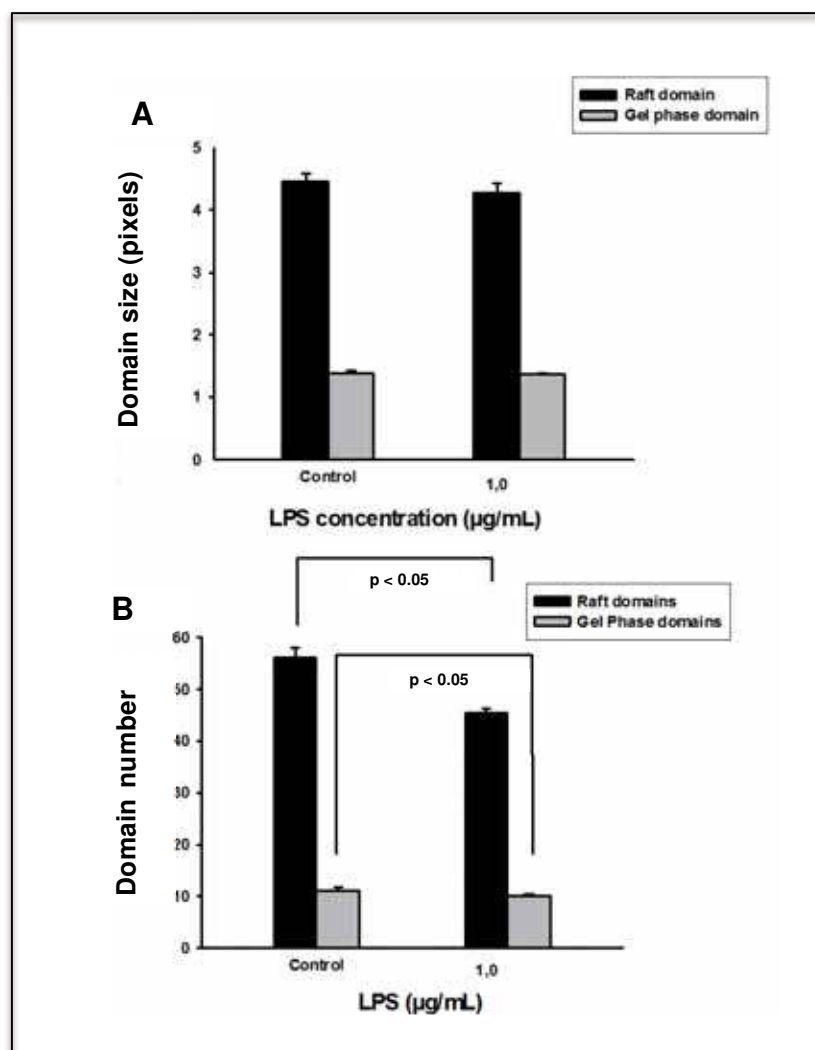
*Figure 28. **Statistical analysis of the size and the number of rigid membrane domains induced by LPS binding.** The mean **size**, in pixels (A), the mean domain **number** (B) of the raft (+0.25 < GP < +0.55) and gel phase domains (GP > +0.55) were plotted for control and LPS activated macrophages. Error bars correspond to SEM. Statistical analysis showed significant differences (p < 0.05) between LPS activated macrophages and control cells in the **number** of both lipid raft and gel phase domains, but not the **size**.*

increase in high GP areas blue-purple colored, corresponding to fluid phases, in LPS activated macrophage membranes compared to non-activated macrophages. A vertical line has been drawn in figure 27D crossing the GP point with common frequencies (GP ~ +0.1), to help defining two zones with different behavior in the GP scale.

For a better observation of these frequency changes, GP frequency distribution values of non-activated macrophages were subtracted from the corresponding values of each GP distribution of LPS activated macrophages (Fig. 27E). This figure shows that LPS binding induces a curve shift towards the lower GP values, fluidifying the plasma membrane. GP values of LPS activated macrophages, from −1.0 to +0.1, increases in frequency while GP values from +0.1 to +1.0 decreases in frequency. These results show that the membranes, of macrophages activated by LPS, become more fluid than non-activated macrophage membranes. We then analyzed how this decrease in fluidity affected the **size** (Fig. 28A) and **number** (Fig. 28B) of lipid domains. Results showed that lipid raft and gel phase domains significantly decrease in **number** when LPS binding occurs (Fig. 28B).

5.2.5- Membrane dynamics in LPS activated macrophages under oxidative stress conditions

As a summary, our results showed that oxidative stress in macrophages increases rigidity of the plasma membrane and that activation due to LPS induces fluidification of the plasma membrane. We then analyzed how LPS-induced activation, under oxidative stress, modifies plasma membrane fluidity in macrophages.

In LPS activated macrophages treated with H_2O_2 there is a substantial gain of positive GP pixels corresponding to rigid domains, colored in orange-red, in macrophage membrane (Fig. 29A–D) as compared to LPS activated macrophages without H_2O_2. Frequency distribution curves (Fig. 29F and G) show that oxidative
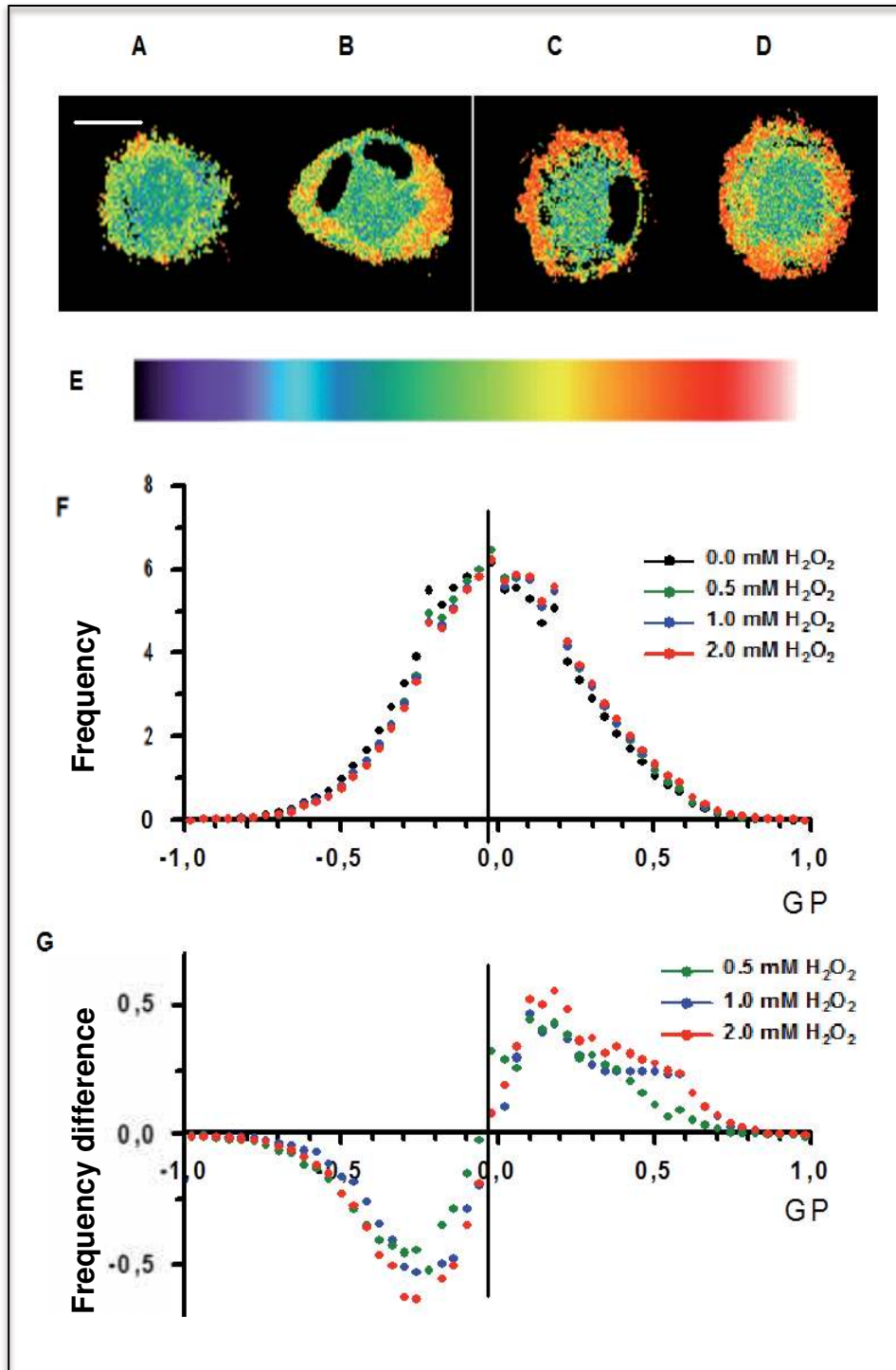
Figure 29. ***Membrane fluidity distribution in LPS activated macrophages under oxidative stress.*** *THP-1 macrophages were incubated without H_2O_2, as control cells, (A) and under oxidative stress conditions: 0.5mM H_2O_2 (B), 1mM H_2O_2 (C) and 2mM H_2O_2 (D) for 24h. During the same 24h incubation with H_2O_2, cells were also activated with LPS for the same time period (24h) with 1µg/ml LPS at 37°C. After the 24h incubation with H_2O_2 and LPS cells were stained with 5µM Laurdan. Scale bar, 5µm. Images were collected (n = 70) at 37°C in a two-photon microscope. GP images were calculated and then pseudocolored with an arbitrary color palette (E). GP images were transformed to GP frequency distribution curves and normalized to the sum of 100 (F). The frequency difference distribution curves are shown in (G). A vertical line has been drawn in F and in G diagrams to help defining two zones with different behavior in the GP scale.*

conditions induces an increase of frequency in GP values from −0.05 to +1.0, whereas

GP values from −0.5 to +1.0 increase in frequency. This means that plasma membrane

of LPS activated macrophages becomes more rigid due to oxidative stress. Interestingly,

this increase from −0.05 < GP < 1.0, corresponds to the GP intervals attributed to non-
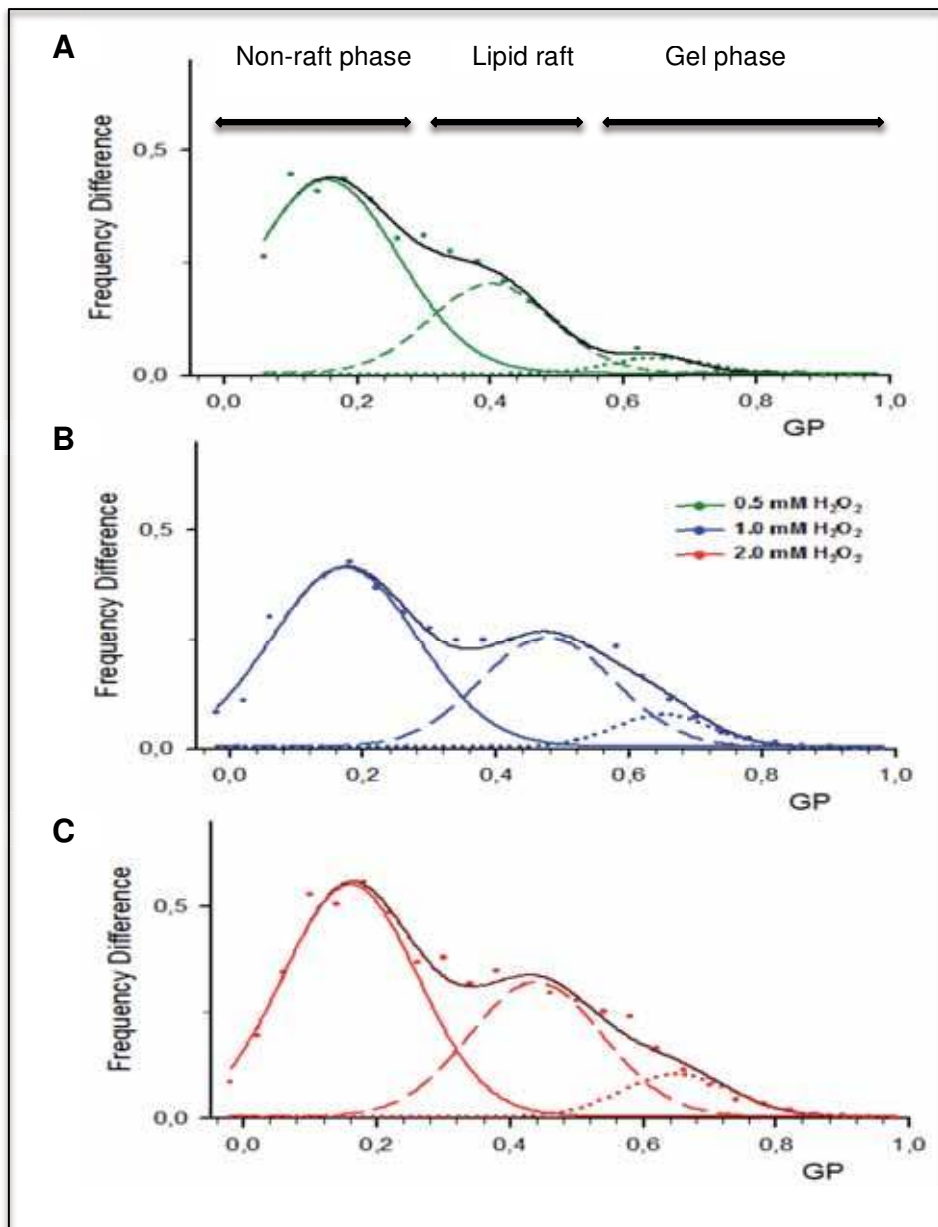
*Figure 30. **Frequency difference analysis of GP values, from -0.05 to +1.00, obtained from LPS bound macrophages under oxidative stress conditions.** THP-1 macrophages were incubated with: 0.5mM H_2O_2 (A), 1mM H_2O_2 (B) and 2mM H_2O_2 (C) for 24h. It can be seen the trimodal Gaussian curve (black lines) and its components: non-raft phase (continuous lines), lipid raft domains (dashed lines) and gel phase (dotted lines).*

raft domains, raft domains and gel phase at the expense of the fluid phas e. Therefore, due to oxidative stress, there is an increase of non-raft, raft and gel phase frequencies in LPS activated macrophages.
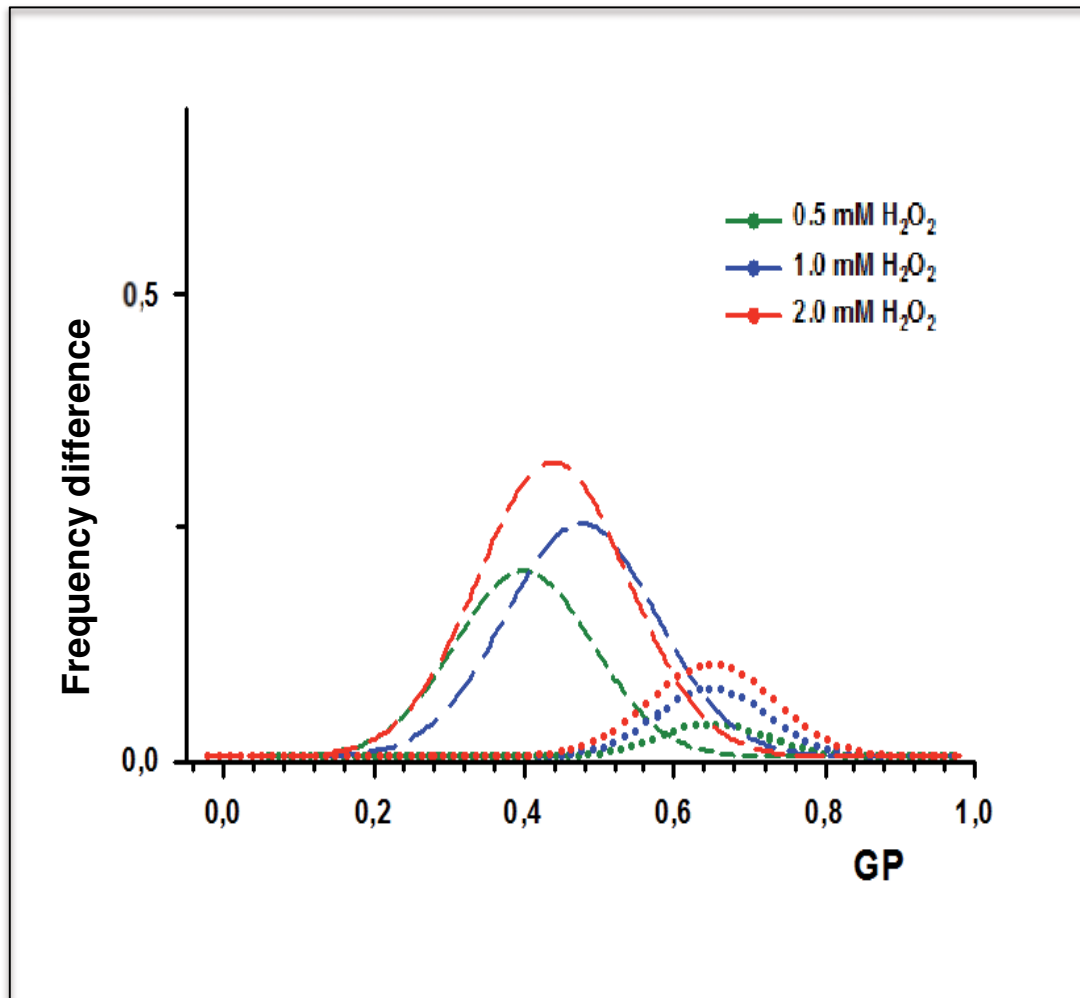
*Figure 31. **H₂O₂ concentration effect on raft and gel phase frequency differences in macrophages.** THP-1 macrophages were incubated with: 0.5mM H₂O₂, 1mM H₂O₂ and 2mM H₂O₂ for 24h. Lipid raft (dashed lines) and gel phase (dotted lines) component curves of the trimodal Gaussian fitting from figure 30, were compared for the three H₂O₂ concentrations: 0.5, 1 and 2mM.*

Due to the complexity of the GP frequency difference changes in the range between –0.05 and +1.0, shown in figure 29G, a more detailed analysis was performed. A trimodal Gaussian function was adjusted to these experimental data in figure 29G to observe the contribution of each biologically interesting phase, lipid raft and gel phase,

to the frequency difference increase. The results of this fitting are observed in figure 30, which shows the original data (dots), the trimodal Gaussian curve (black line) and the Gaussian components: non-raft, lipid raft and gel phase (continuous, dashed and dotted line). The lipid raft and gel phase component curves obtained from this fitting (Fig. 30) were merged into a single graph (Fig. 31) for a better visualization. As can be seen in figure 31, raft frequencies appear at a higher rate than new gel phase domains; interestingly, both kinds of lipid domains under oxidative conditions showed a concentration dependent frequency increase of GP values. Therefore, H_2O_2 causes a
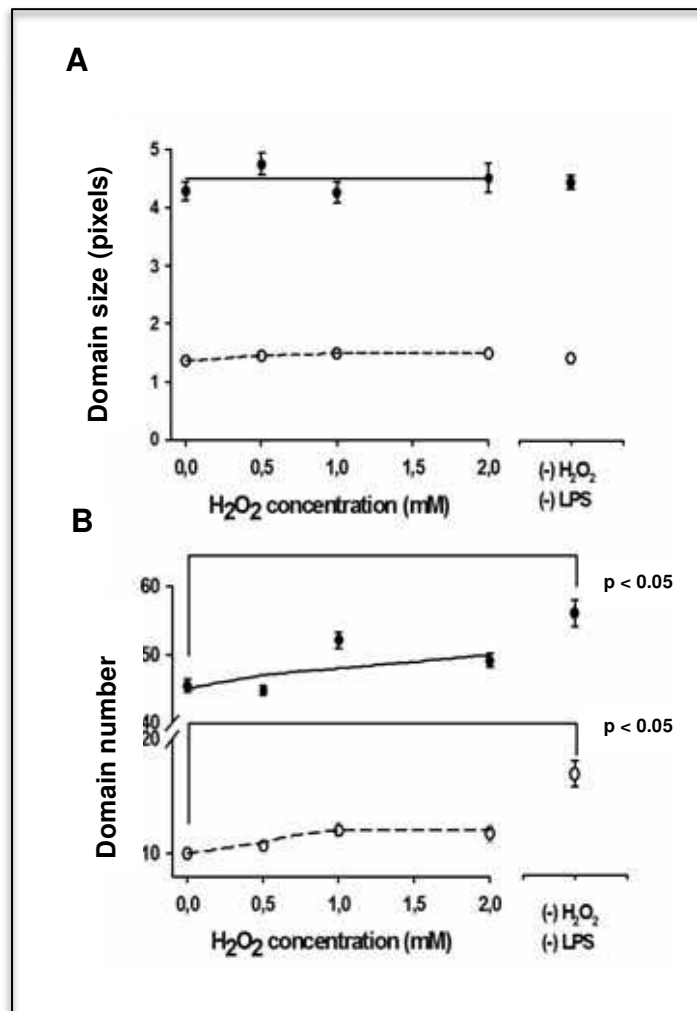
*Figure 32. **Statistical analysis of the size and the number of rigid membrane domains in LPS bound macrophages under oxidative stress conditions.** The mean size, in pixels (A) and the mean domain **number** (B) of the raft (+0.25 < GP < +0.55) and gel phase domains (GP > +0.55) were plotted for LPS bound macrophages and control cells. Error bars correspond to SEM.*

61

concentration dependent increase of frequencies of both lipid raft and gel phase GP values.

Lipid domain analysis of LPS activated macrophages, under oxidative stress, showed an increase in the **number** of both lipid rafts and gel phase domains compared to LPS activated macrophages in the absence of oxidative stress. This means that under oxidative stress, the rigidification observed in figure 29 is due to an increase in the **number** of raft and gel phase domains. The average **number** of raft domains in LPS activated macrophages was significantly lower compared to those from non-activated macrophages in the absence of H_2O_2 (Fig. 32). Although the results for raft domain **numbers** were not significantly different at 0.5, 1 and 2mM, as compared to the control, a concentration dependent increase tendency can be observed due to H_2O_2, showing that H_2O_2 increases the **number** of domains in a concentration manner. Raft domain **size** and gel domain **size** did not vary significantly under oxidative conditions, meaning that clustering was not occurring. Therefore, in LPS-activated macrophages under oxidative stress the appearance of small raft domains and gel phase are induced.

5.3- Effects of oxidative stress induced by H_2O_2 on membrane dynamics in cells of the adaptive immunity

5.3.1- Membrane fluidity changes due to oxidative stress in lymphocytes

Macrophages are highly resistant cells to oxidative stress as shown by our results; however we were also interested in looking at the effect of oxidative stress in lymphocytes, as they are key cells of the adaptive immune response. Therefore we analyzed the effect on membrane fluidity and the consequences of oxidative stress on receptor-ligand interactions.

We then initially analyzed the effects of oxidative stress on lymphocyte membrane fluidity. Under oxidative stress, the GP images and GP frequency
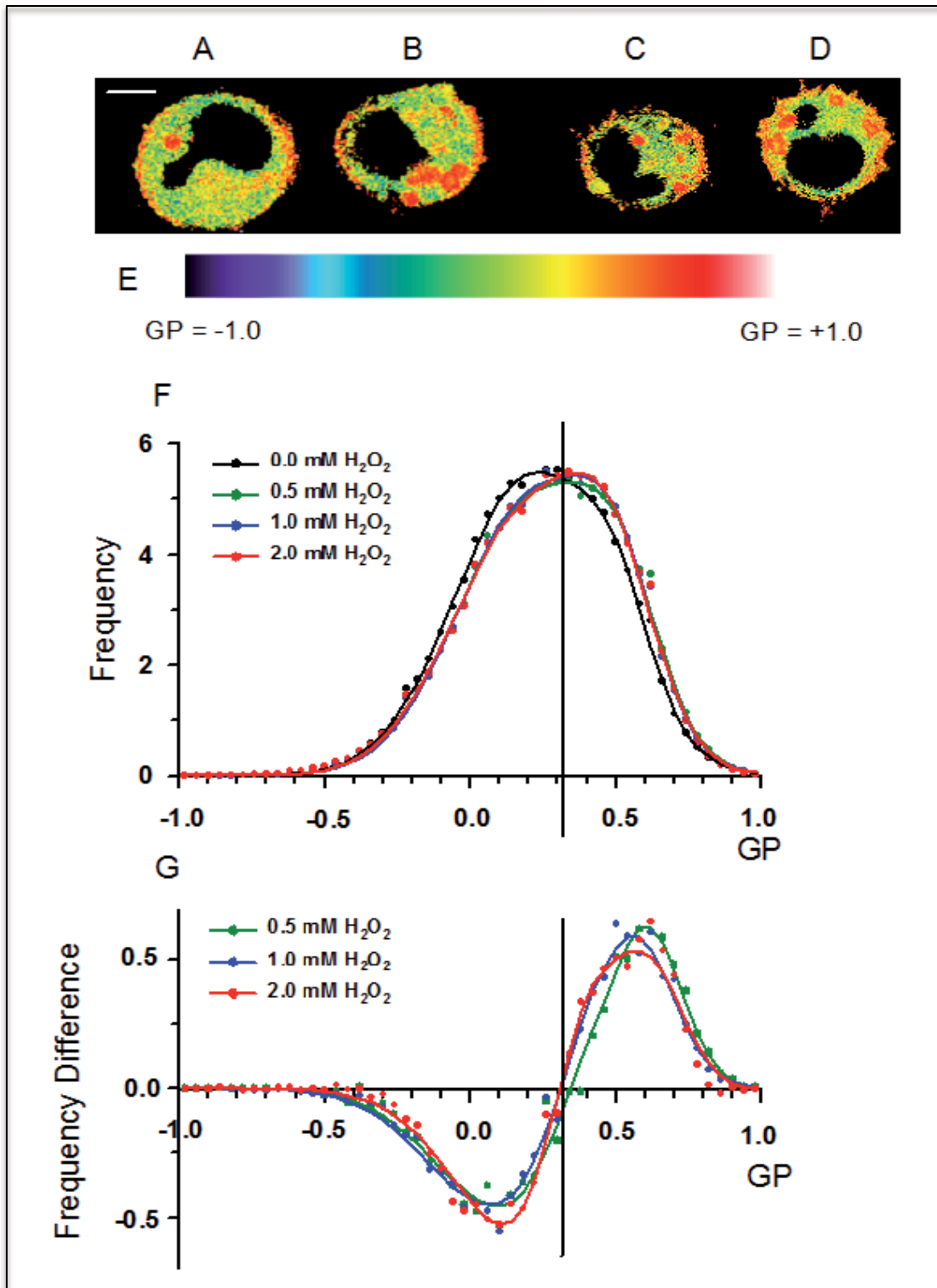
*Figure 33. **GP images and GP frequency distributions Laudan-stained lymphocytes under oxidative stress.** MEC-1 lymphocytes were incubated without H_2O_2, as control cells, (A) and with: 0.5mM H_2O_2 (B), 1mM H_2O_2 (C) and 2mM H_2O_2 (D) for 2h. Scale bar, 5µm. After incubation, lymphocytes were stained with 5µM Laurdan. Images were collected (n = 100) at 37°C in a two-photon microscope, GP images were calculated and then pseudocolored with an arbitrary color palette (E). GP images were transformed to GP frequency distribution curves and normalized to the sum of 100 (F). The frequency difference distribution curves are shown in (G). A vertical line has been drawn in F and G diagrams, crossing the GP point with common frequencies (GP ~ +0.3), to help defining two zones with different behavior in the GP scale.*

distribution graphs of lymphocyte membrane fluidity showed that under oxidative stress membrane fluidity becomes substantially enriched in high GP areas orange-red colored, corresponding to rigid domains.
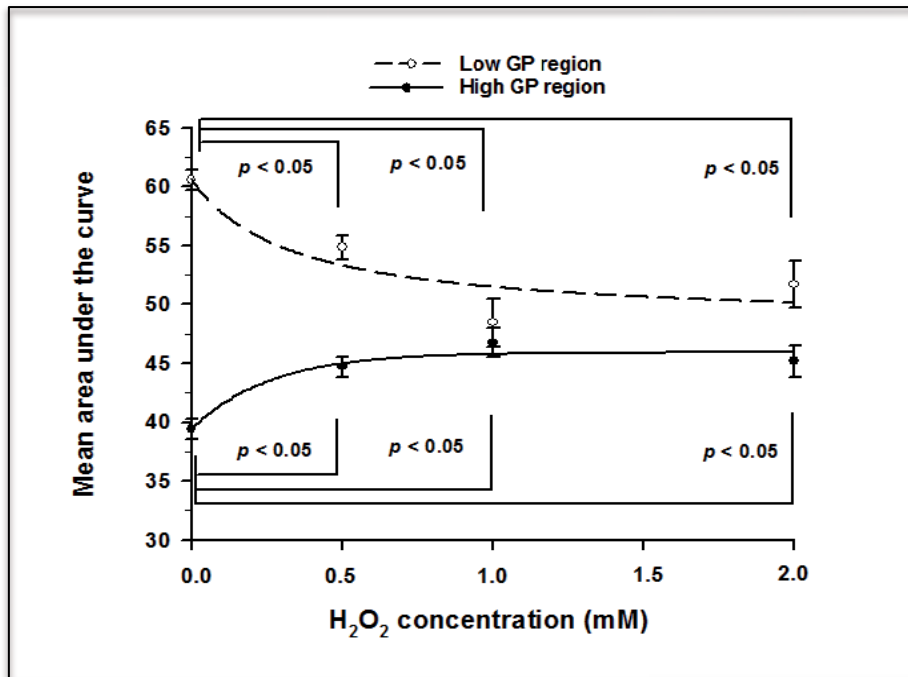
*Figure 34. **Statistical analysis of membrane fluidity distribution in lymphocytes under oxidative stress**. The mean values of the area under the distribution curve for the two GP regions, defined in Figure 33F, were plotted as a function of H_2O_2 concentration. Error bars correspond to SEM. Statistical analysis showed significant differences ($p < 0.05$) between control and treated lymphocytes in the mean area of both fluid and rigid regions.*

GP images were transformed to GP frequency distributions curves for quantification of membrane fluidity differences. GP frequency distributions, at 37ºC, of control and treated lymphocytes are shown in figure 33F. For a better observation of these frequency changes, GP frequency distribution values of control cells were subtracted from the corresponding values of each GP distribution of H_2O_2 treated lymphocytes (Fig. 33F). The resulting frequency difference curves are shown in figure 33G. Oxidative conditions increase the frequency difference in GP values from +0.30 to +1.00, whereas GP values from −0.5 to +0.3 decreases in frequency, meaning that GP

values shift towards rigid frequencies. To statistically analyze the frequency changes for every single cell, the area under the frequency distribution curve (Fig. 33F) of these two GP zones was measured and compared. The result of this analysis showed that higher GP values, from +0.30 to +1.00, in treated cells showed a significant increase ($p < 0.05$) compared to control cells. This increase was at the expense of a significant decrease of the intermediate GP values (from -0.5 to $+0.3$). This means that, as a consequence of oxidative stress, lymphocyte plasma membrane becomes more rigid.

The area under the frequency distribution curve of each of the two GP zones defined in figure 33F, was statistically analyzed. The results of this analysis are shown in figure 34. Both low and high GP regions show significant differences ($p < 0.05$) between the control and each oxidative treatment. In summary, GP values above +0.3 show a significant increase of frequency for lymphocytes under oxidative stress. These frequency differences increase with H_2O_2 concentration and occur at the expense of a significant frequency decrease in the GP interval between -1.0 and $+0.3$. This means that more rigid regions are generated in lymphocyte plasma membrane as a consequence of oxidative conditions.

As described in section 5.2.1 for macrophages under oxidative stress, an increase in the frequency of GP values corresponding to rigid regions, observed for lymphocytes under oxidative stress in figure 33F-G, can be due to: an increase in the mean domain **size**, and/or an increase in the **number** of this kind of domains. A custom-made software was used to statistically analyze these two parameters. The mean and SEM obtained for the **size** of domains with $+0.25 > GP < +0.55$ (lipid rafts) and for the **size** of domains with $GP > +0.55$ (gel phase), for control or H_2O_2 treated lymphocytes are shown in figure 35. No significant changes were found in the **size** of raft domains or in the **size** of gel phase domains as a consequence of H_2O_2 (Fig. 35A). However, the

number of both lipid raft and gel phase domains significantly increased as the H_2O_2 concentration was raised (Fig. 35B). This means that oxidative stress rigidifies plasma membrane by increasing the **number** of raft and gel phase domains.
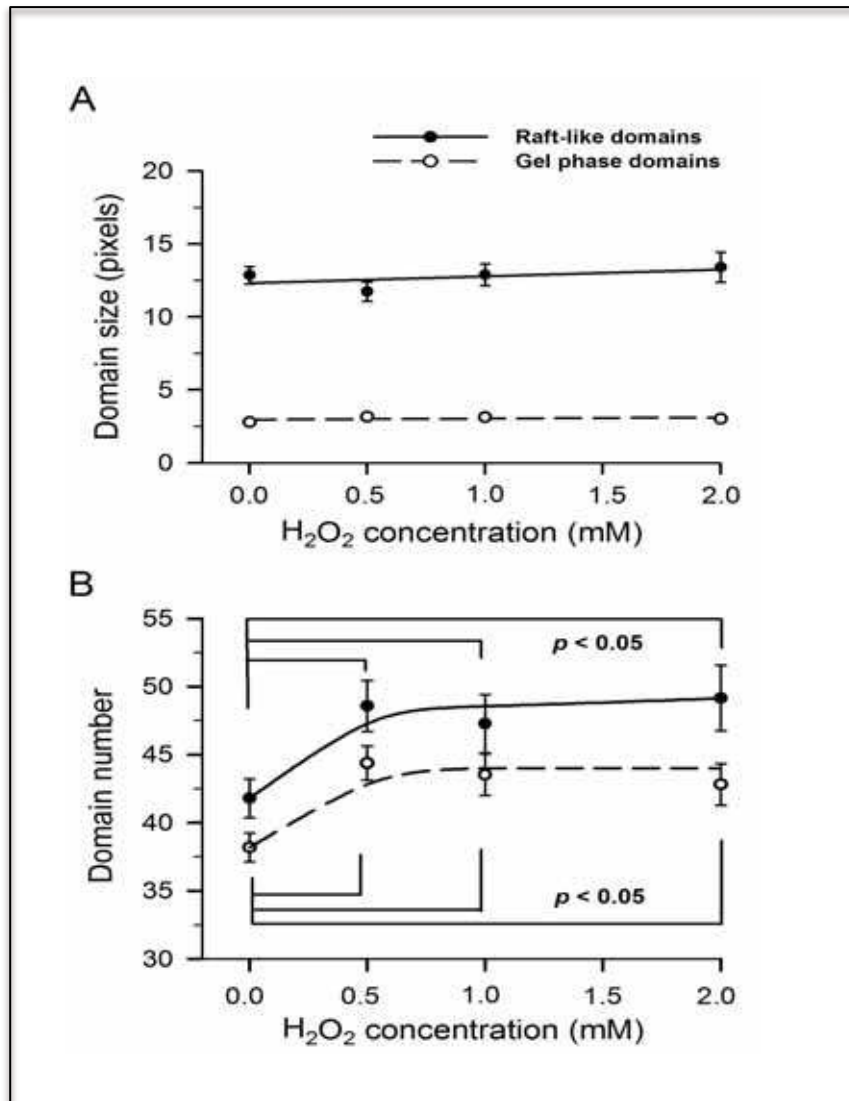
Figure 35. ***Statistical analysis of the size and the number of rigid domains in lymphocyte membranes.*** *The mean **size**, in pixels, (A) and the mean domain **number** (B) of the raft (+0.25 < GP < +0.55) and gel phase domains (GP > +0.55) were plotted as a function of H_2O_2 concentration. Error bars correspond to SEM. Statistical analysis showed significant differences (p < 0.05) between control and treated lymphocytes in the mean domain **number** of both raft and gel phase domains.*

66

5.3.2- Assessment of lymphocyte lipid peroxidation in our oxidative stress conditions

Lipids are the preferential target of free radicals, these altered lipids modify plasma membrane fluidity (Fig. 33). We further investigated if the change in membrane fluidity was due to modifications in fatty acids. MEC-1 lymphocytes under oxidative stress conditions were analyzed in living cells to evaluate fatty acid modifications. We therefore analyzed lipid peroxidation under oxidative stress conditions in lymphocytes.

Lipid peroxidation in cell membranes was assessed by using C11-BODIPY$^{581/591}$, a fluorescent fatty acid analogue which incorporates into membranes. Upon oxidation, both the excitation and emission fluorescence spectra of this dye shift to shorter wavelengths. Oxidation of C11-BODIPY$^{581/591}$ was estimated from the normalized wavelength shift and plotted as a function of H_2O_2 concentration.
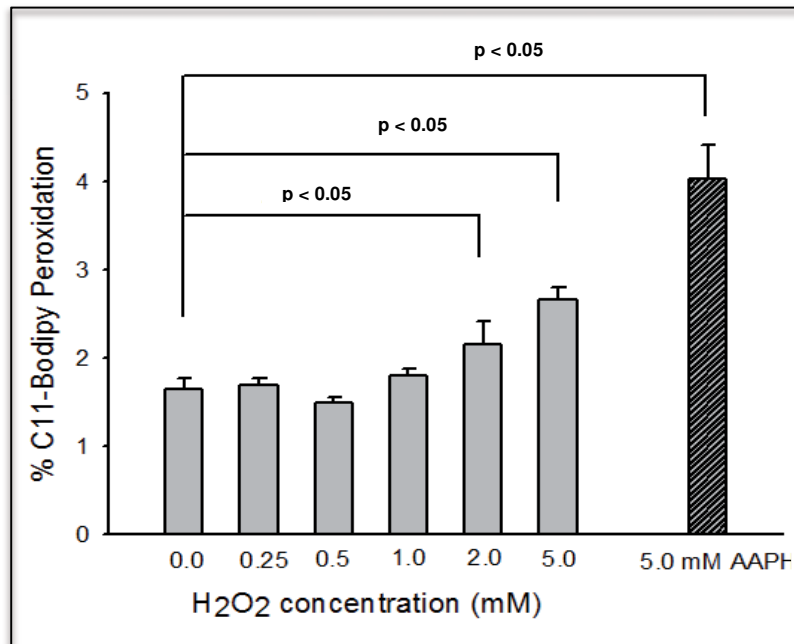
Figure 36. ***Lymphocyte membrane lipid peroxidation under oxidative stress.*** *MEC-1 lymphocytes were stained with the lipid analog C11-BODIPY$^{581/591}$ treated with H_2O_2 for 2h at 37°C. Bars indicate the mean percentage values of C11-BODIPY oxidation. Error bars correspond to SEM. Statistical analysis showed significant differences between oxidizing conditions and control lymphocytes for 2mM H_2O_2 and for 5mM H_2O_2 (p < 0.05). 5mM azo initiator (AAPH) was used as a positive lipid peroxidation control.*

As can be seen in figure 36, lymphocytes under oxidative stress conditions stained with C11-BODIPY[581/591] showed significant levels of lipid peroxidation at 2 and 5mM ($p < 0.05$) H_2O_2 concentrations as compared to lymphocytes without H_2O_2. Membrane lipid peroxidation would be prevented at H_2O_2 concentrations below 2mM because of the intracellular antioxidant activity of the cell. The positive control, the free radical initiator AAPH, also showed significantly ($p < 0.05$) high levels of lipid peroxidation.

5.3.3- PIBF/PIBF-R binding and membrane dynamics in lymphocytes

Our main aim is to understand changes in lipid dynamics and structure due to oxidative stress and how this may impair cellular function in lymphocytes. Results in figures 33 and 36, confirmed that oxidative stress modifies plasma membrane dynamics and lipid structure in lymphocytes. Therefore we evaluated how oxidative stress modifications impair cellular functions; this was achieved by evaluating changes, induced by oxidative stress, in membrane fluidity upon receptor-ligand interactions and the distribution of this binding in different lipid phases. Receptor-ligand binding in lymphocytes was evaluated through the binding of PIBF to its receptor, the PIBF-R. We initially evaluated modifications in membrane fluidity due to the binding of PIBF in physiological conditions, and then we analyzed this binding under oxidative stress conditions.

To analyze how receptor-ligand binding modified lymphocyte membrane fluidity we used conventional confocal microscopy combined two-photon microscopy. Lymphocytes were double stained with AlexaFluor647/PIBF and Laurdan. The excitation and emission wavelengths patterns of these fluorochromes are suitable to yield separate information without interference. PIBF fluorescence images were
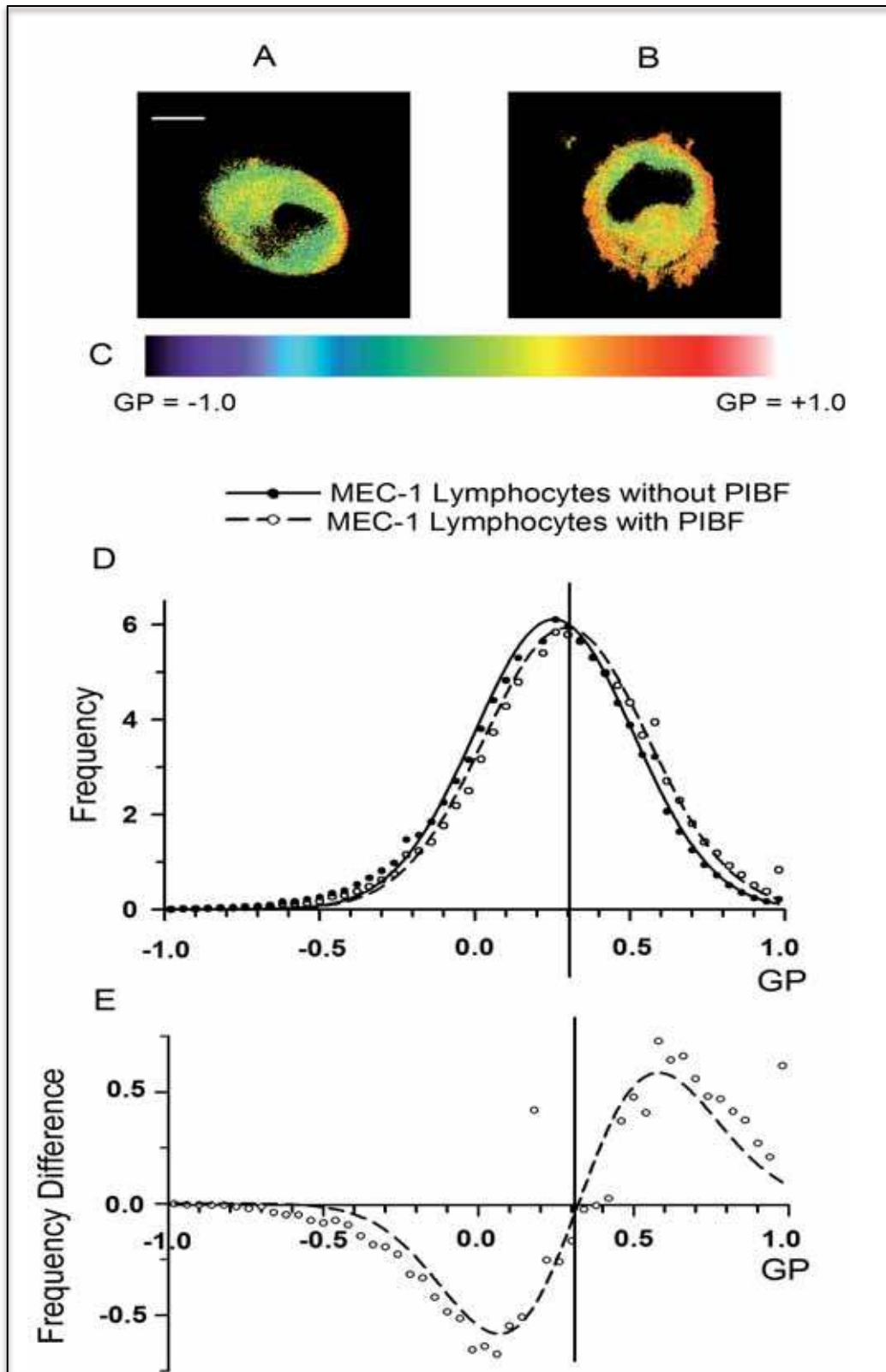
*Figure 37. **Effect of PIBF/PIBF-R on lymphocyte plasma membrane fluidity.** MEC-1 lymphocytes were incubated without PIBF as control cells (A) and with 25µg/mL sPIBF (B) for 1h at 37°C. Scale bar, 5µm. After incubation, lymphocytes were stained with 5µM Laurdan. Images were collected (n = 100) at 37°C in a two-photon microscope. GP images were calculated and then pseudocolored with an arbitrary color palette (C). GP images were transformed to GP frequency distribution curves and normalized to the sum of 100 (D). The frequency difference distribution curves are shown in (E). A vertical line has been drawn in D and E diagrams, crossing the GP point with common frequencies (GP ~ +0.3), to help defining two zones with different behavior in the GP scale.*

69

obtained by conventional microscopy and GP images by two-photon microscopy; both images were consecutively acquired for comparison. Information of PIBF distribution in the different kinds of membrane domains was determined by superposition of GP images to their corresponding PIBF fluorescent images. For two-photon microscopy, MEC-1 lymphocytes were incubated with recombinant PIBF for 1h and membrane fluidity distribution evaluated by two-photon microscopy. The GP images (Fig. 37A-C) show an enrichment of high GP areas orange-red colored in the lymphocyte surface,
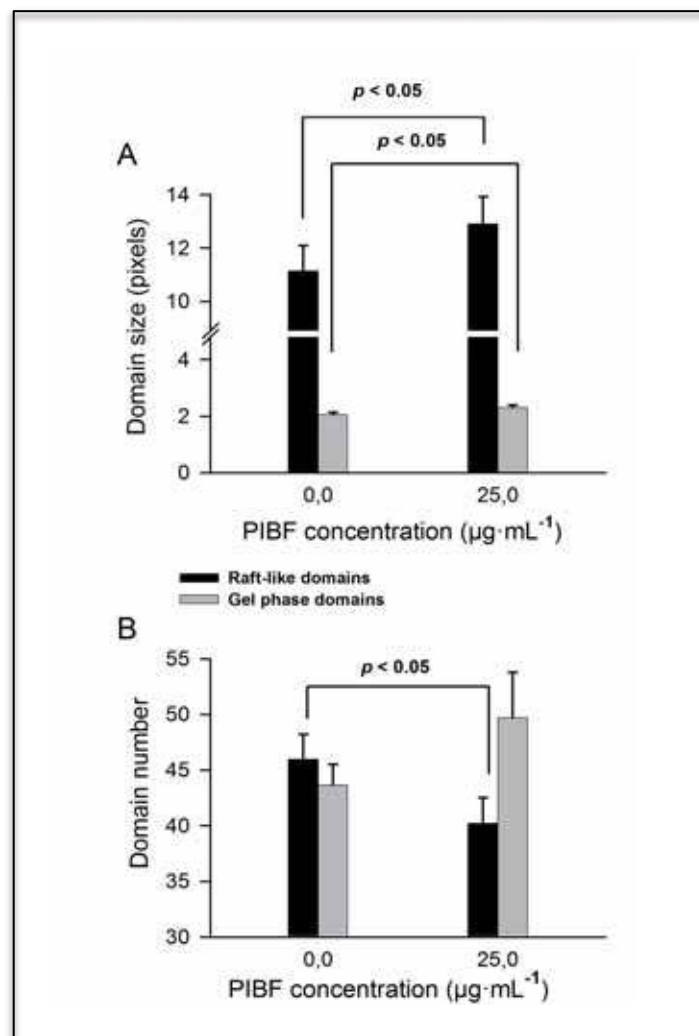
Figure 38. **Statistical analysis of the size and the number of rigid membrane domains induced by PIBF/PIBF-R binding in lymphocyte membranes.** *The mean* **size**, *in pixels, (A) and the mean domain* **number** *(B) of the raft (+0.25 < GP < +0.55) and gel phase domains (GP > +0.55) were plotted for control and PIBF bound lymphocytes. Error bars correspond to SEM. Statistical analysis showed significant differences (p < 0.05) between PIBF bound lymphocytes and control cells in the* **size** *of both lipid raft and gel phase domains, and in the* **number** *of lipid raft domains*

corresponding to rigid regions, due to binding of PIBF to its receptor. GP frequency distributions, at 37ºC, of control and PIBF bound lymphocytes, which presented interesting differences when compared, are shown in figure 37D. One vertical line has been drawn in figure 37D crossing the GP point with common frequencies (GP ~ +0.3), to help defining two zones with different behavior in the GP scale. For a better observation of these frequency changes, GP frequency distribution values of control lymphocytes were subtracted from the corresponding values of each GP distribution of PIBF bound lymphocytes (Fig. 37D). The resulting frequency difference curves are shown in figure 37E where the two above defined GP zones can also been observed. This figure shows that PIBF binding induces a curve shift towards the rigid end of the GP scale. GP values of PIBF bound lymphocytes from −0.5 to +0.3 decrease in frequency while GP values from +0.3 to +1.0 increase in frequency. These results show that plasma membrane of lymphocytes bound to PIBF become more rigid than plasma membranes from lymphocytes without PIBF.

To evaluate if the rigidification observed in figure 37 was due to a clustering effect of PIBF, we performed our analysis of lipid domain **size** and **number**. Results showed that lipid raft domains significantly increase in **size** when PIBF binding occurs (Fig. 38A). The mean **number** (Fig. 38B) of lipid raft domains significantly decreases upon PIBF binding. With this procedure we have evidence that PIBF binding in lymphocytes causes clustering of lipid raft and gel-like domains.

5.3.4- PIBF/PIBF-R binding and membrane dynamics in lymphocytes under oxidative stress conditions

We investigated modifications in plasma membrane dynamics when lymphocytes bound to PIBF were placed under oxidative stress conditions. Results showed that in H_2O_2-treated cells bound to PIBF there is a substantial loss of orange-red
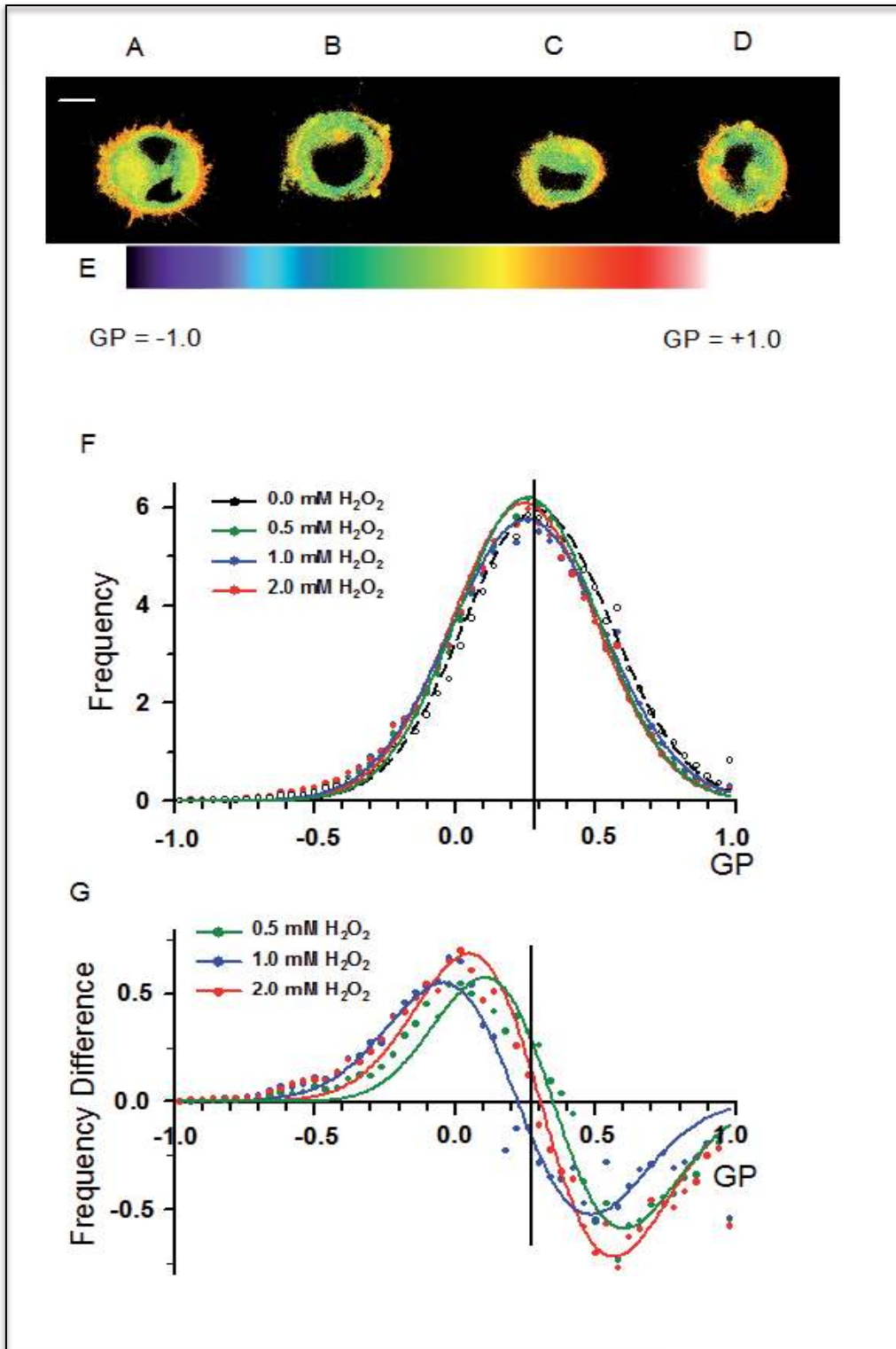
Figure 40. **Membrane fluidity distribution in PIBF bound lymphocytes under oxidative stress.** MEC-1 lymphocytes were incubated without H_2O_2, as control cells, (A) and with: 0.5mM H_2O_2 (B), 1mM H_2O_2 (C) and 2mM H_2O_2 (D) for 2h. Scale bar, 5μm. After incubation all lymphocytes, including control cells, were activated with 25μg/ml sPIBF at 37°C for 1h. Then cells were stained with 5μM Laurdan. Images were collected (n = 150) at 37°C in a two-photon microscope. GP images were calculated and then pseudocolored with an arbitrary color palette (E). GP images were transformed to GP frequency distribution curves and normalized to the sum of 100 (F). The frequency difference distribution curves are shown in (G). A vertical line has been drawn in F and in G diagrams to help defining two zones with different behavior in the GP scale.

pixels compared to lymphocytes bound to PIBF without H_2O_2. Figure 40A-E shows the

Laurdan generalized polarization (GP) images of PIBF bound MEC-1 cells, at 37°C, in

control conditions (0mM H_2O_2) (A) and in oxidizing conditions from 0.5 to 2mM H_2O_2

(B-D). GP frequency distributions, at 37ºC, of control and treated lymphocytes are

shown in figure 40F and the resulting subtracted frequency difference curves are shown

in figure 40G. Frequency distribution curves (Figure 40F-G) show that oxidation

induces a decrease of frequency in GP values from +0.30 to +1.00, whereas GP values

from −0.5 to +0.3 increase in frequency. This results show that plasma membranes of

lymphocytes bound to PIBF under oxidative stress become more fluid than membranes
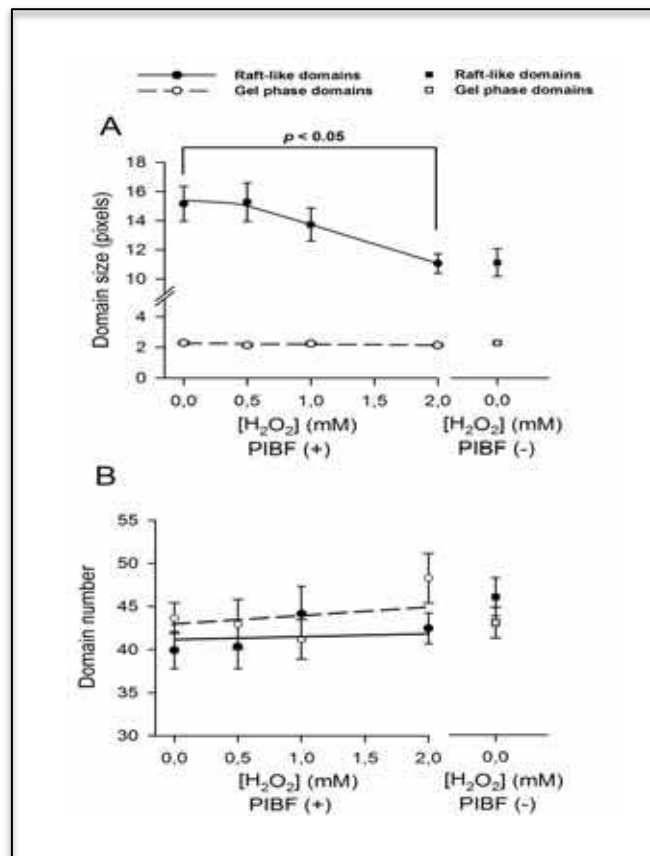
*Figure 41. **Statistical analysis of the size and the number of rigid membrane domains in PIBF bound lymphocytes under oxidative stress conditions.** The mean **size**, in pixels, (A) and the mean domain **number** (B) of the raft (+0.25 < GP < +0.55) and gel phase domains (GP > +0.55) were plotted for PIBF bound lymphocytes and control cells. Error bars correspond to SEM. Oxidative stress by 2mM H_2O_2 induced significant differences (p < 0.05) for raft domain **size** in PIBF bound lymphocytes.*

of non-oxidizing conditions. Therefore, the rigidifying effect previously observed by PIBF is completely inhibited by the action of H_2O_2.

Lipid domain analysis of lymphocytes in the presence of PIBF, under oxidative stress, showed a decrease of lipid raft clustering. The average raft **size** of PIBF bound to its receptor in lymphocytes was reduced significantly by 2mM H_2O_2 (Fig. 41). Although the results for raft **size** were not significantly different at 0.5 and 1mM, as compared to the control, a concentration dependent decrease tendency can be observed. Raft domain **number** and gel domain **number** did not vary significantly under oxidative conditions. This shows that oxidative stress is inhibiting the clustering effect caused by the binding of PIBF.

5.3.5- Effect of oxidative stress on PIBF/PIBF-R membrane distribution

To evaluate how oxidative stress modified normal receptor-ligand binding, we quantified the distribution of PIBF bound to its receptor in the plasma membrane. Two-photon microscopy not only allows to study membrane fluidity in PIBF bound lymphocytes, but combining it with conventional confocal microscopy we were able to evalute the distribution of the PIBF binding in different domains of the plasma membrane. This distribution of PIBF binding to its receptor would allow us to visualize how oxidative stress may modify the localization of PIBF bound to its receptor and if PIBF binding to its receptor occurred in an efficient manner.

Lymphocytes were placed under oxidative stress and incubated with PIBF-AlexaFluor647 for 1h. Figure 42C shows the fluorescence intensity values of PIBF bound to its receptor at different H_2O_2 concentrations. Fluorescence emission intensity of PIBF-AlexaFluor647 bound to PIBF-R was decreased in lymphocytes under oxidative stress, as compared to PIBF bound lymphocytes without oxidative stress. This indicates that less binding of PIBF to its receptor is achieved.
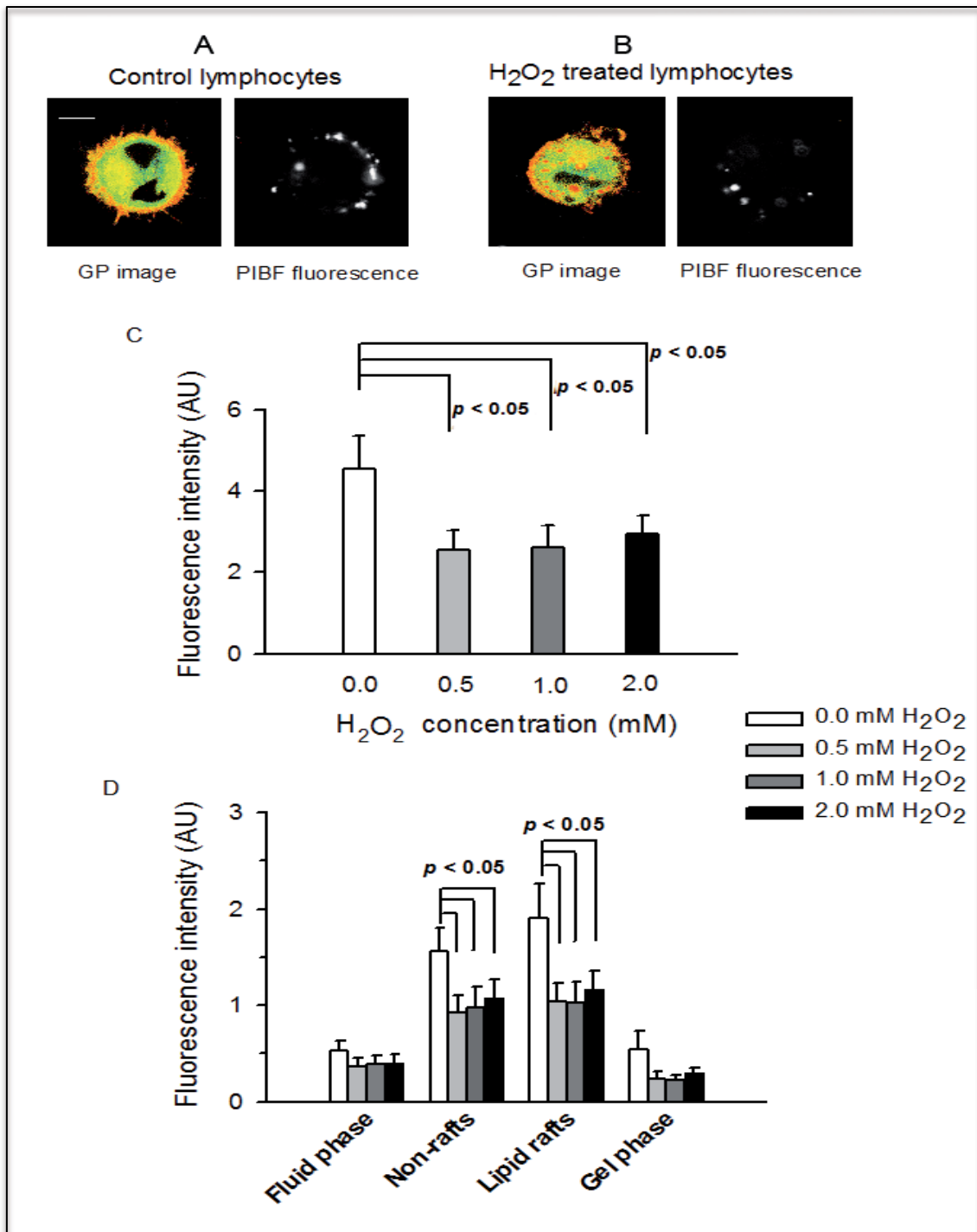
Figure 42. **PIBF/PIBF-R binding distribution in lymphocytes under oxidative stress conditions.**
MEC-1 lymphocytes were incubated without H_2O_2, as control cells, and with: 0.5mM H_2O_2, 1mM H_2O_2 and 2mM H_2O_2 for 2h. Scale bar, 5µm. After incubation all lymphocytes, including control cells, were activated with 25µg/ml sPIBF at 37°C for 1h. Then cells were stained with 5µM Laurdan. This figure shows GP and PIBF fluorescence images of representative PIBF bound lymphocytes in the absence (A) and in the presence (B) of 2mM H_2O_2. Scale bar, 5µm. PIBF fluorescence images were collected (n = 160 cells) at 37°C in a conventional confocal microscope. The PIBF fluorescence of whole cells was analyzed at each H_2O_2 concentration (C) and significant differences (p < 0.05) were found as compared to the control. PIBF/PIBF-R binding distribution was analyzed and compared among the different kinds of domains in plasma membrane under oxidative stress (D). All H_2O_2 concentrations, significant differences (p < 0.05) were found in raft and non-raft PIBF distribution when compared to lymphocytes in the absence of H_2O_2.

Taking advantage of the double staining approach, we obtained PIBF intensities allocated to each lipid phase of plasma membrane. We matched the PIBF fluorescence intensity of each pixel with their corresponding pixels of Laurdan GP image. We grouped all the PIBF fluorescent pixels in the different membrane phases using their corresponding GP values, as follows: fluid phase (GP < −0.05), non-raft (−0.05 < GP < 0.25), lipid raft (+0.25 < GP < 0.55) and gel phase (GP > 0.55). Results are shown in figure 42D. The fluorescence intensity upon PIBF binding decreased under oxidative stress conditions as compared to control lymphocytes bound to PIBF: around 20% in the fluid phase, 30% in the non-raft, 40% in the lipid raft and 50% in the gel phase. This means that PIBF binding to its receptor is reduced under oxidative stress conditions, which is significantly more reduced in lipid raft domains.

6- Discussion

6.1- Standardization of the two-photon technique

6.1.1- Standardization for model membranes

Model membranes, such as liposomes, are very useful for technique standardizations and membrane fluidity studies: the experimental fluidity values of artificial membranes composed by only one type of lipid can be easily compared with the fluidity properties of more complex lipid systems, like biological membranes. In order to standardize the two-photon microscopy technique we generated DPPC liposomes and analyzed their membrane fluidity at different temperatures (Fig. 13). This allowed us to obtain their transition curve (Fig. 14) and to determine the phase transition temperature (T_m) of these liposomes to compare it with previous data from the literature [119, 120]. The T_m is the temperature at which half of the phospholipid molecules have "transited" to the fluid phase whereas the other half still remains in the rigid, gel phase. The rapid decrease of rigidity shown by the *S* shaped curve obtained (Fig. 14), from 35ºC to 50ºC, and the value of the T_m obtained, 43ºC, is consistent with the T_m values described in the literature for DPPC liposomes [112-114]. Consequently, results shown in figures 13 and 14 prove that the standardization of two-photon microscopy in our laboratory was valid due to the fact that the present results are similar to those obtained by the authors above. In summary, in our hands the technique has been validated to analyze fluidity distribution in Laurdan stained model membranes.

6.1.2- Optimization for living cell samples

After two-photon microscopy was validated with liposomes, this technique was optimized for the study in living cells: macrophages and lymphocytes cell lines. This

optimization for living cells was performed for several parameters, that are listed below and that had to be adjusted:

1. Laurdan staining medium for living cell samples.

2. Optimal cellular cut section to be analyzed.

3. Agitation or not during Laurdan staining of living cell samples.

4. Number of consecutive images that can be obtained from a single plane due to a photobleaching effect.

5. Scan speed threshold to avoid image distortion.

6. Suitable probe concentration to obtain enough image fluorescence intensity.

7. Optimal image resolution to avoid altered membrane fluidity values.

All the above mentioned parameters were standardized, but the most critical parameter was the composition of the staining medium. A significant decrease in fluorescence emission of Laurdan-stained macrophages was observed as compared to emission intensity of DPPC liposomes. The presence of serum in the medium was the main experimental difference between both protocols. We then analyzed if the reduced Laurdan fluorescence intensity was due to the serum present in the medium. In the literature it has been shown that bovine serum albumin molecules present in serum are able to sequester hydrophobic molecules such as fluorescein dyes, probes, lipids and drugs, with similar structure to Laurdan. These probes cannot efficiently stain cellular membranes [121-123]. We evaluated Laurdan-stained cells in the presence and in the absence of serum. Our results showed that stained cells in medium without serum maintain the fluorescence of Laurdan compared to cells stained in medium with serum; therefore we attributed this fluorescence decrease to the presence of albumin in the serum during the 1h staining procedure.

6.2- Membrane fluidity distribution of THP-1 macrophages under oxidative stress conditions induced by H_2O_2

Following the optimization of two-photon microscopy for living cells, we applied this technique to analyze membrane fluidity distribution of control THP-1 macrophages and to compare our results with those described in the literature, in order to validate our membrane fluidity studies. Membrane fluidity distribution of our control macrophages (Fig. 22) was not the same to those obtained by Gaus *et al.* with THP-1 macrophages by using two-photon microscopy [124]. Plasma membrane fluidity of our THP-1 macrophages, obtained at physiological temperature (37ºC), was significantly higher when compared to fluidity obtained by Gaus *et al.* at 22ºC [124]. The temperature at which membrane fluidity is evaluated explains this difference, because plasma membrane fluidity significantly increases as temperature is increased [26].

Our results show that macrophages under oxidative stress undergo a H_2O_2 concentration dependent significant increase in the frequency of both rigid lipid domains: gel phase and raft domains. This is observed, in figure 22, as a shift of the fluidity curve towards the high GP zone that corresponds to these rigid domains. An induction of lipid raft formation by oxidative stress, similar to the observed in our *in vivo* results, has been previously described by Yang *et al.* in endothelial cells; nevertheless, these results were obtained from isolated detergent resistant membrane (DRM) preparations [125]. Yang *et al.* concluded that oxidative stress induces lipid raft formation for an efficient activation of the Akt signaling pathway, which is essential for the cell to survive oxidative stress [125].

In the present thesis we planned to generate a new tool, associated to two-photon microscopy, able to detect and evaluate lipid raft clustering. We therefore devised a novel software that analyzes lipid domain **size** and **number** from the previously

obtained GP images. The application of this analysis on macrophages under oxidative stress conditions demonstrated, for the first time with two-photon microscopy, that the increase of both raft and gel phase frequencies is attributable to a significant increase in the **number** of these rigid domains (Fig. 24B), whereas the mean **size** remains unaltered (Fig. 24A).

In order to compare lipid domain analysis results, we transformed pixels into metric units and defined a domain **size**. Our transformation allowed us to estimate the average domain **sizes** of approximately 170nm × 170nm for raft-like domains and 120nm × 120nm for gel phase domains. One of the characteristic of our microscope configuration is a spatial resolution of 100nm × 100nm, this means that any domain below this surface value cannot be detected. The **sizes** obtained by our transformation are within the accepted **size** range of lipid rafts, that may vary from 10nm up to 200nm, as reported in previous literature [126].

The increase in the **number** of lipid raft domains observed may be interpreted either as a consequence of a *de novo* condensation of domains with intermediate GP values, or as a coalescence of undetectable preexisting lipid rafts below the resolution of the microscope [43]. Our results show that clustering of detectable lipid domains does not occur, as their average **size** did not increase; nevertheless, as the technique is only able to distinguish large domains, above 100nm × 100nm, clustering of smaller domains might occur, giving rise to larger detectable domains that would account for the increase in visible domain **number**.

Data of macrophages under oxidative stress conditions have shown an increase in two kinds of lipid rigid domains: lipid rafts and gel-like domains. While the characteristics and behavior of lipid rafts have been extensively studied in the last fifteen years, the gel-like domains have more recently been subject of study. Goñi and

Alonso [127] have reviewed that gel-like domains are present in cellular membranes and are highly rigid ceramide-enriched domains. Ceramide (Cer) is a lipid precursor of sphingolipids that can be generated by *de novo* synthesis and/or by the enzyme acid sphingomyelinase (ASM) [128]. These kind of rigid domains are suggested to be involved in cell function such as in apoptosis [129].

As stated by Silva *et al*, ceramide *per se* is not able to induce neither the formation of large platforms in model membranes nor domain coalescence [130]. It has been proposed that, in complex systems like plasma membranes, gel-like Cer-enriched domains do not appear to exist as large platforms but, instead, they appear as small "islands" of gel phase [127]. This can explain the differences observed in our results which show that lipid rafts are larger in **size** than gel-like domains. We suggest that these gel-like domains could correspond, as indicated by their high GP values, at least partially to ceramide-enriched domains.

6.3- Assessment of macrophage plasma membrane lipid peroxidation in our oxidative stress conditions

This study has shown that oxidative stress modifies membrane fluidity (Fig. 22), which might be due to peroxidation of unsaturated fatty acid tails. We evaluated lipid peroxidation to assess the presence of structural modifications in macrophage membrane lipids under oxidative stress conditions.

Our results showed that oxidative stress significantly increased the levels of oxidized lipids within the macrophage plasma membrane, which means that lipid fatty acyl chains become structurally modified. This is consistent with a previous report showing that lipid peroxidation, induced by oxidative stress, decreases the fluidity of erythrocyte membranes [131]. Therefore, during oxidative conditions, lipids become

initially oxidized affecting physical membrane properties that could account for an increased rigidity.

6.4- Effect of oxidative stress on macrophage function

The relationship between plasma membrane modifications and cellular functions is essential for cellular homeostasis. The results above mentioned have shown that lipid peroxidation modifications, induced by oxidative stress, alter membrane fluidity in macrophages. We then analyzed if this decreased membrane fluidity observed in figure 22, can inhibit macrophage function.

Several authors have reported a decrease in cellular functions due to oxidative stress. Abraham *et al.* have described, in two different articles, that oxidative stress negatively affects proinflammatory responses, inhibiting TNFα production, of LPS activated neutrophils [132, 133]. In another study, Filosto *et al.* [68] analyzed the epidermal growth factor (EGF), a molecule involved in proliferation, differentiation and cellular migration in A549 adenocarcinoma cells, upon EGF binding to EGF-R. These authors [68] showed that, under oxidative stress, EGF-R signaling is inhibited due to an impaired receptor dimerization. Consequently, under oxidative stress A549 adenocarcinoma cells show impaired proliferation, differentiation and migration functions. However, Filosto *et al.* [68] also reported that oxidative stress activates a different ligand-independent signaling pathway [68] through c-Src, which is involved in survival, angiogenesis and invasion.

Another review, by Shackelford, Kaufmann and Paules, described that oxidative stress is able to inhibit cell division, which is essential for many biological processes, such as cell growth and immune response, in different cell types [134]. This inhibition leads the cell to enter an irreversible G_0 state (resting phase), which causes the cell not be able to divide under oxidative stress conditions. Studies by He *et al.* [135] observed a

reduced ATP production by mitochondria in retinal pigment epithelial cells under oxidative stress conditions, meaning that the ability of cells to produce ATP is altered, not allowing efficient homeostatic cell function. The studies described above confirm that under oxidative stress several crucial cell functions are impaired. In addition, our results further expand this fact, showing that macrophages are not activated efficiently under oxidative stress. This inefficient activation would cause macrophages to produce low levels of TNFα, which might cause an altered proinflammatory state.

One of the above articles by Abraham *et al.* [133], described that macrophages under oxidative stress secreted the same amount of TNFα as in non-oxidizing conditions. This differs from our results which show a significantly reduced TNFα production under oxidative stress conditions. This discrepancy, between Abraham *et al.* and our data, can be explained by the different oxidative stress conditions established: in our study, the oxidative stress conditions were induced by 0.5mM to 2mM H_2O_2 and by a long incubation period of 24h, while the conditions used by Abraham [133] were 0.05mM to 0.25mM H_2O_2 only for 4h.

To date, most of the oxidative stress studies analyze modifications of the protein compartment and/or the signaling pathways which involve receptors [66, 136, 137]. Many studies have observed, under oxidatives stress conditions, structural modifications of the cholinergic receptors [66], impaired coupling of the dopamine receptors [137] and reduced binding of aldosterone to mineralocorticoid receptor crucial for the regulation of cellular H_2O and Na^+ levels [136]. All these studies observed modifications that negatively affect receptor functions; nevertheless, as lipids are the preferential target for oxidative stress, it would have been desirable to evaluate membrane fluidity to gain insights in the role of membrane dynamics concerning these impaired receptor functions.

6.5- LPS-TLR2/4 binding and membrane dynamics in macrophages

Membrane fluidity is an important physicochemical property which is thought to be essential for an efficient receptor-ligand binding. Our results showed that upon LPS binding to its receptor, in living cells, macrophage plasma membrane becomes more fluid. As described in section 1.3 and 1.4, it is known that many receptors are distributed within lipid rafts while other receptors are specifically distributed in non-raft. Nevertheless, whereas the presence of receptors in lipid rafts has been extensively studied, very little is known about the biological importance of receptors within non-raft phases. Several authors [138-140] have shown, using detergent resistant membrane (DRMs) preparations, that non-activated TLR4 is distributed within the non-raft phases (fluid phases) of plasma membrane, while other non-activated members of the LPS-TLR4 complex, such as CD14, are distributed in lipid rafts.

It is generally accepted that the activation of receptors distributed in lipid rafts increases the abundance of lipid rafts. This aids cell function upon receptor-ligand binding [16, 19, 40-42]; an example of this occurs in the immunological synapse where the abundance of lipid rafts increases upon antigen presentation by MHC of antigen presenting cells to the TCR/CD3 complex in T-cells [43].

As non-activated TLR4 are distributed in fluid phase domains, an increase in abundance of these domains upon TLR4 activation would also be expected. Such increase in fluidity has been shown in figure 27, which has not been described previously in macrophages. The only data regarding the fluidification effect of LPS is in renal cortex cells by using fluorescence polarization [141]. Yosiba *et al*. [141] only analyzed average membrane fluidity and no further discussion was performed on significance of the fluidification effect on renal cortex cells. We show a more detailed evaluation of membrane fluidity as our methodology allows to determine fluidity

distribution and to quantify domain **size** and **number** across the entire macrophage plasma membrane. This confirms that, upon LPS binding, plasma membrane of macrophages increases in fluidity which might be necessary for cellular activation and secretion of cytokines.

Binding of LPS to TLR4 is a very complex mechanism which requires several stages. LPS, present in a soluble form, must be delivered by LPS binding protein (LBP) from the extracellular matrix to CD14, which is bound to a glycosylphosphatidylinositol (GPI) anchor in plasma membrane [70]. CD14 is able to separate the LPS-aggregates into LPS-monomers which can then be recognized by the TLR4 [70]. Several reports have demonstrated that TLR4, after stimulation with LPS, migrates from fluid phase to lipid rafts where CD14 is distributed [138-140]. This migration into lipid rafts would allow TLR4 to interact with CD14 to generate the TLR4/CD14 complex which induces intracellular signaling and leads to cytokine expression via NFκB signaling. These reports [138-140] were performed by using detergent resistant membrane (DRMs) preparations and did not provide information from living cells and how LPS binding can modify membrane fluidity. By contrast, in the present study it is shown, in living macrophages, a regionalized fluidification effect that might be necessary for an efficient activation and that might also be required for the migratory ability of TLR4 into lipid rafts.

Binding of TLR2/4 to LPS can lead to an endocytic pathway that internalizes the receptor complex bound to LPS. In order to internalization occur, membrane fusion is consequently necessary. It is generally accepted by many authors [142-144] that the higher is membrane fluidity, the more efficient membrane fusion occurs [145]. We suggest that fluidification of macrophage plasma membrane, induced by LPS binding, would be required for membrane fusion and internalization of TLR4 upon activation.

85

6.6- Effects of oxidative stress on membrane fluidity in LPS activated macrophages

In the literature there are no previous data associating membrane fluidity modifications, due to oxidative stress, and macrophage activation. In the present study we showed for the first time that LPS activated macrophages undergo a rigidifying effect due to oxidative stress. In the above sections, we have demonstrated a rigidification effect in macrophages under oxidative stress, which might be due to the following events: 1) direct fatty acid modifications which account for the increase in rigidity (Fig. 25), and/or 2) oxidative stress which causes an increase in the **number** of lipid rafts (Fig. 22). The rigidification might also be caused by the fact that: 3) receptor oxidative modifications inhibit receptor-ligand binding, and/or, 4) oxidized lipids inhibit the migratory ability of the TLR4 receptor.

LPS binding to macrophage receptors is the initial step in recognition leading to a proinflammatory response. If this initial binding does not occur efficiently, the proinflammatory response might develop in an inefficient manner. As membrane dynamics is crucial for many biological processes, it might be possible that the rigidification of the plasma membrane under oxidative stress, observed in our study, might cause this impaired macrophage activation, also detected.

6.7- Membrane fluidity distribution of MEC-1 lymphocytes under oxidative stress induced by H_2O_2

Lymphocytes are very important cells of the adaptive immune response and in immune regulation. Membrane fluidity distribution in this study with B-lymphocytes in non-oxidizing conditions, showed similar membrane fluidity values to those obtained with the cell line JCaM2 T-lymphocytes at $37^{o}C$ by Gaus *et al.* [43].

When MEC-1 B-lymphocytes were placed under oxidative stress conditions,

results showed an increase in rigidity of lymphocyte membranes (Fig. 33), in a similar manner to the results obtained in macrophage membranes under oxidative stress conditions (Fig. 22). The importance and the meaning of such rigidification effect in macrophages under oxidative stress have been discussed previously in section 6.2: this rationale underlying the rigidification effect can also be applied to lymphocytes.

Lipid domain analysis in this study showed that the increase in rigidity of lymphocyte membranes under oxidative stress was due to an increase in **number**, rather than in **size**, of rigid domains which is consistent with the results described above for macrophages, where an increase in raft domain **number** may be due to *de novo* synthesis of lipid rafts or due to clustering of small undetectable lipid rafts. Several studies have also reported an increase of lipid rafts by using detergent resistant membrane (DRM) preparations from endothelial and monocytic cells, previously placed under oxidative stress conditions [125, 146]. Cuschieri *et al.* [146] showed that under oxidative stress the expression of membrane CD16 in monocytic cells is upregulated, also in lipid rafts, thus altering the cytokine secretion pattern by the cell. Nevertheless, the experimental approach of these studies, by using DRMs, does not allow to evaluate if the observed increase in rigidity is due to an increase in **size** and/or **number** of lipid rafts.

6.8- Assessment of lymphocyte plasma membrane lipid peroxidation

We analyzed lipid peroxidation in order to assess if the rigidifying changes in membrane fluidity, induced by oxidative stress, were due to oxidized lipid in these membranes. We showed that oxidative stress significantly increased the levels of lipid peroxidation within the lymphocyte plasma membrane. Therefore, the rigidifying effect can be explained by the presence of lipid peroxidation. Similar results were also

obtained in macrophages and discussed previously in section 6.3. The rigidification effect during lipid peroxidation, has been attributed to the appearance of lipid derivatives with truncated acyl chains which contain aldehyde and hydroperoxide groups and to cross-linking of the lipid radicals [147].

6.9- PIBF-PIBF/R binding and membrane dynamics in lymphocytes

During pregnancy, cell function of the immune system is regulated to allow tolerance to the fetus. Without this regulation the immune system would initiate an immune response against the fetus that would impair pregnancy. Progesterone is essential as a regulatory molecule during pregnancy. Among the progesterone regulation mechanisms, the induction of the PIBF release modulates an anti-abortive effect. PIBF contributes to a Th2 dominant cytokine production by lymphocytes, a microenvironment necessary for pregnancy [85, 148, 149] and induces uNK cytokine regulatory functions. Hudic *et al*. [150] have shown that patients with low (50%) PIBF levels, compared to normal (100%) PIBF levels, experience recurrent spontaneous abortions. Under normal pregnancy conditions the concentration of PIBF continuously increases during gestation [151]. Check *et al.* [152] reported that the absence of PIBF in weeks 3rd - 5th of apparently normal pregnancies is associated with high miscarriage rate.

Binding of PIBF to its receptor, PIBF-R, is one of the crucial factors of a correct immune regulation for a successful pregnancy. Therefore, we analyzed membrane dynamics upon PIBF/PIBF-R binding and how oxidative stress modifies it. MEC-1 lymphocytes were used to investigate PIBF binding to PIBF-R. Upon PIBF binding to its receptor *in vivo* conditions, the membrane of lymphocytes becomes more rigid. An increase in rigidity caused by receptor-ligand interactions has also been described by Gaus *et al.* [43] in T-lymphocyte membranes after the interaction of CD3 with anti-

CD3-coated polystyrene beads by using two-photon microscopy. Larbi *et al.* [153] have also shown, by using detergent resistant membrane (DRM) preparations from T-lymphocytes activated with anti-CD3, an increase in rigidity. Another report by Gaus *et al.* [43] has described a rigidification process in cell-to-cell interactions. They also observed a frequency increase in rigid GP values, which means rigidification, at the site of formation of the immunological synapse in studies with T-lymphocytes and dendritic cells (DCs). In the present thesis we have been able, for the first time, to observe in individualized living cells, that the rigidity of lymphocyte plasma membrane is increased upon binding of PIBF to its receptor.

Moreover, our results from the lipid domain analysis demonstrated that, upon PIBF binding, the rigidification observed was due to lipid raft clustering, observed as an increase in domain **size**. A similar clustering effect has also been observed upon ligand binding to raft-preferring receptors, inducing large stabilized lipid rafts from small unstable rafts [40, 154, 155]. Lipid raft clustering has also been observed by Altrock *et al.* [156], by using conventional confocal microscopy, upon cellular adhesion in human acute myelogenous leukemia KG-1 myeloblasts mediated by fibronectin anchoring to the base of the plate [156]; it was concluded that lipid raft clustering is an essential process for an efficient adhesion of stem cells.

Results show that binding of PIBF to PIBF-R involves the action of lipid raft clustering for an efficient activation of the signaling pathway that leads to a Th2 cytokine expression.

6.10- Effect of oxidative stress on PIBF/PIBF-R binding and membrane fluidity in lymphocytes

No data are present in the literature describing a relationship between membrane fluidity modifications, due to oxidative stress, and PIBF binding. Our results showed

(Fig. 40) an increase in membrane fluidity as a consequence of oxidative stress in PIBF bound lymphocytes. We suggest that this increase in fluidity is due to direct oxidative receptor modifications that inhibit PIBF binding to its receptor and/or by oxidative modifications of lipid dynamics that consequently inhibit PIBF-PIBF/R binding.

Lipid domain analysis of lymphocytes in the presence of PIBF revealed that oxidative stress caused a drastic decrease in lipid raft clustering. These results indicate that oxidative stress produces modifications in plasma membrane dynamics that inhibits the ability of lipid rafts to form clusters upon receptor-ligand binding. This inhibition of the clustering effect might reduce PIBF signaling which in turn would not allow PIBF to regulate the immune system and consequently pregnancy would not proceed to term.

6.11- Lymphocyte membrane distribution of PIBF-PIBF/R binding under oxidative stress

One of the main aims of this thesis was to analyze the localization of PIBF receptor among the different lipid domains in order to understand how oxidative modifications of the specific lipid phases can affect ligand recognition. We devised additional new software to quantify the distribution of PIBF bound to its receptor in the different lipid domains. It is shown that PIBF bound to its receptor is mainly distributed in lipid rafts and that oxidative stress induced modifications that had the most pronounced decrease in binding of PIBF within these lipid domains.

The preferential distribution of PIBF/PIBF-R in MEC-1 lymphocyte lipid rafts is not surprising as Kozma *et al.* [1] showed in peripheral blood lymphocytes that PIBF-R is a GPI anchored receptor located in these type of lipid domains. Interestingly, the GPI anchored family of receptors is well known to be highly associated to lipid rafts [157, 158]. As PIBF-R is mainly distributed in lipid rafts, upon PIBF binding a clustering effect is expected, which was confirmed by the lipid domain analysis (Fig. 38).

Our results showed that oxidative stress: decreased the binding of PIBF to its receptor by 40% and simultaneously increased fluidity of lymphocyte plasma membranes. The reduced binding can be interpreted as: 1) a structural modification of PIBF-R, due to oxidative stress and/or 2) a disruption of lipid raft formation or clustering necessary for intracellular signaling. In both cases it would be expected an inhibition of a cytokine profile compatible with gestation.

6.12- Comparative analysis of lipid membrane composition and fluidity in macrophages and lymphocytes

From the information obtained in the present study, a comparative analysis can be drawn of plasma membrane fluidity of two very important types of cells in the immune system. We have described that control macrophages have substantially more fluid membrane when compared to control lymphocytes. It is not unexpected that under physiological conditions both cells have different plasma membrane fluidities, as the key element in determining membrane fluidity is the fatty acid composition of lipid components, as described in section 1.2. We can therefore assume that membrane fluidity differences between macrophages and lymphocytes, observed in our results, are due to differences in lipid composition. One of the most abundant fatty acids, in both macrophages and lymphocytes, is palmitic acid: 43% of fatty acids being palmitic in lymphocytes while only 34% in macrophages [6], the presence of these saturated fatty acid is directly correlated to membrane rigidity. The second most abundant fatty acid in both cells is the monounsaturated oleic acid. This fatty acid is present in large amounts in macrophage membranes (25%) while in lymphocytes it is only present at 18% [6]; this correlates to our results as oleic acyl chains are associated with increased fluidity. These differences in lipid composition help us to understand the difference between membrane fluidities of both cells.

Interestingly, our results on receptor-ligand interaction effect on membrane fluidity varied greatly between the two cell types, macrophages and lymphocytes. Upon receptor-ligand binding, macrophages became more fluid while lymphocytes became more rigid. It is generally accepted that upon receptor-ligand binding, a clustering effect of lipid rafts occurs which aids receptor signaling. The data obtained in our study suggests that lipid raft clustering may occur only for certain receptor-ligand interactions, such as the PIBF binding, but in other receptor-ligand interactions, such as LPS binding in macrophages, lipid raft clustering may not occur.

*Table 1. **Fatty acids comparison between macrophages and lymphocytes.***

	Macrophages	*Lymphocytes*
Palmitic acid (Induces rigidity)	34%	43%
Oleic acid (Induces fluidity)	25%	18%

Data obtained from C.R. Felippe et al. (1997) [6].

Our results show how membrane modifications due to oxidative stress can affect cellular functions in cells of the immune system, although our findings could be applied to many other cells through the entire body: an universal phenomenon that could probably be reproduced in all types of cells: neuronal, epithelial, etc. When cells are placed under oxidative stress, lipids in the plasma membrane are modified, which would in turn cause an impaired cellular response, as demonstrated by our studies in macrophages.

6.13- Concluding model proposal

In summary, the reaction to oxidative stress of macrophages and lymphocytes upon receptor-ligand binding is completely different. Macrophage plasma membrane needs to be fluid for phagocytosis and becomes rigidified (Fig. 42), while activated lymphocytes develop lipid raft clustering in plasma membrane for signal transduction and cytokine secretion, but oxidizing conditions disturbs the lipid raft clustering.
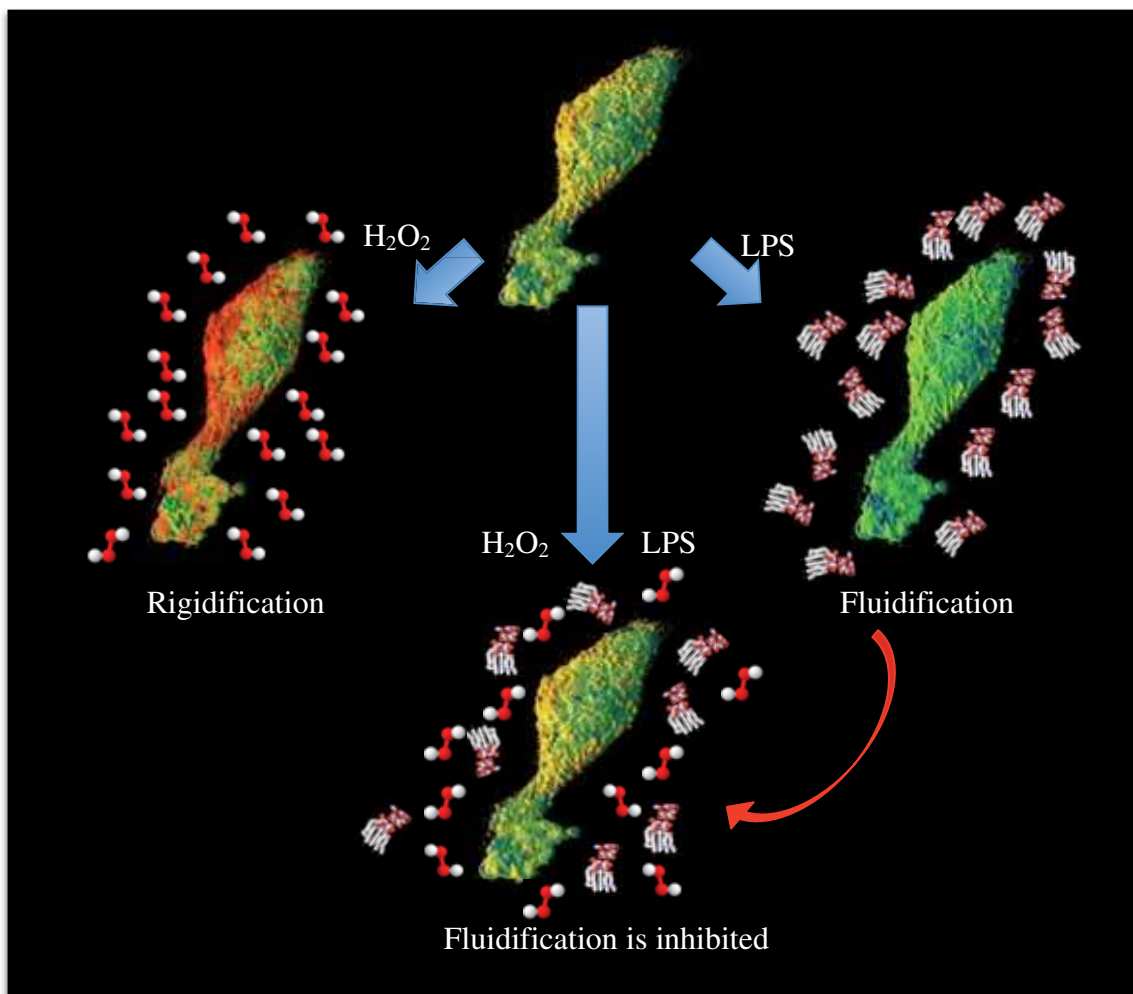
*Figure 43. **Macrophage membrane fluidity changes.** 3D representation of macrophage membrane fluidity changes with: H_2O_2, LPS and H_2O_2 + LPS.*
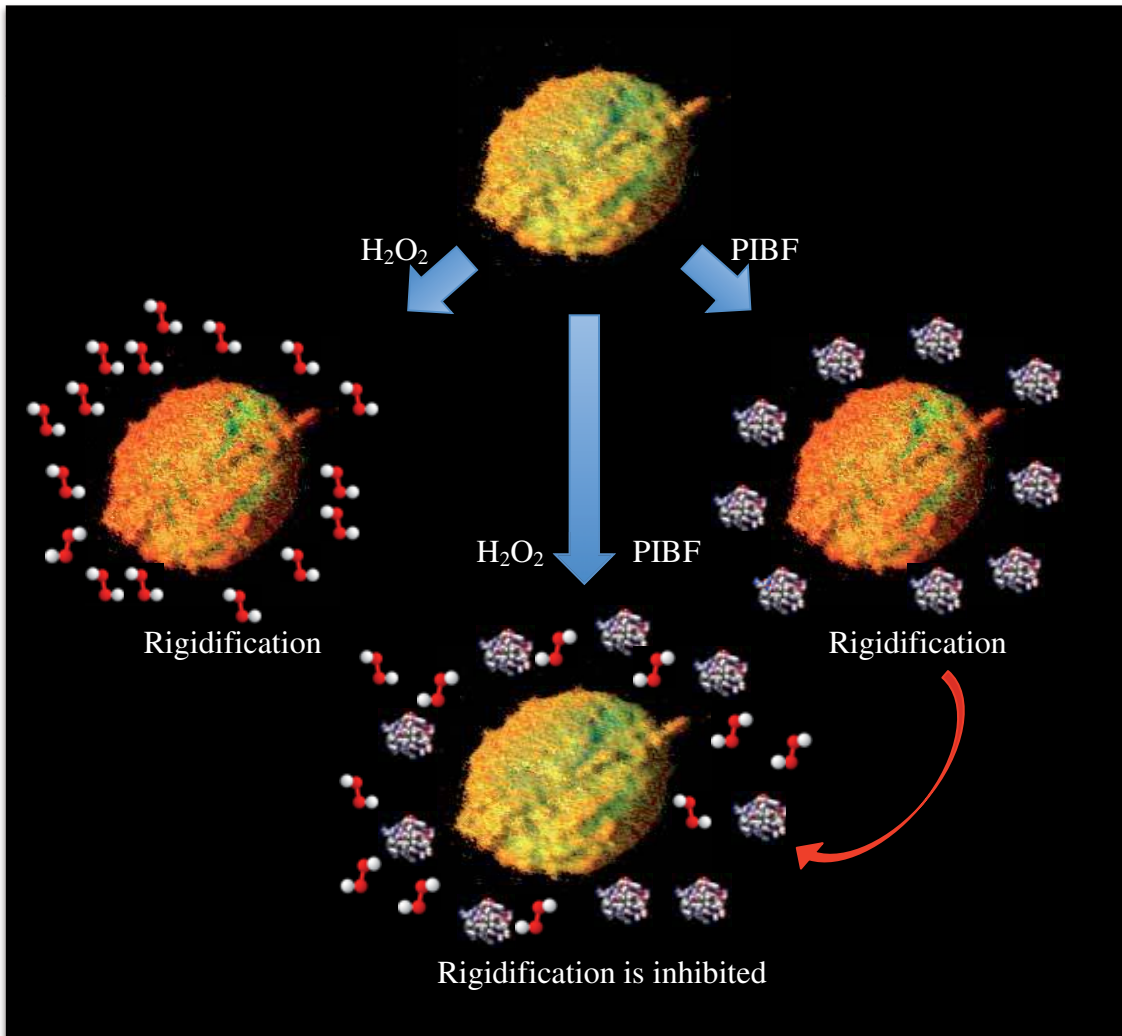
*Figure 44. **Lymphocyte membrane fluidity changes.** 3D representation of lymphocyte membrane fluidity with: H_2O_2, PIBF and H_2O_2 + PIBF.*

7- Conclusions

1. Under oxidative stress conditions, THP-1 macrophage plasma membrane shows significant levels of lipid peroxidation and becomes rigidified, with an increase in the **number** of lipid raft and gel phase domains at the expense of the fluid phase.

2. LPS induces fluidification of plasma membrane in THP-1 activated macrophages by decreasing the **number** of lipid raft and gel phase domains. However, under oxidative stress this fluidification is lost.

3. Macrophage inflammatory response ability, induced by LPS, was evaluated through the secretion of TNF-α. This ability is significantly reduced under oxidative stress conditions, as compared to LPS-activated macrophages without oxidative stress.

4. Under oxidative stress, MEC-1 lymphocyte plasma membrane shows significant levels of lipid peroxidation and becomes rigidified, with an increase in the **number** of lipid raft and gel phase domains, but not in the **size**.

5. Receptor-ligand binding in case of PIBF/PIBF-R induces rigidification of lymphocyte plasma membrane, with an increase in the **size** of lipid raft and gel phase domains, indicating a domain clustering effect. However, under oxidative stress, lipid raft clustering, which is important for cellular signaling, is inhibited.

6. PIBF/PIBF-R binding, under oxidative stress conditions, significantly decreases in all kinds of lipid domains, but mainly in lipid rafts and gel phase domains.

8- References

[1]   N. Kozma, M. Halasz, B. Polgar, T. G. Poehlmann, U. R. Markert, T. Palkovics, M. Keszei, G. Par, K. Kiss, J. Szeberenyi, L. Grama and J. Szekeres-Bartho (2006) Progesterone-induced blocking factor activates STAT6 via binding to a novel IL-4 receptor. *Journal of Immunology* 176(2): 819-26

[2]   L. A. O'Neill, D. Golenbock and A. G. Bowie (2013) The history of Toll-like receptors - redefining innate immunity. *Nature Reviews: Immunology* 13(6): 453-60

[3]   N. Mimica-Dukic, N. Simin, E. Svircev, D. Orcic, I. Beara, M. Lesjak and B. Bozin (2012) Lipid Peroxidation. Ch 9 The Effect of Plant Secondary Metabolites on Lipid Peroxidation and Eicosanoid Pathway. *InTech* (1):193-210

[4]   N. Bellance, P. Lestienne and R. Rossignol (2009) Mitochondria: from bioenergetics to the metabolic regulation of carcinogenesis. *Frontiers in Bioscience* 14:4015-34

[5]   D. A. Brown (2006) Lipid rafts, detergent-resistant membranes, and raft targeting signals. *Physiology* 21:430-39

[6]   C. R. Felippe, P. C. Calder, M. G. Vecchia, M. R. Campos, J. Mancini-Filho, E. A. Newsholme and R. Curi (1997) Fatty acid composition of lymphocytes and macrophages from rats fed fiber-rich diets: a comparison between oat bran- and wheat bran-enriched diets. *Lipids* 32(6):587-91

[7]   S. Degroote, J. Wolthoorn and G. van Meer (2004) The cell biology of glycosphingolipids. *Seminars in Cell and Developmental Biology* 15(4):375-87

[8]   L. J. Johnston (2007) Nanoscale imaging of domains in supported lipid membranes. *Langmuir* 23(11):5886-95

[9]   D. R. V. Gerrit van Meer and Gerald W. Feigenson (2008) Membrane lipids: where they are and how they behave. *Nature Reviews: Molecular Cell Biology* 9(2):112-124

[10]   M. Sud, E. Fahy, D. Cotter, A. Brown, E. A. Dennis, C. K. Glass, A. H. Merrill, Jr., R. C. Murphy, C. R. Raetz, D. W. Russell and S. Subramaniam (2007) LMSD: LIPID MAPS structure database. *Nucleic Acids Research* 35:527-32

[11]   G. van Meer (2005) Cellular lipidomics. *EMBO Journal* 24(18):3159-65

[12]   S. J. Singer and G. L. Nicolson (1972) The fluid mosaic model of the structure of cell membranes. *Science* 175(4023):720-31

References

[13]   F. M. Goñi (2014) The basic structure and dynamics of cell membranes: an update of the Singer-Nicolson model. *Biochimica et Biophysica Acta* 1838(6):1467-76

[14]   G. L. Nicolson (2014) The Fluid-Mosaic Model of Membrane Structure: still relevant to understanding the structure, function and dynamics of biological membranes after more than 40 years. *Biochimica et Biophysica Acta* 1838(6):1451-66

[15]   L. J. Pike (2006) Rafts defined: a report on the Keystone Symposium on Lipid Rafts and Cell Function. *Journal of Lipid Research* 47(7):1597-98

[16]   K. Simons and J. L. Sampaio (2011) Membrane organization and lipid rafts. *Cold Spring Harbor Perspectives in Biology* 3(10):a004697

[17]   D. M. Owen, A. Magenau, D. Williamson and K. Gaus (2012) The lipid raft hypothesis revisited--new insights on raft composition and function from super-resolution fluorescence microscopy. *Bioessays* 34(9):739-47

[18]   D. M. Owen, A. Magenau, D. Williamson and K. Gaus (2012) The lipid raft hypothesis revisited. New insights on raft composition and function from super-resolution fluorescence microscopy. *Bioessays* 34(9):739-47

[19]   B. P. Head, H. H. Patel and P. A. Insel (2014) Interaction of membrane/lipid rafts with the cytoskeleton: impact on signaling and function: membrane/lipid rafts, mediators of cytoskeletal arrangement and cell signaling. *Biochimica et Biophysica Acta* 1838(2):532-45

[20]   G. R. Chichili and W. Rodgers (2009) Cytoskeleton-membrane interactions in membrane raft structure. *Cellular and Molecular Life Sciences* 66(14):2319-28

[21]   J. A. Lundbaek (2006) Regulation of membrane protein function by lipid bilayer elasticity-a single molecule technology to measure the bilayer properties experienced by an embedded protein. *Journal of physics: Condensed matter* 18(28):S1305-44

[22]   M. O. Jensen and O. G. Mouritsen (2004) Lipids do influence protein function-the hydrophobic matching hypothesis revisited. *Biochimica et Biophysica Acta* 1666(1-2):205-26

[23]   O. S. Andersen (2013) Membrane proteins: Through thick and thin. *Nature Chemical Biology* 9(11):667-68

[24]   J. Kaur and S. N. Sanyal (2010) Alterations in membrane fluidity and dynamics in experimental colon cancer and its chemoprevention by diclofenac. *Molecular and Cellular Biochemistry* 341(1-2):99-108

[25]   G. Lenaz (1987) Lipid fluidity and membrane protein dynamics. *Bioscience Reports* 7(11):823-37

[26] K. Gaus, E. Gratton, E. P. Kable, A. S. Jones, I. Gelissen, L. Kritharides and W. Jessup (2003) Visualizing lipid structure and raft domains in living cells with two-photon microscopy. *Proceedings of the National Academy of Sciences of the United States of America* 100(26):15554-59

[27] G. M'Baye, Y. Mely, G. Duportail and A. S. Klymchenko (2008) Liquid ordered and gel phases of lipid bilayers: fluorescent probes reveal close fluidity but different hydration. *Biophysical Journal* 95(3):1217-25

[28] D. M. Owen and K. Gaus (2013) Imaging lipid domains in cell membranes: the advent of super-resolution fluorescence microscopy. *Front in Plant Science* 4:503

[29] W. Stilwell (2013) An Introduction to Biological Membranes: From Bilayers to Rafts. Ch 3 Membrane Lipids: Fatty Acids. *ELSEVIER* 1st Ed:43-56

[30] R. B. Gennis (1989) Biomembranes: Molecular Structure and Function. Ch 2 The Structures and Properties of Membrane Lipids. *Springer* 1st Ed:36-84

[31] P. L. Yeagle (2013) The structure of Bological Membranes. Ch 1 Introduction to Lipid Bilayers. *CRC Press* 3rd Ed:1-6

[32] P. Kuo, M. Weinfeld, M. A. Rudd, P. Amarante and J. Loscalzo (1990) Plasma membrane enrichment with cis-unsaturated fatty acids enhances LDL metabolism in U937 monocytes. *Arteriosclerosis* 10(1):111-18

[33] H. J. Heipieper, F. Meinhardt and A. Segura (2003) The cis-trans isomerase of unsaturated fatty acids in Pseudomonas and Vibrio: biochemistry, molecular biology and physiological function of a unique stress adaptive mechanism. *FEMS Microbiology Letters* 229(1):1-7

[34] P. V. Escriba, P. B. Wedegaertner, F. M. Goñi and O. Vogler (2007) Lipid-protein interactions in GPCR-associated signaling. *Biochimica et Biophysica Acta* 1768(4):836-52

[35] R. Alemany, J. S. Perona, J. M. Sanchez-Dominguez, E. Montero, J. Canizares, R. Bressani, P. V. Escriba and V. Ruiz-Gutierrez (2007) G protein-coupled receptor systems and their lipid environment in health disorders during aging. *Biochimica et Biophysica Acta* 1768(4):964-75

[36] T. S. Tillman and M. Cascio (2003) Effects of membrane lipids on ion channel structure and function. *Cell Biochemistry and Biophysics* 38(2):161-90

[37] U. Coskun and K. Simons (2011) Cell membranes: the lipid perspective. *Structure* 19(11):1543-48

[38] K. Boesze-Battaglia and R. Schimmel (1997) Cell membrane lipid composition and distribution: implications for cell function and lessons learned from photoreceptors and platelets. *Journal of Experimental Biology* 200(23):2927-36

[39]   P. V. Escriba, J. M. Gonzalez-Ros, F. M. Goñi, P. K. Kinnunen, L. Vigh, L. Sanchez-Magraner, A. M. Fernandez, X. Busquets, I. Horvath and G. Barcelo-Coblijn (2008) Membranes: a meeting point for lipids, proteins and therapies. *Journal of Cellular and Molecular Medicine* 12(3):829-75

[40]   U. Coskun and K. Simons (2010) Membrane rafting: from apical sorting to phase segregation. *FEBS Letters* 584(9):1685-93

[41]   L. J. Pike (2009) The challenge of lipid rafts. *Journal of Lipid Research* 50:323.28

[42]   K. Jacobson, O. G. Mouritsen and R. G. Anderson (2007) Lipid rafts: at a crossroad between cell biology and physics. *Nature Cell Biology* 9(1):7-14

[43]   K. Gaus, E. Chklovskaia, B. Fazekas de St Groth, W. Jessup and T. Harder (2005) Condensation of the plasma membrane at the site of T lymphocyte activation. *Journal of Cell Biology* 171(1):121-31

[44]   L. A. Bagatolli, J. H. Ipsen, A. C. Simonsen and O. G. Mouritsen (2010) An outlook on organization of lipids in membranes: searching for a realistic connection with the organization of biological membranes. *Progress in Lipid Research* 49(4):378-89

[45]   G. Radeva and F. J. Sharom (2004) Isolation and characterization of lipid rafts with different properties from RBL-2H3 (rat basophilic leukaemia) cells. *Biochemical Journal* 380(1):219-30

[46]   L. J. Pike, X. Han, K. N. Chung and R. W. Gross (2002) Lipid rafts are enriched in arachidonic acid and plasmenylethanolamine and their composition is independent of caveolin-1 expression: a quantitative electrospray ionization/mass spectrometric analysis. *Biochemistry* 41(6):2075-88

[47]   L. Rajendran, S. Le Lay and H. Illges (2007) Raft association and lipid droplet targeting of flotillins are independent of caveolin. *Biological Chemistry* 388(3):307-14

[48]   T. Lang (2007) SNARE proteins and "membrane rafts". *Journal of Physiology* 585(3):693-98

[49]   S. Sonnino and A. Prinetti (2008) Membrane lipid domains and membrane lipid domain preparations: are they the same thing ? *Thends in Glycoscience and Glycotechnolgie* 20(116):315-340

[50]   H. Gallala and K. Sandhoff (2008) Principles of microdomain formation in biological membranes- Are there lipid liquid ordered domains in living cellular membranes ? *Trends in Glycoscience and Glycotechnologie* 20(116):277-95

[51]   D. Lichtenberg, F. M. Goñi and H. Heerklotz (2005) Detergent-resistant membranes should not be identified with membrane rafts. *Trends in Biochemical Sciences* 30(8):430-36

[52] H. Sies (1997) Oxidative stress: oxidants and antioxidants. *Experimental Physiology* 82(2):291-95

[53] A. Meister (1994) Glutathione-ascorbic acid antioxidant system in animals. *Journal of Biological Chemistry* 269(13):9397-400

[54] V. Lobo, A. Patil, A. Phatak and N. Chandra (2010) Free radicals, antioxidants and functional foods: Impact on human health. *Pharmacognosy Reviews* 4(8):118-26

[55] O. Blokhina, E. Virolainen and K. V. Fagerstedt (2003) Antioxidants, oxidative damage and oxygen deprivation stress: a review. *Annals of Botany* 91:179-94

[56] S. Estany, J. R. Palacio, R. Barnadas, M. Sabes, A. Iborra and P. Martinez (2007) Antioxidant activity of N-acetylcysteine, flavonoids and alpha-tocopherol on endometrial cells in culture. *Journal of Reproductive Immunology* 75(1):1-10

[57] N. Makino, K. Sasaki, K. Hashida and Y. Sakakura (2004) A metabolic model describing the H2O2 elimination by mammalian cells including H2O2 permeation through cytoplasmic and peroxisomal membranes: comparison with experimental data. *Biochimica et Biophysica Acta* 1673(3):149-59

[58] J. M. Slauch (2011) How does the oxidative burst of macrophages kill bacteria? Still an open question. *Molecular Microbiology* 80(3):580-83

[59] R. G. Knowles and S. Moncada (1994) Nitric oxide synthases in mammals. *Biochemical Journal* 298(2):249-58

[60] E. Galea and D. L. Feinstein (1999) Regulation of the expression of the inflammatory nitric oxide synthase (NOS2) by cyclic AMP. *FASEB Journal* 13(15):2125-37

[61] B. Rada and T. L. Leto (2008) Oxidative innate immune defenses by Nox/Duox family NADPH oxidases. *Contributions to Microbiology* 15(1):164-87

[62] M. Freitas, J. L. Lima and E. Fernandes (2009) Optical probes for detection and quantification of neutrophils' oxidative burst. A review. *Analytica Chimica Acta* 649(1):8-23

[63] B. Uttara, A. V. Singh, P. Zamboni and R. T. Mahajan (2009) Oxidative stress and neurodegenerative diseases: a review of upstream and downstream antioxidant therapeutic options. *Current Neuropharmacology* 7(1):65-74

[64] B. Halliwell (1994) Free radicals, antioxidants, and human disease: curiosity, cause, or consequence? *Lancet* 344(8924):721-24

[65]   J. H. Houtgraaf, J. Versmissen and W. J. van der Giessen (2006) A concise review of DNA damage checkpoints and repair in mammalian cells. *Cardiovascular Revascularization Medicine* 7(3):165-72

[66]   Z. Z. Guan (2008) Cross-talk between oxidative stress and modifications of cholinergic and glutaminergic receptors in the pathogenesis of Alzheimer's disease. *Acta Pharmacologica Sinica* 29(7):773-80

[67]   W. Jun-Feng and T. Hua (2013) Oxidative protein modification of soluble N-ethylmaleimide-sensitive factor attachment protein receptors. *FASEB Journal* 27(1):890.7

[68]   S. Filosto, E. M. Khan, E. Tognon, C. Becker, M. Ashfaq, T. Ravid and T. Goldkorn (2011) EGF receptor exposed to oxidative stress acquires abnormal phosphorylation and aberrant activated conformation that impairs canonical dimerization. *PloS One* 6(8):e23240

[69]   H. Kumar, T. Kawai and S. Akira (2011) Pathogen recognition by the innate immune system. *International Reviews of Immunology* 30(1):16-34

[70]   B. S. Park and J. O. Lee (2013) Recognition of lipopolysaccharide pattern by TLR4 complexes. *Experimental and Molecular Medicine* 45(12):e66

[71]   A. M. Mowat and W. W. Agace (2014) Regional specialization within the intestinal immune system. *Nature Reviews: Immunology* 14(10):667-85

[72]   D. R. Bainbridge (2000) Evolution of mammalian pregnancy in the presence of the maternal immune system. *Reviews of Reproduction* 5(2):67-74

[73]   U. Kammerer, M. von Wolff and U. R. Markert (2004) Immunology of human endometrium. *Immunobiology* 209(7):569-74

[74]   M. J. van den Heuvel, S. Chantakru, X. Xuemei, S. S. Evans, F. Tekpetey, P. A. Mote, C. L. Clarke and B. A. Croy (2005) Trafficking of circulating pro-NK cells to the decidualizing uterus: regulatory mechanisms in the mouse and human. *Immunological Investigations* 34(3):273-93

[75]   S. Kalkunte, C. O. Chichester, F. Gotsch, C. L. Sentman, R. Romero and S. Sharma (2008) Evolution of non-cytotoxic uterine natural killer cells. *American Journal of Reproductive Immunology* 59(5):425-32

[76]   J. K. Riley (2008) Trophoblast immune receptors in maternal-fetal tolerance. *Immunological Investigations* 37(5):395-426

[77]   S. J. Renaud and C. H. Graham (2008) The role of macrophages in utero-placental interactions during normal and pathological pregnancy. *Immunological Investigations* 37(5):535-64

[78]   A. Rapacz-Leonard, M. Dabrowska and T. Janowski (2014) Major histocompatibility complex I mediates immunological tolerance of the trophoblast during pregnancy and may mediate rejection during parturition. *Mediators of Inflammation* 2014:579279

[79]   I. L. Sargent, A. M. Borzychowski and C. W. Redman (2006) NK cells and human pregnancy--an inflammatory view. *Trends in Immunology* 27(9):399-404

[80]   L. Fainboim and L. Arruvito (2011) Mechanisms involved in the expansion of Tregs during pregnancy: role of IL-2/STAT5 signalling. *Journal of Reproductive Immunology* 88(2):93-98

[81]   J. S. Hunt, M. G. Petroff, R. H. McIntire and C. Ober (2005) HLA-G and immune tolerance in pregnancy. *FASEB Journal* 19(7):681-93

[82]   L. Lynge Nilsson, S. Djurisic and T. V. Hviid (2014) Controlling the Immunological Crosstalk during Conception and Pregnancy: HLA-G in Reproduction. *Frontiers in Immunology* 5:198

[83]   C. Dosiou and L. C. Giudice (2005) Natural killer cells in pregnancy and recurrent pregnancy loss: endocrine and immunologic perspectives. *Endocrine Reviews* 26(1):44-62

[84]   R. Raghupathy, E. Al-Mutawa, M. Al-Azemi, M. Makhseed, F. Azizieh and J. Szekeres-Bartho (2009) Progesterone-induced blocking factor (PIBF) modulates cytokine production by lymphocytes from women with recurrent miscarriage or preterm delivery. *Journal of Reproductive Immunology* 80(1-2):91-99

[85]   J. Szekeres-Bartho, A. Barakonyi, B. Polgar, G. Par, Z. Faust, T. Palkovics and L. Szereday (1999) The role of gamma/delta T cells in progesterone-mediated immunomodulation during pregnancy: a review. *American Journal of Reproductive Immunology* 42(1):44-48

[86]   J. Szekeres-Bartho, Z. Faust and P. Varga (1995) The expression of a progesterone-induced immunomodulatory protein in pregnancy lymphocytes. *American Journal of Reproductive Immunology* 34(6):342-48

[87]   J. Szekeres-Bartho, A. Barakonyi, G. Par, B. Polgar, T. Palkovics and L. Szereday (2001) Progesterone as an immunomodulatory molecule. *International Immunopharmacology* 1(6):1037-48

[88]   I. Hudic and Z. Fatusic (2009) Progesterone - induced blocking factor (PIBF) and Th(1)/Th(2) cytokine in women with threatened spontaneous abortion. *Journal of Perinatal Medicine* 37(4):338-42

[89]   M. Dykstra, A. Cherukuri, H. W. Sohn, S. J. Tzeng and S. K. Pierce (2003) Location is everything: lipid rafts and immune cell signaling. *Annual Review of Immunology* 21:457-81

[90]   G. Szabo, A. Dolganiuc, Q. Dai and S. B. Pruett (2007) TLR4, ethanol, and lipid rafts: a new mechanism of ethanol action with implications for other receptor-mediated effects. *Journal of Immunology* 178(3):1243-49

[91]   E. C. Jury, F. Flores-Borja and P. S. Kabouridis (2007) Lipid rafts in T cell signalling and disease. *Seminars in Cell and Developmental Biology* 18(5):608-15

[92]   V. Horejsi, K. Drbal, M. Cebecauer, J. Cerny, T. Brdicka, P. Angelisova and H. Stockinger (1999) GPI-microdomains: a role in signalling via immunoreceptors. *Immunology Today* 20(8):356-61

[93]   I. Parolini, S. Topa, M. Sorice, A. Pace, P. Ceddia, E. Montesoro, A. Pavan, M. P. Lisanti, C. Peschle and M. Sargiacomo (1999) Phorbol ester-induced disruption of the CD4-Lck complex occurs within a detergent-resistant microdomain of the plasma membrane. Involvement of the translocation of activated protein kinase C isoforms. *Journal of Biological Chemistry* 274(20):14176-87

[94]   A. Arcaro, C. Gregoire, N. Boucheron, S. Stotz, E. Palmer, B. Malissen and I. F. Luescher (2000) Essential role of CD8 palmitoylation in CD8 coreceptor function. *Journal of Immunology* 165(4):2068-76

[95]   A. Stacchini, M. Aragno, A. Vallario, A. Alfarano, P. Circosta, D. Gottardi, A. Faldella, G. Rege-Cambrin, U. Thunberg, K. Nilsson and F. Caligaris-Cappio (1999) MEC1 and MEC2: two new cell lines derived from B-chronic lymphocytic leukaemia in prolymphocytoid transformation. *Leukemia Research* 23(2):127-36

[96]   E. H. Pap, G. P. Drummen, V. J. Winter, T. W. Kooij, P. Rijken, K. W. Wirtz, J. A. Op den Kamp, W. J. Hage and J. A. Post (1999) Ratio-fluorescence microscopy of lipid oxidation in living cells using C11-BODIPY(581/591). *FEBS Letters* 453(3):278-82

[97]   G. P. Drummen, L. C. van Liebergen, J. A. Op den Kamp and J. A. Post (2002) C11-BODIPY(581/591), an oxidation-sensitive fluorescent lipid peroxidation probe: (micro)spectroscopic characterization and validation of methodology. *Free Radical Biology and Medicine* 33(4):473-90

[98]   E. H. Pap, G. P. Drummen, J. A. Post, P. J. Rijken and K. W. Wirtz (2000) Fluorescent fatty acid to monitor reactive oxygen in single cells. *Methods in Enzymology* 319(1):603-12

[99]   D. M. Owen, K. Gaus, A. I. Magee and M. Cebecauer (2010) Dynamic organization of lymphocyte plasma membrane: lessons from advanced imaging methods. *Immunology* 131(1):1-8

[100]   D. Marguet, P. F. Lenne, H. Rigneault and H. T. He (2006) Dynamics in the plasma membrane: how to combine fluidity and order. *EMBO Journal* 25(15):3446-57

[101] A. P. Demchenko, Y. Mely, G. Duportail and A. S. Klymchenko (2009) Monitoring biophysical properties of lipid membranes by environment-sensitive fluorescent probes. *Biophysical Journal* 96(9):3461-70

[102] T. Parasassi, E. Gratton, W. M. Yu, P. Wilson and M. Levi (1997) Two-photon fluorescence microscopy of laurdan generalized polarization domains in model and natural membranes. *Biophysical Journal* 72(6):2413-29

[103] L. A. Bagatolli (2006) To see or not to see: lateral organization of biological membranes and fluorescence microscopy. *Biochimica et Biophysica Acta* 1758(10):1541-56

[104] L. A. Bagatolli and E. Gratton (2000) Two photon fluorescence microscopy of coexisting lipid domains in giant unilamellar vesicles of binary phospholipid mixtures. *Biophysical Journal* 78(1):290-305

[105] L. A. Bagatolli and E. Gratton (1999) Two-photon fluorescence microscopy observation of shape changes at the phase transition in phospholipid giant unilamellar vesicles. *Biophysical Journal* 77(4):2090-101

[106] L. A. Bagatolli, S. A. Sanchez, T. Hazlett and E. Gratton (2003) Giant vesicles, Laurdan, and two-photon fluorescence microscopy: evidence of lipid lateral separation in bilayers. *Methods in Enzymology* 360:481-500

[107] K. Gaus, S. Le Lay, N. Balasubramanian and M. A. Schwartz (2006) Integrin-mediated adhesion regulates membrane order. *Journal of Cell Biology* 174(5):725-34

[108] W. Yu, P. T. So, T. French and E. Gratton (1996) Fluorescence generalized polarization of cell membranes: a two-photon scanning microscopy approach. *Biophysical Journal* 70(2):626-36

[109] P. N. Dean (2001) Confocal microscopy: principles and practices. *Current protocols in cytometry* Chapter 2:Unit 2-8.

[110] P. T. So, C. Y. Dong, B. R. Masters and K. M. Berland (2000) Two-photon excitation fluorescence microscopy. *Annual Review of Biomedical Engineering* 2:399-429

[111] K. Gaus, T. Zech and T. Harder (2006) Visualizing membrane microdomains by Laurdan 2-photon microscopy. *Molecular Membrane Biology* 23(1):41-48

[112] D. Marsh (1990) CRC handbook of lipid bilayers. *CRC press.* 2nd Ed

[113] R. Koynova and M. Caffrey (1998) Phases and phase transitions of the phosphatidylcholines. *Biochimica et Biophysica Acta* 1376:91-145

[114] M. Caffrey (1993) NIST Standard Reference Database 34, Lipid thermotropic phase transition database (LIPIDAT). (http://www.lipidat.chemistry.ohio-state.edu). *Book NIST Standard Reference Database 34, Lipid thermotropic phase transition database (LIPIDAT). (*http://www.lipidat.chemistry.ohio-state.edu): Version 1

[115] T. Parasassi, G. Ravagnan, R. M. Rusch and E. Gratton (1993) Modulation and dynamics of phase properties in phospholipid mixtures detected by Laurdan fluorescence. *Photochemistry and Photobiology* 57(3):403-10

[116] M. M. Dodes Traian, F. L. Gonzalez Flecha and V. Levi (2012) Imaging lipid lateral organization in membranes with C-laurdan in a confocal microscope. *Journal of Lipid Research* 53(3):609-16

[117] C. Dietrich, L. A. Bagatolli, Z. N. Volovyk, N. L. Thompson, M. Levi, K. Jacobson and E. Gratton (2001) Lipid rafts reconstituted in model membranes. *Biophysical Journal* 80(3):1417-28

[118] L. A. Bagatolli, T. Parasassi and E. Gratton (2000) Giant phospholipid vesicles: comparison among the whole lipid sample characteristics using different preparation methods: a two photon fluorescence microscopy study. *Chemistry and Physics of Lipids* 105(2):135-47

[119] K. N. Barton, M. M. Buhr and J. S. Ballantyne (1999) Effects of urea and trimethylamine N-oxide on fluidity of liposomes and membranes of an elasmobranch. *American Journal of Physiology* 276(2):397-406

[120] U. Subuddhi and A. K. Mishra (2006) Prototropism of 1-hydroxypyrene in liposome suspensions: implications towards fluorescence probing of lipid bilayers in alkaline medium. *Photochemical & Photobiological Sciences* 5(3):283-90

[121] K. Egbaria and M. Friedman (1992) Adsorption of fluorescein dyes on albumin microspheres. *Pharmaceutical Research* 9(5):629-35

[122] K. Egbaria and M. Friedman (1992) Physicochemical properties of albumin microspheres determined by spectroscopic studies. *Journal of Pharmaceutical Sciences* 81(2):186-90

[123] L. C. Bartholow and R. P. Geyer (1981) Sterol release in mammalian cells. The role of a liposomal-free albumin-phospholipid complex. *Biochimica et Biophysica Acta* 665(1):40-47

[124] K. Gaus, M. Rodriguez, K. R. Ruberu, I. Gelissen, T. M. Sloane, L. Kritharides and W. Jessup (2005) Domain-specific lipid distribution in macrophage plasma membranes. *Journal of Lipid Research* 46(7):1526-38

[125] B. Yang, T. N. Oo and V. Rizzo (2006) Lipid rafts mediate H2O2 prosurvival effects in cultured endothelial cells. *FASEB Journal* 20(9):1501-03

[126] L. J. Pike (2003) Lipid rafts: bringing order to chaos. *Journal of Lipid Research* 44(4):655-67

[127] F. M. Goñi and A. Alonso (2009) Effects of ceramide and other simple sphingolipids on membrane lateral structure. *Biochimica et Biophysica Acta* 1788(1):169-77

[128] A. E. Cremesti, F. M. Goñi and R. Kolesnick (2002) Role of sphingomyelinase and ceramide in modulating rafts: do biophysical properties determine biologic outcome? *FEBS Letters* 531(1):47-53

[129] S. N. Pinto, F. Fernandes, A. Fedorov, A. H. Futerman, L. C. Silva and M. Prieto (2013) A combined fluorescence spectroscopy, confocal and 2-photon microscopy approach to re-evaluate the properties of sphingolipid domains. *Biochimica et Biophysica Acta* 1828(9):2099-110

[130] L. C. Silva, R. F. de Almeida, B. M. Castro, A. Fedorov and M. Prieto (2007) Ceramide-domain formation and collapse in lipid rafts: membrane reorganization by an apoptotic lipid. *Biophysical Journal* 92(2):502-16

[131] H. Watanabe, A. Kobayashi, T. Yamamoto, S. Suzuki, H. Hayashi and N. Yamazaki (1990) Alterations of human erythrocyte membrane fluidity by oxygen-derived free radicals and calcium. *Free Radical Biology and Medicine* 8(6):507-14

[132] D. Strassheim, K. Asehnoune, J. S. Park, J. Y. Kim, Q. He, D. Richter, S. Mitra, J. Arcaroli, K. Kuhn and E. Abraham (2004) Modulation of bone marrow-derived neutrophil signaling by H2O2: disparate effects on kinases, NF-kappaB, and cytokine expression. *American Journal of Physiology: Cell Physiology* 286(3):683-92

[133] J. W. Zmijewski, X. Zhao, Z. Xu and E. Abraham (2007) Exposure to hydrogen peroxide diminishes NF-kappaB activation, IkappaB-alpha degradation, and proteasome activity in neutrophils. *American Journal of Physiology: Cell Physiology* 293(1):255-66

[134] R. E. Shackelford, W. K. Kaufmann and R. S. Paules (2000) Oxidative stress and cell cycle checkpoint function. *Free Radical Biology and Medicine* 28(9):1387-404

[135] Y. He, K. W. Leung, Y. Ren, J. Pei, J. Ge and J. Tombran-Tink (2014) PEDF improves mitochondrial function in RPE cells during oxidative stress. *Investigative Ophthalmology and Visual Science* 55(10):6742-55

[136] G. Piwien-Pilipuk, A. Ayala, A. Machado and M. D. Galigniana (2002) Impairment of mineralocorticoid receptor (MR)-dependent biological response by oxidative stress and aging: correlation with post-translational modification of MR and decreased ADP-ribosylatable level of elongating factor 2 in kidney cells. *Journal of Biological Chemistry* 277(14):11896-903

[137] A. A. Banday, F. R. Fazili and M. F. Lokhandwala (2007) Oxidative stress causes renal dopamine D1 receptor dysfunction and hypertension via mechanisms that involve NF-kB and protein kinase C. *Journal of the American Society of Nephrology* 18(5):1446-57

[138] M. Triantafilou, K. Miyake, D. T. Golenbock and K. Triantafilou (2002) Mediators of innate immune recognition of bacteria concentrate in lipid rafts and facilitate lipopolysaccharide-induced cell activation. *Journal of Cell Science* 115(12):2603-11

[139] S. W. Wong, M. J. Kwon, A. M. Choi, H. P. Kim, K. Nakahira and D. H. Hwang (2009) Fatty acids modulate Toll-like receptor 4 activation through regulation of receptor dimerization and recruitment into lipid rafts in a reactive oxygen species-dependent manner. *Journal of Biological Chemistry* 284(40):27384-92

[140] J. Cuschieri, J. Billigren and R. V. Maier (2006) Endotoxin tolerance attenuates LPS-induced TLR4 mobilization to lipid rafts: a condition reversed by PKC activation. *Journal of Leukocyte Biology* 80(6):1289-97

[141] M. Yoshida, J. Tanaka, J. Tamura, K. Fujita, T. Kasamatsu, M. Kohmoto and T. Kaido (1995) Significance of altered fluidity of plasma membranes of the liver and kidney in rats with sepsis. *Journal of Surgical Research* 58(2):131-36

[142] J. Wilschut, N. Duzgunes, D. Hoekstra and D. Papahadjopoulos (1985) Modulation of membrane fusion by membrane fluidity: temperature dependence of divalent cation induced fusion of phosphatidylserine vesicles. *Biochemistry* 24(1):8-14

[143] J. I. Howell, Q. F. Ahkong, F. C. Cramp, D. Fisher, W. Tampion and J. A. Lucy (1972) Membrane fluidity and membrane fusion. *Biochemical Journal* 130(1):44

[144] J. Prives and M. Shinitzky (1977) Increased membrane fluidity precedes fusion of muscle cells. *Nature* 268(5622):761-63

[145] Y. Tokudome, Y. Saito, F. Sato, M. Kikuchi, T. Hinokitani and K. Goto (2009) Preparation and characterization of ceramide-based liposomes with high fusion activity and high membrane fluidity. *Colloids and Surfaces B: Biointerfaces* 73(1):92-96

[146] J. Cuschieri, S. Sakr, E. Bulger, M. Knoll, S. Arbabi and R. V. Maier (2009) Oxidant alterations in CD16 expression are cytoskeletal induced. *Shock* 32(6):572-77

[147] J. Wong-Ekkabut, Z. Xu, W. Triampo, I. M. Tang, D. P. Tielema and L. Monticelli (2007) Effect of lipid peroxidation on the properties of lipid bilayers: a molecular dynamics study. *Biophysical Journal* 93(12):4225-36

[148] J. Szekeres-Bartho, G. Szekeres, P. Debre, B. Autran and G. Chaouat (1990) Reactivity of lymphocytes to a progesterone receptor-specific monoclonal antibody. *Cellular Immunology* 125(2):273-83

[149] B. Polgar, A. Barakonyi, I. Xynos and J. Szekeres-Bartho (1999) The role of gamma/delta T cell receptor positive cells in pregnancy. *American Journal of Reproductive Immunology* 41(4):239-44

[150] I. Hudic, J. Szekeres-Bartho, Z. Fatusic, B. Stray-Pedersen, L. Dizdarevic-Hudic, A. Latifagic, N. Hotic, L. Kameric and A. Mandzic (2010) Dydrogesterone supplementation in women with threatened preterm delivery--the impact on cytokine profile, hormone profile, and progesterone-induced blocking factor. *Journal of Reproductive Immunology* 92(1-2):103-07

[151] B. Polgar, E. Nagy, E. Miko, P. Varga and J. Szekeres-Bartho (2004) Urinary progesterone-induced blocking factor concentration is related to pregnancy outcome. *Biology of Reproduction* 71(5):1699-705

[152] J. H. Check, E. Levin, A. Bollendorf and J. Locuniak (2005) Miscarriage in the first trimester according to the presence or absence of the progesterone-induced blocking factor at three to five weeks from conception in progesterone supplemented women. *Clinical and Experimental Obstetrics and Gynecology* 32(1):13-14

[153] A. Larbi, N. Douziech, G. Dupuis, A. Khalil, H. Pelletier, K. P. Guerard and T. Fulop, Jr. (2004) Age-associated alterations in the recruitment of signal-transduction proteins to lipid rafts in human T lymphocytes. *Journal of Leukocyte Biology* 75(2):373-81

[154] A. Kusumi, I. Koyama-Honda and K. Suzuki (2004) Molecular dynamics and interactions for creation of stimulation-induced stabilized rafts from small unstable steady-state rafts. *Traffic* 5:213-230

[155] K. Simons and D. Toomre (2000) Lipid rafts and signal transduction. *Nature Reviews: Molecular Cell Biology* 1(1):31-39

[156] E. Altrock, C. A. Muth, G. Klein, J. P. Spatz and C. Lee-Thedieck (2012) The significance of integrin ligand nanopatterning on lipid raft clustering in hematopoietic stem cells. *Biomaterials* 33(11):3107-18

[157] K. Simons and E. Ikonen (1997) Functional rafts in cell membranes. *Nature* 387(6633):569-72

[158] D. A. Brown and E. London (1998) Functions of lipid rafts in biological membranes. *Annual Review of Cell and Developmental Biology* 14:111-36

ANNEX I: DPPC GUVs generation

The chosen phospholipid was 1,2-dipalmitoyl-sn-glycero-3-phosphocholine (DPPC), with a phase transition temperature of T_m= 41ºC, not far from physiological conditions. This T_m allows for ideal analysis of phase transition from rigid phase to fluid phase as the confocal microscope can be adjusted to temperatures below (30ºC, rigid phase) and above (50ºC, fluid phase) the T_m. DPPC has a molecular weight of 734.05 g/mol, empirical formula $C_{40}H_{80}NO_8P$, and the schematic structural formula shown in figure 45.
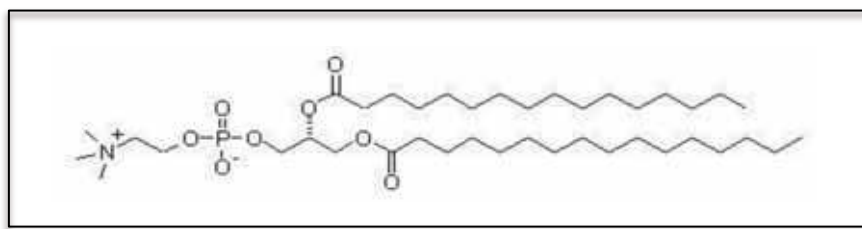

*Figure 45. **Structure of DPPC**.*

In our experimental approach we used giant unilamellar vesicles (GUVs) instead of large unilamellar vesicles (LUVs) or small unilamellar vesicles (SUVs) due to their size: GUVs are very similar in size, from 1µm up to 50µm, to eukaryotic cells while LUVs are about 80 - 800nm and SUVs 30 – 50nm.

In the two-photon confocal microscope it would be very difficult to visually distinguish SUVs due to their small size, LUV would also be too small for analysis, as their surface area is too small.

Appropriate amounts of DPPC (Avanti Polar Lipids) and of the membrane fluidity probe Laurdan were dissolved in chloroform. The solvent was evaporated under an oxygen-free N_2 stream and the resulting film was maintained under high vacuum

overnight to remove organic solvent traces. Giant vesicles were obtained by gently applying PBS, pH 7.4, at a temperature 10ºC above the DPPC phase transition (T_m= 41ºC) on the film, to a final DPPC concentration of 2.5mM (0.5mg/ml) and Laurdan concentration of 5µM. The sample was incubated at this temperature in resting conditions and in the dark for 24h. This method rends mainly giant unilamellar vesicles (GUVs) of about 20µm of mean diameter, although some oligolamellar vesicles could also be observed. For the fluorescence measurements by confocal microscope only GUV were selected.

ANNEX II: Publications in BBA-Biomembranes

Effect of oxidative stress on plasma membrane fluidity of THP-1 induced macrophages (2013) C. de la Haba, JR Palacio, P Martínez, A Morros. *Biochimica et Biophysica Acta (BBA)-Biomembranes*, 1828 (2), 357-364

Oxidative stress effect on progesterone-induced blocking factor (PIBF) binding to PIBF-receptor in lymphocytes (2014) C. de la Haba, José R. Palacio, Tamas Palkovics, Júlia Szekeres-Barthó, Antoni Morros, Paz Martínez. *Biochimica et Biophysica Acta (BBA)-Biomembranes,* 1838 (1), Part B, 148–157